Electronic Band Structures and Physical Properties of Intercalation Compounds of 1T-Type TiS_2

Tatsuya TESHIMA

January 1992

Abstracts

Intercalation of 3d transition-metal atoms, silver atoms and alkali-metal atoms into the layered transition-metal dichalcogenide 1T-TiS_2 has been studied extensively, and quite dramatic changes in the physical properties of the host TiS_2 have been observed depending on the intercalant species and concentration. To provide a basis for understanding a rich variety of physical properties of the intercalation compounds, knowledge of electronic structures of a given compound holds an important key.

Electronic band structures of 1T-TiS_2 intercalated with 3d transition-metal atoms have been carried out for the non-magnetic states of $M_{1/3}TiS_2$ (M = Ti, V, Cr) and for the ferromagnetic state of $Cr_{1/3}TiS_2$ and $Co_{1/3}TiS_2$ by using a self-consistent augmented-plane-wave (APW) method. We have also made linearlized augmented-plane-wave (LAPW) band calculations for $Ag_{1/3}TiS_2$, $Li_{1/3}TiS_2$ and $K_{1/3}TiS_2$. The principal results are summarized as follows:

(a) The 3d states of the intercalant transition-metal atoms hybridize with the Ti 3d and S 3p states and form a new band between the bonding and non-bonding bands of the host TiS_2. The original band structures of the mother crystal TiS_2 are modified considerably by the intercalation and hence the so-called rigid-band model cannot be applied. In contrast with $Co_{1/3}TiS_2$ or $Ni_{1/3}TiS_2$, the 3d states of the guest atoms in $M_{1/3}TiS_2$ (M = Ti, V, Cr) hybridize mainly with the Ti 3d states and hybridization with the S 3p states is small.

(b) The magnetic moment obtained from the ferromangetic band calculation is close to the experimental value for $Co_{1/3}TiS_2$, but for $Cr_{1/3}TiS_2$ the calculated value is about four times larger than the experimental one.

(c) The calculated densities of states at the Fermi level explain well the observed M-dependence of the coefficient γ of electronic specific heat observed in $M_{1/3}TiS_2$ (M = transition-metal).

(d) In $Ag_{1/3}TiS_2$, the Ag 4d states hybridize strongly with the S 3p state and destroy the covalent-like bond between the Ti 3d and the S 3p states, but the strong hybridization between the Ag 4d and the S 3p states does not yield an energy gain because almost all the states of the hybridized bands of the Ag 4d and S 3p states are occupied.

(e) In $Li_{1/3}TiS_2$ and $K_{1/3}TiS_2$ there is little hybridization between the 2s or 4s states of the guest atoms and the host Ti 3d or S 3p states. The modification of the electronic band structure of the host is small.

As for stacking of the guest atoms along the c-axis, ABC-stacking is realized in $M_{1/3}TiS_2$ (M=transition-metal atom, alkali metal atom), and AB-stacking is realized in $Ag_{1/3}TiS_2$. In order to discuss which stacking is most favorable we have performed the total energy calculation for both the AB- and ABC-stacking of $Ag_{1/3}TiS_2$ and $Fe_{1/3}TiS_2$ by using the band structures obtained by the LAPW method. It is concluded that the AB-stacking is more stable than the ABC-stacking in $Ag_{1/3}TiS_2$ whereas ABC-stacking is

stable in $Fe_{1/3}TiS_2$. To get deeper insight into the difference of cohesive properties of $Fe_{1/3}TiS_2$, $Ag_{1/3}TiS_2$ $Li_{1/3}TiS_2$ and $K_{1/3}TiS_2$, we have also carried out the total energy calculation for $Li_{1/3}TiS_2$ and $K_{1/3}TiS_2$ and compared the total energies of these compounds. It has been found that the energy gain due to intercalation of Fe atoms is large compared with those of Ag atom and K atom. This result corresponds to the experimental fact that the guest alkali atoms can move easily in the van der Waals gap layers and the guest Ag stoms shows the temperature-induced order-disorder transitions.

To provide the starting point understanding the magnetism of the low-concentration intercalates of the 3d transition element and the intercalation compounds of the rare earth element, RKKY interaction has been calculated by using the realistic electronic band structure of the host TiS_2.

Acknowlegements

The author would like to express his sincere appreciations to Professor K. Motizuki, under whose guidance this work has been done, for helpful suggestions and valuable discussions. He also would like to express his sincere appreciations to Assistant-Professor N. Suzuki for stimulative and valuable discussions and helpful suggestions. Also he thanks for their help in preparing the manuscript. Without their continuous encouragement and help, this work would not have been completed. His thanks are also due to Doctor M. Shirai for valuable advice and discussions.

He thanks greatly Professor A. Yanase of University of Osaka Prefecture for providing him the computer programs for band calculations and for helpful advice on band calculations. He also gratefully acknowledge helpful advice of Professor K. Terakura of Institute of Solid State Physics on total energy calculations. Thanks are also due to Doctor H. Harima for helpful advice and comments on band calculations and operations of computer.

*** CONTENTS ***

§1. Introduction

The layered titanium disulfide TiS_2 is a narrow-gap semiconducter, and has the 1T-type (CdI_2-type) crystal structure which consists of a sequence of Ti layers sandwiched between two S layers.[1,2] This compound is an important material as the mother crystal for intercalation compounds. In fact, various atoms and organic molecules can be intercalated into van der Waals gap sites of TiS_2. In particular, intercalation of 3d transition-metal atoms,[2-16] silver atoms [17-23] and alkali-metal atoms [24-27] has been studied intensively, and quite dramatic changes in the physical properties of the host TiS_2 have been observed depending on the intercalation species and their concentration.

In the transition-metal intercalation compounds M_xTiS_2 (M=transition-metal atoms), intercalated M atoms occupy the octahedral interstitial sites between the neighboring sulphur layers (van der Waals gap layers) and form regular array for particular x-values such as x=1/4, 1/3, or 1. For x=1/3 the intercalant atoms form a $\sqrt{3}a\times\sqrt{3}a$ triangular lattice in the van der Waals gap layer, and such triangular lattice of M atoms stacks along the c-axis as ABCABC$\cdots$. Experimental investigations, including electrical, optical and magnetic measurements, have been made actively on M_xTiS_2. The analysis of their physical properties had been done by using what is called rigid-band model which assumes that the intercalant atoms

act as electron donors to the host-TiS_2 without changing its original band structures, and the 3d states of intercalants are assumed to be localized. However, the observed results reveal itinerant character of the intercalant 3d electrons [6-8,13-15] and they indicate also the inapplicability of the rigid-band model. Recent measurements of the photoemission suggest strong hybridization of the M-3d states with Ti-3d and S-3p states of the mother crystal.[16] Furthermore, among $M_{1/3}TiS_2$, the three compounds, $Fe_{1/3}TiS_2$, $Cr_{1/3}TiS_2$ and $Co_{1/3}TiS_2$, become ferromagnets below T_c= 50 K, 14 K, and 118 K, respectively,[6] and the observed saturation moment of each compound is much smaller than that expected from the localized M-3d states. This fact also suggests an itinerant character of M-3d states.

In the silver intercalation compounds Ag_xTiS_2, there are three intercalated phases, gas phase for small concentration, a second-stage phase for intermediate concentration (x=1/6 being an ideal concentration) and a first-stage phase for large concentration (x=1/3 being an ideal concentration).[21] The upper limit of the silver concentration is x=0.42.[17] For samples with nominal composition x>0.42, the powder patterns show lines of metallic silver. In the first-stage intercalate, $Ag_{1/3}TiS_2$, all the van der Waals gap layers are partially filled by Ag atoms and a super-structure due to three-dimensional order of Ag atoms, $\sqrt{3}a\times\sqrt{3}a\times\sqrt{2}c$, is present at low temperatures.[22] The stacking of Ag atom layers along the c-axis is ABAB$\cdots$,[18] in contrast with the ABC stacking of M atom layers in $M_{1/3}TiS_2$. The transition to

the disordered structure at T_c=300 K is of the second-order nature.[19] In the second-stage phase the van der Waals gap layers are alternatively partially-occupied and unoccupied by silver atoms. In partially-occupied layer the Ag atoms form also $\sqrt{3}a \times \sqrt{3}a$ super-structure at low temperatures, but along the c-axis there is no ordering at low temperatures.[20,22] The staging structure and the temperature-induced order-disorder transition of intercalant atoms are characteristic to silver intercalate compared with transition-metal intercalate.

In the alkali-metal intercalation compounds, Li_xTiS_2 had been studied for a cathode in chargable battery cell.[24,26] Experimental observation of transport properties of the guest indicates that the Li-ions are hopping among octahedral sites in interstitial layers with period of 10^{-16}sec at 300K.[27] And this suggests a weakness of bonding between the guest-Li and the host-TiS_2. In alkali-metal intercalation compounds, many workers have been also studied for structural ordering of the guest and modification of the host by intercalation. The Li atoms are intercalated in TiS_2 with small changes in lattice parameter because of its small ionic radius. In contrast to Li_xTiS_2, the larger alkali metals such as K or Na are intercalated with changing in the structure of the host.[25] The Na occupies an octahedral site at low concentration ($x < 0.3$), and at mediate concentration the stacking of the host are changed to trigonal prismatic.[26] In K_xTiS_2 with $x<1/3$, only one sort of superstructure which is $\sqrt{3} \times \sqrt{3}$ has been found even in low

concentration and it coexists with non-intercalated region.[26] This indicates that interaction between host and guest is weak compared with that among the guests.

To provide a basis for understanding the physical properties of the intercalation compounds, knowledge of electronic structures of a given compound holds an important key. For that purpose, Yamasaki et al.[28-31] have made the electronic band structure calculations for the non-magnetic states of $M_{1/3}TiS_2$ (M=heavy 3d transition-metal atoms, Mn, Fe, Co, Ni), and for the ferromagnetic state of $Fe_{1/3}TiS_2$. A self-consistent APW method was used. The calculated electronic band structures indicate clearly the itinerant character of the M-3d electrons and also inapplicability of the rigid band model. Furthermore, they have calculated the bond orders in $Fe_{1/3}TiS_2$ and $FeTiS_2$, and found that in Fe_xTiS_2 the Fe-dγ orbitals hybridize strongly with the 3p orbitals of the surronunding S ions whereas the Fe-dε orbitals hybridize with the dε orbitals of the nearest neighboring Ti atoms.

In this paper, first we have made, for completeness, systematic APW band calculations for the non-magnetic states of $M_{1/3}TiS_2$ (M=light transition-metal atoms such as Cr, V, Ti) and for the ferromagnetic states of $Cr_{1/3}TiS_2$ and $Co_{1/3}TiS_2$. Secondly, we focus our attention to the electronic band structures of silver intercalation compound $Ag_{1/3}TiS_2$ as well as alkali-metal intercalation compounds, which show interesting physical properties different from those of transition-metal

intercalation compounds M_xTiS_2. We have made band calculations of the ordered $Ag_{1/3}TiS_2$, $Li_{1/3}TiS_2$ and $K_{1/3}TiS_2$ with use of the linearized APW (LAPW) method. In order to compare the obtained results directly with the eletronic structure of $M_{1/3}TiS_2$ in which M atom layers stack as ABCABC$\cdots$, the band calculation for $Ag_{1/3}TiS_2$ have been carried out for hypothetical ABC-stacking as well as for the first stage AB-stacking $Ag_{1/3}TiS_2$. Thirdly, to make clear why AB-stacking is realized in $Ag_{1/3}TiS_2$ while ABC-stacking is realized in $Fe_{1/3}TiS_2$, by using the band structures obtained by the LAPW method we have calculated the total electronic energy for both AB- and ABC-stacking and compared them. The total energy calculation has been also made for $Fe_{1/3}TiS_2$, $Li_{1/3}TiS_2$ and $K_{1/3}TiS_2$ to discuss cohesive property of each compoud. Finally we have calculated RKKY interaction by using the realistic band structure of the host-TiS_2 to provide the starting point for understanding the magnetism of the intercalation compound of the rare earth element and the low-concentrate intercalation compound of 3d transition element.

§2. Method for Calculations

2-1 Band Calculation

2-1-1 Basic Concept in APW and LAPW Method

First-principle calculations of electronic band structures based on Slater's APW method [32,33] have been performed for many kinds of crystals, during the last 30 years. Recently linearized versions of this method have been developed and applied to many cases. In this section, the principles of APW and Linearized-APW (LAPW) methods [34] are reviewed for later use.

In general any kind of first-principle band calculations is reduced to solve the following one-electron Schrödinger equation (in atomic units):

$$[\ -\nabla^2 + V(\mathbf{r})\ ]\Psi_{\mathbf{k}}(\mathbf{r}) = E_{\mathbf{k}}\Psi_{\mathbf{k}}(\mathbf{r})\ . \qquad (2\text{-}1)$$

where $V(\mathbf{r})$ is the periodic crystal potential for an electron, $\Psi_{\mathbf{k}}(\mathbf{r})$ the eigenfunction which satisfies the Bloch condition, and $\mathbf{k}$ the wave vector in the Brillouin zone. The potential $V(\mathbf{r})$ consists of the interaction of an electron with the nuclear charges and with other electrons. The electron-electron interaction is usually treated within the local spin density approximation (LSDA) [35-41] which will be described in detail in section 2-2.

Both APW and LAPW methods use the Muffin-Tin (MT) approxi-

mation to the crystal potential $V(\mathbf{r})$. A unit cell is divided into two kinds of regions, inside region of spheres (MT spheres) centered at each atomic site and outside of it. Inside the MT spheres the potential is assumed to be spherically symmetric, and outside it is taken to be constant. The radii of MT spheres are set as large as possible unless they overlap each other.

Eignefunction $\Psi_{\mathbf{k}}(\mathbf{r})$ is expanded in terms of the what is called augmented plane waves (APWs) $\chi_{\mu}(\mathbf{r})$ as follows:

$$\Psi_{\mathbf{k}}(\mathbf{r}) = \sum_{\mu} C_{\mu}\chi_{\mu}(\mathbf{r}) \tag{2-2}$$

where μ represents $\mathbf{k}_{\mu} \equiv \mathbf{k} + \mathbf{G}_{\mu}$ with $\mathbf{G}_{\mu}$ being a reciprocal lattice vector. The expansion coefficients C_{μ} can be determined by variational principle. Outside the MT spheres the APW $\chi_{\mu}(\mathbf{r})$ is represented by a single plane wave and inside the MT spheres it can be expanded in terms of atomic-like orbitals as follows:

$$\chi_{\mu}(\mathbf{r}) = \begin{cases} e^{i\mathbf{k}_{\mu}\cdot\mathbf{r}} & \text{(outside MT spheres)} \\ \sum_{\ell m\lambda} A^{\nu}_{\ell m}(\mathbf{k}_{\mu},\lambda) Y_{\ell m}(\hat{\mathbf{r}}_{\nu}) R_{\ell}(r_{\nu};\lambda) & \text{(inside } \nu\text{th MT sphere).} \end{cases} \tag{2-3}$$

Here $\mathbf{r}_{\nu}$ denotes $\mathbf{r}-\mathbf{R}_{\nu}$ with $\mathbf{R}_{\nu}$ being the position vector of the center of the νth MT sphere, $\hat{\mathbf{r}}_{\nu}$ represents the angular components of $\mathbf{r}_{\nu}$, $Y_{\ell m}$ is a spherical harmonics, and $R_{\ell}(r_{\nu};\lambda)$ is a solution

of radial Schrödinger equation

$$\left[-\frac{1}{r^2}\frac{d}{dr}\left(r^2\frac{d}{dr}\right) + \frac{\ell(\ell+1)}{r^2} + V_\nu(r) \right] R_\ell(r;\lambda) = \lambda R_\ell(r;\lambda) \qquad (2\text{-}4)$$

where $V_\nu(r)$ is the spherical potential inside the νth MT sphere. At the present stage λ is not an eigenvalue for the crystal, but is only a parameter that determines the shape of the basis function $\chi_\mu(\mathbf{r})$. The expansion coefficients $A^\nu_{\ell m}(\mathbf{k}_\mu,\lambda)$ in eq.(2-3) can be determined by boundary conditions on the MT sphere given in each method.

2-1-2 APW Method

In the APW method we use only one kind of λ and the value of λ is set to be $E_\mathbf{k}$, the eigenvalue itself to be determined. This choice of λ may make the number of basis functions to be small, however it also makes the secular equation highly non-linear owing to the dependence of $R_\ell(\mathbf{r})$ on $E_\mathbf{k}$. The expansion coefficients $A^\nu_{\ell m}(\mathbf{k}_\mu,E_\mathbf{k})$ in eq.(2-3) are determined so that the APW $\chi_\mu(\mathbf{r})$ is continuous on the MT sphere:

$$A^\nu_{\ell m}(\mathbf{k}_\mu,E_\mathbf{k}) = 4\pi\, i^\ell\, e^{i\mathbf{k}_\mu\cdot\mathbf{R}_\nu}\, Y^*_{\ell m}(\hat{\mathbf{k}}_\mu) j_\ell(k_\mu S_\nu)/R(S_\nu;E_\mathbf{k}) \qquad (2\text{-}5)$$

where $\hat{\mathbf{k}}_\mu$ represents the angular component of $\mathbf{k}_\mu$, S_ν denotes the radius of the νth MT sphere and j_ℓ is a spherical Bessel function of order ℓ. In obtaining eq.(2-5) we have used the following

expansion formula for $e^{i\mathbf{k}\cdot\mathbf{r}}$:

$$e^{i\mathbf{k}\cdot\mathbf{r}} \quad e^{i\mathbf{k}\cdot\mathbf{R}_\nu} \sum_{\ell=0}^{\infty} \sum_{m=-\ell}^{\ell} i^{\ell}\, j_{\ell}(kr_\nu) Y^{*}_{\ell m}(\hat{\mathbf{k}}) Y_{\ell m}(\hat{\mathbf{r}}_\nu) \tag{2-6}$$

It should be noted that the derivative of the APW basis function, $\chi_\mu(\mathbf{r})$, is discontinuous on the MT spheres. Owing to this discontinuity the momentum operator becomes non-Hermitian and there appear additional terms in the variational energy expression which are expressed by integration over the surface of MT spheres. Details of the variational procedure in the APW method are given by Loucks.[33] The final expressions of the equations to determine the expansion coefficients C_μ are given as follows:

$$\sum_{\mu} M_{\xi\mu}(E_{\mathbf{k}})\, C_{\mu} \quad 0 \tag{2-7}$$

and the secular equation to determine the eigenvalue $E_{\mathbf{k}}$ is

$$\det\left| M_{\xi\mu}(E_{\mathbf{k}}) \right| \quad = 0 \tag{2-8}$$

Here the expression of $M_{\xi\mu}$ is given as follows:

$$M_{\xi\mu}(E_{\mathbf{k}}) = \Omega_0(k_\mu^2 \quad E_{\mathbf{k}})\delta_{\xi\mu} \quad 4\pi \sum_{\nu} S_\nu^2 e^{i\mathbf{k}_{\xi\mu}\cdot\mathbf{R}_\nu} G^{\nu}_{\xi\mu}(E_{\mathbf{k}}) \tag{2-9}$$

with

$$G^{\nu}_{\xi\mu}(E_{\mathbf{k}}) = (\mathbf{k}_{\xi}\cdot\mathbf{k}_{\mu}-E_{\mathbf{k}})j_1(k_{\xi\mu}S_{\nu})/k_{\xi\mu} - \sum_{\ell}(2\ell+1)P_{\ell}(\hat{\mathbf{k}}_{\xi}\cdot\hat{\mathbf{k}}_{\mu})j_{\ell}(k_{\xi}S_{\nu})R'_{\ell}(S_{\nu};E_{\mathbf{k}})/R_{\ell}(S_{\nu};E_{\mathbf{k}}) \quad (2\text{-}10)$$

where Ω_0 denotes the unit cell volume, P_{ℓ} is the Legendre polynomial of order ℓ, and $k_{\xi\mu}\equiv|\mathbf{k}_{\xi}-\mathbf{k}_{\mu}|$. As seen from the above expression, $M_{\xi\mu}(E_{\mathbf{k}})$ is complicated as a function of $E_{\mathbf{k}}$ because it contains the function $R_{\ell}(\mathbf{r};E_{\mathbf{k}})$ which depends on $E_{\mathbf{k}}$ through eq.(2-4). Thus it takes rather much computer time to determine the eigenvalue $E_{\mathbf{k}}$ from the secular equaiton eq.(2-8).

2-1-3 LAPW Method

In the LAPW method we use two kinds of λ for every (ℓ,ν) and their values are fixed to appropriate values, $E^1_{\ell\nu}$ and $E^2_{\ell\nu}$ $(E^1_{\ell\nu}<E^2_{\ell\nu})$. Then the expansion coefficients, $A^{\nu}_{\ell m}(\mathbf{k}_{\mu},E^1_{\ell\nu})$ and $A^{\nu}_{\ell m}(\mathbf{k}_{n},E^2_{\ell\nu})$, in eq.(2-3) can be determined so that both the value and the derivative of $\chi_{\mu}(\mathbf{r})$ are continuous on the MT spheres. By making use of eq.(2-6) the expressions of $A^{\nu}_{\ell m}(\mathbf{k}_{\mu},E^{\alpha}_{\ell\nu})$ $(\alpha=1,2)$ are determined as follows:

$$A^{\nu}_{\ell m}(\mathbf{k}_{\mu},E^{\alpha}_{\ell\nu}) = 4\pi\, i^{\ell}\, e^{i\mathbf{k}_{\mu}\cdot\mathbf{R}_{\nu}}\, Y^{*}_{\ell m}(\hat{\mathbf{k}}_{\mu})\; a^{\alpha}_{\ell\nu\mu} \quad (2\text{-}11)$$

with

$$a^{\alpha}_{\ell\nu\mu} = \frac{R'_{\ell}(S_{\nu};E^{\beta}_{\ell\nu})j_{\ell}(k_{\mu}S_{\nu}) - R_{\ell}(S_{\nu};E^{\beta}_{\ell\nu})k_{\mu}j_{\ell}(k_{\mu}S_{\nu})}{R_{\ell}(S_{\nu};E^{1}_{\ell\nu})R'_{\ell}(S_{\nu};E^{2}_{\ell\nu}) - R'_{\ell}(S_{\nu};E^{1}_{\ell\nu})R_{\ell}(S_{\nu};E^{2}_{\ell\nu})} \quad (\beta\neq\alpha) \quad (2\text{-}12)$$

Since in the LAPW method the APW basis functions are continuous both in value and slope on the MT spheres, the usual variational procedure can be used. As a result the expansion coefficients C_μ are determined from

$$\sum_\mu [H_{\xi\mu} \quad E_{\mathbf{k}}\Delta_{\xi\mu}]C_\mu = 0 \tag{2-13}$$

and the eigenvalue $E_{\mathbf{k}}$ is determined from the secular equation

$$\det| H_{\xi\mu} \quad E_{\mathbf{k}}\Delta_{\xi\mu} | = 0 \tag{2-14}$$

Here $H_{\xi\mu}$ and $\Delta_{\xi\mu}$ are elements of the Hamiltonian and overlap matrices, and their explicit expressions are given as follows:

$$H_{\xi\mu} = k_\mu^2\Omega_0\delta_{\xi\mu} \quad \frac{1}{2}(k_\xi^2+k_\mu^2)D_{\xi\mu} + 4\pi\sum_\ell(2\ell+1)P_\ell(\hat{\mathbf{k}}_\xi\cdot\hat{\mathbf{k}}_\mu)A_{\ell\xi\mu} \tag{2-15}$$

$$\Delta_{\xi\mu} = \Omega_0\delta_{\xi\mu} \quad D_{\xi\mu} + 4\pi\sum_\ell(2\ell+1)P_\ell(\hat{\mathbf{k}}_\xi\cdot\hat{\mathbf{k}}_\mu)B_{\ell\xi\mu} \tag{2-16}$$

where $D_{\xi\mu}$, $A_{\ell\xi\mu}$ and $B_{\ell\xi\mu}$ are defined by

$$D_{\xi\mu} = \sum_\nu \frac{4\pi S_\nu}{k_{\xi\mu}} j_1(k_{\xi\mu}S_\nu) \tag{2-17}$$

$$A_{\ell\xi\mu} = \sum_{\nu}\sum_{\alpha} E^{\alpha}_{\ell\nu} a^{\alpha}_{\ell\nu\xi} a^{\alpha}_{\ell\nu\mu} \Theta^{\alpha\alpha}_{\ell\nu} + \frac{1}{2}\sum_{\nu}\sum_{\alpha,\beta}^{\alpha\neq\beta} (E^{\alpha}_{\ell\nu}+E^{\beta}_{\ell\nu})(a^{\alpha}_{\ell\nu\xi} a^{\beta}_{\ell\nu\mu} + a^{\beta}_{\ell\nu\xi} a^{\alpha}_{\ell\nu\mu})\Theta^{\alpha\beta}_{\ell\nu} \tag{2-18}$$

$$B_{\ell\xi\mu} = \sum_{\alpha,\beta} a^{\alpha}_{\ell\nu\xi} a^{\beta}_{\ell\nu\mu} \Theta^{\alpha\beta}_{\ell\nu} \tag{2-19}$$

with

$$\Theta^{\alpha\beta}_{\ell\nu} = \int_0^{S_\nu} R_\ell(r_\nu; E^{\alpha}_{\ell\nu}) R_\ell(r_\nu; E^{\beta}_{\ell\nu}) r_\nu^2 dr_\nu \tag{2-20}$$

Comparing with the APW method the matrix elements $H_{\xi\mu}$ and $\Delta_{\xi\mu}$ do not depend on the eigenvalue $E_{\mathbf{k}}$. Thus, determination of eigenvalues in the LAPW method is reduced to usual algebraic procedure for Hermitian matrix, which saves much computer time.

2-1-4 Practical Aspects in APW and LAPW Band Calculations

For APW and LAPW calculations one has to prepare the following parameters.

a) Parameters related to the crystal structure

(1) lattice constants.

(2) species of atoms and their positions in the unit cell.

These parameters are characteristic of the material.

b) Parameters related directly to accuracy

(1) K_{max}: the absolute value of reciprocal lattice vector which determines the number of basis functions. The basis sets are built from reciprocal lattice vectors inside the sphere of radius K_{max}.

(2) ℓ_{max}: the maximum value of angular momentum quantum number of spherical functions which are used to expand the basis functions inside the MT sphere.

(3) k-points which are used to calculate self-consistently the charge density (or partial DOS).

c) Parameters related to approximations

(1) MT radius of each atom.

(2) kinds of orbits which are solved self-consistently. These orbits are called 'valence orbits'. Inner orbits (core orbits) which are deep in energy are treated by frozen-core approximation or by semi-core approximation.

d) Electron configuration of constituent atoms

The initail charge density (or potential) is constructed by superposing the free atomic charge density (or potential) determined by the given atomic electron configuration. It is not always necessary to use the electron configuration of the ground state. One often chooses an electron configuration different from that of the ground state in order to achieve a rapid convergence of the self-consistent calculation.

In actual calculations it is the spherically symmetric

charge desnity of valence electrons, $\rho_\nu(r_\nu)$, in each MT sphere that is determined self-consistently. $\rho_\nu(r_\nu)$ is defined by the spherical average of the valence charge density in the νth MT sphere:

$$\rho_\nu(r_\nu) = \frac{1}{4\pi}\int \rho(\mathbf{r}_\nu)\, d\hat{r}_\nu \tag{2-21}$$

and the valence charge density $\rho(\mathbf{r})$ is calculated in general from

$$\rho(\mathbf{r}) = \sum_{n\mathbf{k}}^{occup} |\Psi_{n\mathbf{k}}(\mathbf{r})|^2 \tag{2-22}$$

where $\Psi_{n\mathbf{k}}(\mathbf{r})$ represents the eigenfunction obtained for valence electrons with n being the band index, and the summation is taken over the occupied states.

In the APW method we have constructed the charge density by using directly the eigenfunctions $\Psi_{n\mathbf{k}}(\mathbf{r})$ In the LAPW method, on the other hand, we have constructed the charge density by making use of the partial density of state as described in the Appendix-1.

2-2 Calculation of Total Energy

A total energy is the most reliable physical quantity in the density functional theory.[35,36] It has been calculated for many kinds of free atoms, molecules, simple metals and compounds,[37,38] by using the local spin density approximation (LSDA).[39-41] The obtained results have been used in order to discuss structural instability, lattice dynamics and cohesive properties. We have evaluated the total energy for the intercalation compounds of 1T-TiS_2 to discuss the bonding strength between the guest atoms and the host. In this section the density functional theory is reviewed briefly and an expression for the total energy in the LSDA is given.

We consider a many electron system which is described by the following Hamiltonian in the second quantized form (in atomic unit):

$$H = T + V + U \tag{2-23}$$

with

$$T = \int \Psi^*(\mathbf{r})\,(-\nabla^2)\,\Psi(\mathbf{r})\,d\mathbf{r} \tag{2-24}$$

$$V \int \Psi^*(\mathbf{r})\,v(\mathbf{r})\,\Psi(\mathbf{r})\,d\mathbf{r} \tag{2-25}$$

$$U \iint \Psi^*(\mathbf{r})\Psi^*(\mathbf{r}')\,|\mathbf{r}-\mathbf{r}'|\,\Psi(\mathbf{r}')\Psi(\mathbf{r})d\mathbf{r}d\mathbf{r}' \tag{2-26}$$

where $\Psi(\mathbf{r})$ represents the field operator, T denotes the kinetic energy, V is a contribution from the external potential $v(\mathbf{r})$ (interaction with the nuclear charges is included in this term), and finally U represents the electron-electron interaction energy.

Acording to the Hohenberg-Kohn [35] theorem the total energy, E_G, in the ground state of the above system is given by a functional of the electron density, $\rho(\mathbf{r})\equiv\langle G|\Psi^{*}(\mathbf{r})\Psi(\mathbf{r})|G\rangle$, where $|G\rangle$ denotes the ground state. We can express E_G in the following functional form of $\rho(\mathbf{r})$:

$$E_G = K[\rho(\mathbf{r})] + \int v(\mathbf{r})\rho(\mathbf{r})d\mathbf{r} + \iint \frac{\rho(\mathbf{r})\rho(\mathbf{r}')}{|\mathbf{r}-\mathbf{r}'|} d\mathbf{r}d\mathbf{r}' + E_{xc}[\rho(\mathbf{r})]. \tag{2-27}$$

Here the first term denotes the functional for the kinetic energy when the electron-electron interaction is absent, the second term the interaction energy with external field $v(\mathbf{r})$,and the third term the direct Coulomb (classical) interaction energy between electrons. The fourth term represents the remaining energy called exchange-correlation energy, and the explicit functional form of E_{xc} is unknown.

Now, the ground state energy E_G can be determined by a variational procedure, $\delta E_G=0$, with respect to $\rho(\mathbf{r})$ under the condition $\int\rho(\mathbf{r})d\mathbf{r}$=constant. Then, the variational condition is given by

$$\int \{ \frac{\delta K[\rho(\mathbf{r})]}{\delta\rho} + w(\mathbf{r}) \quad E \} \delta\rho(\mathbf{r})d\mathbf{r} = 0 \tag{2-28}$$

with

$$w(\mathbf{r}) \equiv v(\mathbf{r}) + v_c(\mathbf{r}) + v_{xc}(\mathbf{r}) \tag{2-29}$$

$$v_c(\mathbf{r}) = 2\int \frac{\rho(\mathbf{r}')}{|\mathbf{r}-\mathbf{r}'|} d\mathbf{r}' \tag{2-30}$$

$$v_{xc}(\mathbf{r}) = \frac{\delta E_{xc}[\rho(\mathbf{r})]}{\delta \rho(\mathbf{r})} \tag{2-31}$$

where E is a Lagrange's multiplier, and $\delta K/\delta\rho$ and $\delta E_{xc}/\delta\rho$ represent functional derivatives. $v_{xc}(\mathbf{r})$ is called exchange-correlation potential.

The variational condition given by eq.2-28 is equivalent to that for a non-interacting electron gas system subjected to an external potential $w(\mathbf{r})$. Therefore, the electron density, $\rho(\mathbf{r})$, of the ground state can be obtained from

$$\rho(\mathbf{r}) = \sum_{i}^{occup} |\phi_i(\mathbf{r})|^2 \tag{2-32}$$

where ϕ_i denotes the one-electron eigenfunction of the following Schrödinger equation for an electron under the external potential $w(\mathbf{r})$:

$$[\ -\nabla^2 + w(\mathbf{r})\ ]\phi_i(\mathbf{r}) = \varepsilon_i \phi_i(\mathbf{r}) \tag{2-33}$$

Once the charge density $\rho(\mathbf{r})$ is determined, we can evaluate the

total energy from eq.2-27 or from the following equation:

$$E_G = \sum_i^{occup} \varepsilon_i - \int \frac{\rho(\mathbf{r})\rho(\mathbf{r}')}{|\mathbf{r}-\mathbf{r}'|} d\mathbf{r}d\mathbf{r}' - \int v_{xc}(\mathbf{r})\rho(\mathbf{r})d\mathbf{r} + E_{xc}[\rho(\mathbf{r})]. \tag{2-34}$$

This equation is derived by using the following relation:

$$\sum_i^{occup} \varepsilon_i = K[\rho(\mathbf{r})] + \int v(\mathbf{r})\rho(\mathbf{r})d\mathbf{r} + 2\int \frac{\rho(\mathbf{r})\rho(\mathbf{r}')}{|\mathbf{r}-\mathbf{r}'|} d\mathbf{r}d\mathbf{r}' + \int v_{xc}(\mathbf{r})\rho(\mathbf{r})d\mathbf{r} . \tag{2-35}$$

In order to perform actaul calculations we have to determine a functional form of $E_{xc}[\rho(\mathbf{r})]$. Usually we assume the following form for E_{xc}:

$$E_{xc}[\rho(\mathbf{r})] = \int \varepsilon_{xc}(\rho)\rho(\mathbf{r})d\mathbf{r} , \tag{2-36}$$

where $\varepsilon_{xc}(\rho)$ is called exchange-correlation energy density. Then, the exchange-correlation potential, $v_{xc}(\mathbf{r})$, is expressed as

$$v_{xc}(\mathbf{r}) = \frac{\delta E_{xc}}{\delta \rho} = \varepsilon_{xc}(\rho) + \rho \frac{\partial \varepsilon_{xc}}{\partial \rho} . \tag{2-37}$$

This approximation is called the local spin density approximation (LSDA). As for $\varepsilon_{xc}(\rho)$ we usually employ the exchange correlation energy density in the electron gas system. Even for the electron

gas system any exact expression of $\varepsilon_{xc}(\rho)$ has not been derived, and many approximate expressions have been proposed for $\varepsilon_{xc}(\rho)$ by von Barth and Hedin,[39] Hedin and Lundqvist,[40] Moruzzi, Janak and Williams,[37] Ceperly and Alder,[42] and Gunnarsson and Lundqvist.[41] Their expressions are summarized in Appendix-2. In this paper we have used the following expression of ε_{xc} given by Gunnarsson and Lundqvist:

$$\varepsilon^{xc}=\varepsilon_p^{xc} + (\varepsilon_f^{xc} - \varepsilon_p^{xc}) \frac{(1+\zeta)^{4/3}+ (1-\zeta)^{4/3}-2}{2(2^{1/3} - 1)}$$

where

$$\varepsilon_p^{xc} = - \varepsilon_p^{x} - 0.0666 \left[(1+ x_p^3)\ln(1+ \frac{1}{x_p}) + \frac{1}{2} x_p^2 - \frac{1}{3}\right] ,$$

$$\varepsilon_f^{xc} = - \varepsilon_f^{x} - 0.0406 \left[(1+ x_f^3)\ln(1+ \frac{1}{x_f}) + \frac{1}{2} x_f^2 - \frac{1}{3}\right] , \qquad (2\text{-}38)$$

$$\varepsilon_p^{x} = - (\frac{9\pi}{4})^{1/3} \frac{3}{2\pi r_s} , \qquad \varepsilon_f^{x} = - (\frac{9\pi}{2})^{1/3} \frac{3}{2\pi r_s} ,$$

and

$$x_p = \frac{r_s}{11.4} , \qquad x_f = \frac{r_s}{15.9} .$$

The r_s is a density parameter defined by $r_s=(3/4\pi\rho)^{1/3}$, and the polarization parameter ζ is given by $\zeta=(\rho\uparrow-\rho\downarrow)/\rho$.

In actual calculation we first give an appropriate initial charge density to evaluate the Coulomb and exchange-correlation

potential, $v_c(\mathbf{r}) + v_{xc}(\mathbf{r})$. Then, we solve the one-electron Schrödinger equation eq.(2-33) and construct the charge density from eq.(2-32). Next, this newly determined charge density is used to evaluate the Coulomb and exchange-correlation potential and again we solve the one-electron Schrödinger equation and construct the charge density. This iterating procedure is to be repeated until the charge density is determined self-consistently.

In band calculation the one particle states $\phi_{\mathbf{k}}(\mathbf{r})$ are regarded as the eigenstates for the bulk (Bloch states). Note that the density functional formulation guarantees that the total energy and the electronic charge density, $\phi(\mathbf{r})=\Sigma|\phi_{\mathbf{k}}|$, will be obtained exactly. The true ground state can be represented by using the one particle states provided that the LSDA is appropriate for the system.

In band calculation, once the eigenvalue and charge density are obtained within a certain accuracy, the total energy can be evaluated by using eq.(2-34) and eq.(2-38). In practice it is difficult to evaluate total energy for compounds consisting of many atoms to discuss the absolute magnitude of it. The self-consistent band calculation for such compounds takes much more computational resources compared with that for atoms or simple metals; the larger number of atoms in the unit cell demands the larger number of the basis set, then large capacity of computer memory has to be occupied and CPU time for one iteration is enlarged. Thus this brings hardness into the discussion for

absolute value of total energy of the compounds. However it should be emphasized that one can obtain the total energy with sufficient accuracy to discuss relative magnitude of them. We will discuss total energies within the order of 0.1 Ryd.

§3. Electronic Structures of Transition-Metal Intercalation Compounds

We have made the band calculation for non-magnetic states of $M_{1/3}TiS_2$ (M=Cr,V,Ti) and ferromagnetic states of $Cr_{1/3}TiS_2$ and $Co_{1/3}TiS_2$ by using the self-consistent APW method. The MT approximation has been used for the crystal potential and the exchange and correlation interaction are treated in the local spin density approximation by Gunnarson and Lundqvist. The core states of all atoms have been assumed to be unchanged in self-consistent calculation (frozen-core approximation).

The host 1T-type TiS_2 has the CdI_2-type crystal structure (Fig. 3-1(a)), which consists of a sequence of titanium layer sandwiched by two layers of sulfur. Guest atoms occpy the octahedral interstitial sites between the neighboring sulfur layers. As the concentration of the guest is equal to 1/3, the guest atoms form $\sqrt{3}a\times\sqrt{3}a$ super lattice in the plane and a period of the super lattice along the c-direction is 3c (ABC-stacking).[3-5] The crystal structure of $M_{1/3}TiS_2$ with ABC stacking are shown in Fig. 3-2. The generators for a space group of this structure (C_{3i}) are I and C_3. The lattice parameters of each compound are given Tabel 3-1.

Table 3-1. Lattice constants [3-5)]

	a	c
host-TiS_2	3.410	5.690
$Ti_{1/3}TiS_2$	5.911	17.151
$V_{1/3}TiS_2$	5.911	17.094
$Cr_{1/3}TiS_2$	5.929	17.133
$Co_{1/3}TiS_2$	5.887	16.887

(unit in Å)

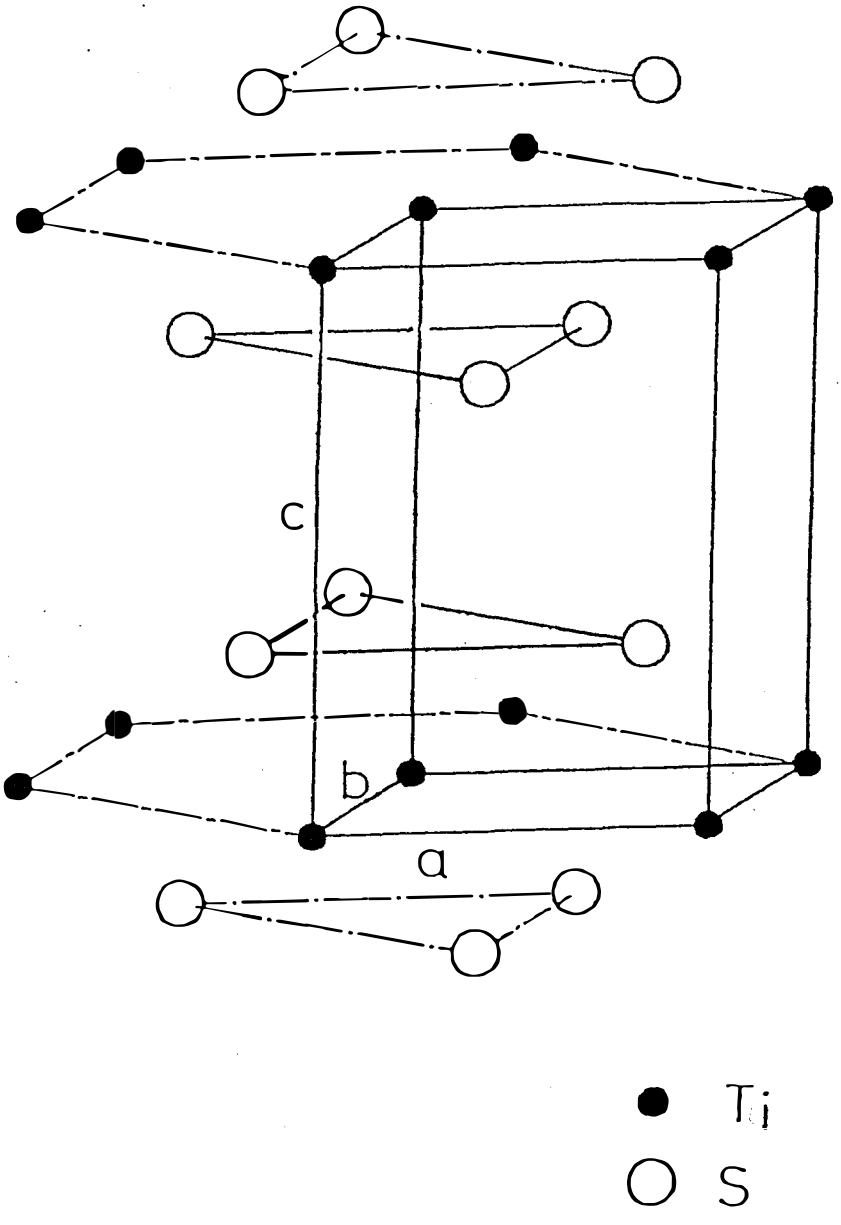

Fig. 3-1(a). The crystal structure of 1T-TiS_2 (CdI_2 structure).

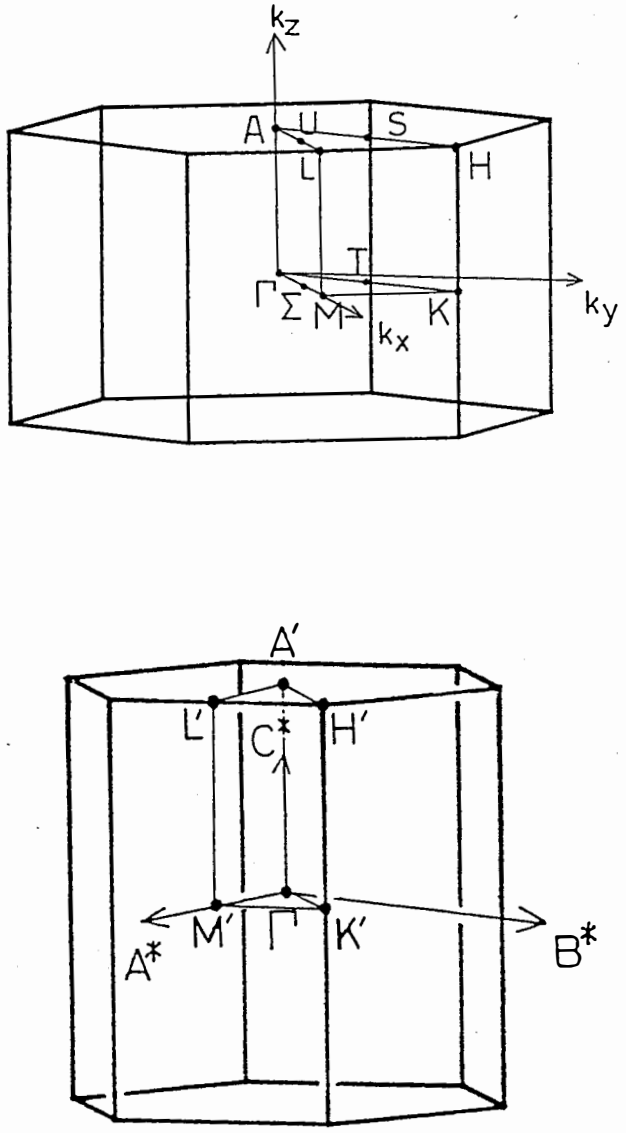

Fig. 3-1(b). The first Brilloun zone of D_{3d} (above) and C_{3i} (below). Space group for TiS_2 and $M_{1/3}TiS_2$ (AB-stacking) is D_{3d}, for $M_{1/3}TiS_2$ (ABC-stacking) space group is C_{3i}.

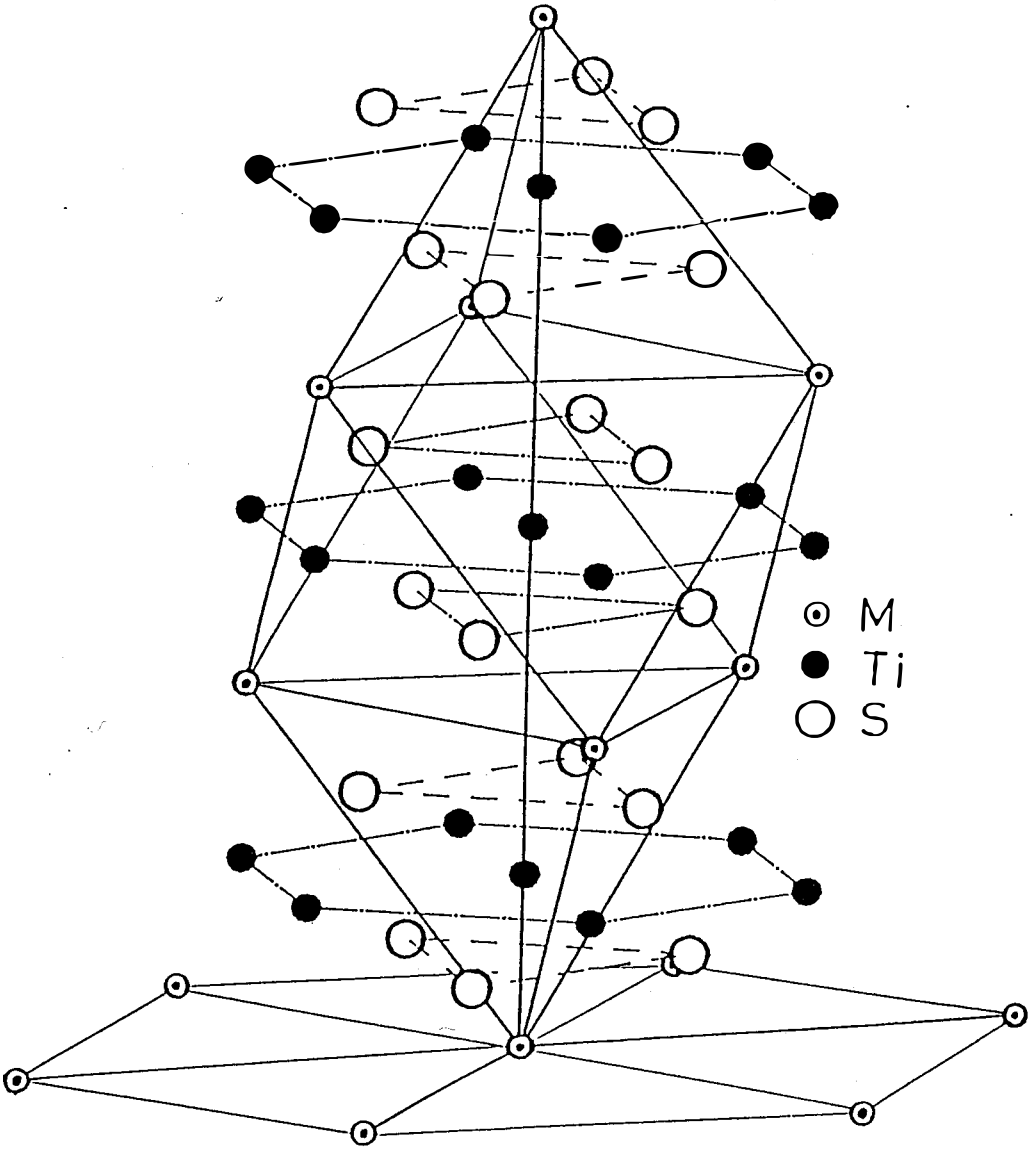

Fig. 3-2. The crystal structure of $M_{1/3}TiS_2$.

3-1 Band Structure of Non-Magnetic $M_{1/3}TiS_2$ (M= Ti,V,Cr)

The APW band calculation for the non-magnetic state of $M_{1/3}TiS_2$ (M=Ti,V,Cr) has been performed first. We have used the criterion, $K_{max}=3.8\times(2\pi/a)$ and $_{max}=7$, for all of the above three compounds. The number of basis APWs corresponding this K_{max} is about 300. The electronic configurations and MT radii are shown in Table.3-2.

The dispersion curves along the symmetry lines for $Ti_{1/3}TiS_2$, $V_{1/3}TiS_2$ and $Cr_{1/3}TiS_2$ are shown in Fig.3-3, Fig.3-4, and Fig.3-5, respectively. Lowest six bands consist mainly of 3s-states of sulfur and the 38 bands above the gap are mixing bands of Ti-3d, S-3p, and M-3d states (M=Ti,V,Cr). The gross feature of the dispersion curves for these compounds resemble each other.

The densities of states (DOS) calculated for the 38 mixing bands of $M_{1/3}TiS_2$ (M=Ti, V, Cr) are shown in Fig.3-6, Fig.3-7 and Fig.3-8, respectively, together with the partial DOS. For all of these compounds, the energy range in DOS may be divided into three parts as shown in the figures.

The part (1) and (3) correspond to the bonding and anti-bonding bands between S-3p and Ti-3dγ, respectively. The part (2) consists mainly of the Ti-3dε and M-3d states. In part (1) the majority components are the 3p-states of sulfur, and the 3dε-states of titanium are contained mainly in part (2). The hybridization between the Cr-3d and S-3p states is small and the hybridization between the Cr-3d and Ti-3d states is large as seen

from Fig.3-4. The Cr-3d states are hybridized with the Ti-3d states chiefly in part (2), but there are certain hybridizaion both in (1) and (3). These behaviors are also seen in $Ti_{1/3}TiS_2$ and in $V_{1/3}TiS_2$ (see Fig.3-7 and Fig.3-8), but quite different from those of $M_{1/3}TiS_2$ (M=heavy 3d-transition elements),[28-31] in which the 3d-states of guests are hybridized mainly with the S-3p states. This difference can be ascribed to the difference in the atomic energy levels of the 3d-states of the guest atoms. In light 3d-transition elements the atomic 3d-levels are higher than those in heavy 3d-transition elements. Namely the energy level of the 3d-states of light transition elements is close to that of host Ti-3d and therefore the M-3d states are mixed well with Ti-3d. On the other hand, with increasing atomic number of the guest the 3d levels of the guests are lowered and approach to S-3p level. A small gap exits between (2) and (3) for the intercalation compounds except for $Ti_{1/3}TiS_2$ and $V_{1/3}TiS_2$, and its value increases with increasing atomic number of the guest atom. With decreasing atomic number of the guest, the part (2) is pushed up, and the gap vanishs for $V_{1/3}TiS_2$ and $Ti_{1/3}TiS_2$.

The width of the partial DOS of the guest 3d-states is more than 0.1 Ryd for all intercalation compounds $M_{1/3}TiS_2$ (M=Ti,V,$\cdots$,Ni). Thus it will be required that the guest 3d-states are treated as itinerant states rather than localized states. Particularly, the width is large for $Ni_{1/3}TiS_2$ or $Ti_{1/3}TiS_2$. The energy levels of the 3d states of Ni (or Ti) atoms are near to those of the S-3p (or Ti-3d) states, thus the

guest-3d bands can be well hybridized to the host S-3p (or Ti-3d) bands whose width is large. Thus the DOS at E_f becomes small and therefore the compounds of Ni and Ti do not show magnetic order, while the compounds of Cr, Fe and Co become ferromagnets at low temperatures. The situation mentioned above is consistent with the experimental results. Recently, Tazuke et.al.[13] have measured the magnetic susceptibility in Cu_xTiS_2 ($x < 0.3$). Paramagnetic behavior was observed in a temperature range of $4.2\,K < T < 300\,K$ and effective Bohr magneton is $0.15\text{-}0.32\,\mu_B$. It is also consistent with the tendency mentioned above.

Table.3-2. The electronic configurations and MT radii for non-magnetic $M_{1/3}TiS_2$ (M= Ti,V,Cr)

	configuration		M.T. radii (in a)		
			guest	Ti	S
$Ti_{1/3}TiS_2$	Ti	$[Ar](3d)^2(4s)^2$	0.1855	0.1850	0.2260
	S	$[Ne](3s)^2(3p)^4$			
$V_{1/3}TiS_2$	V	$[Ar](3d)^3(4s)^2$	0.1855	0.1850	0.2260
$Cr_{1/3}TiS_2$	Cr	$[Ar](3d)^{4.4}(4s)^{1.6}$	0.1855	0.1850	0.2260

The orbits in [ ] are considered to be frozen.

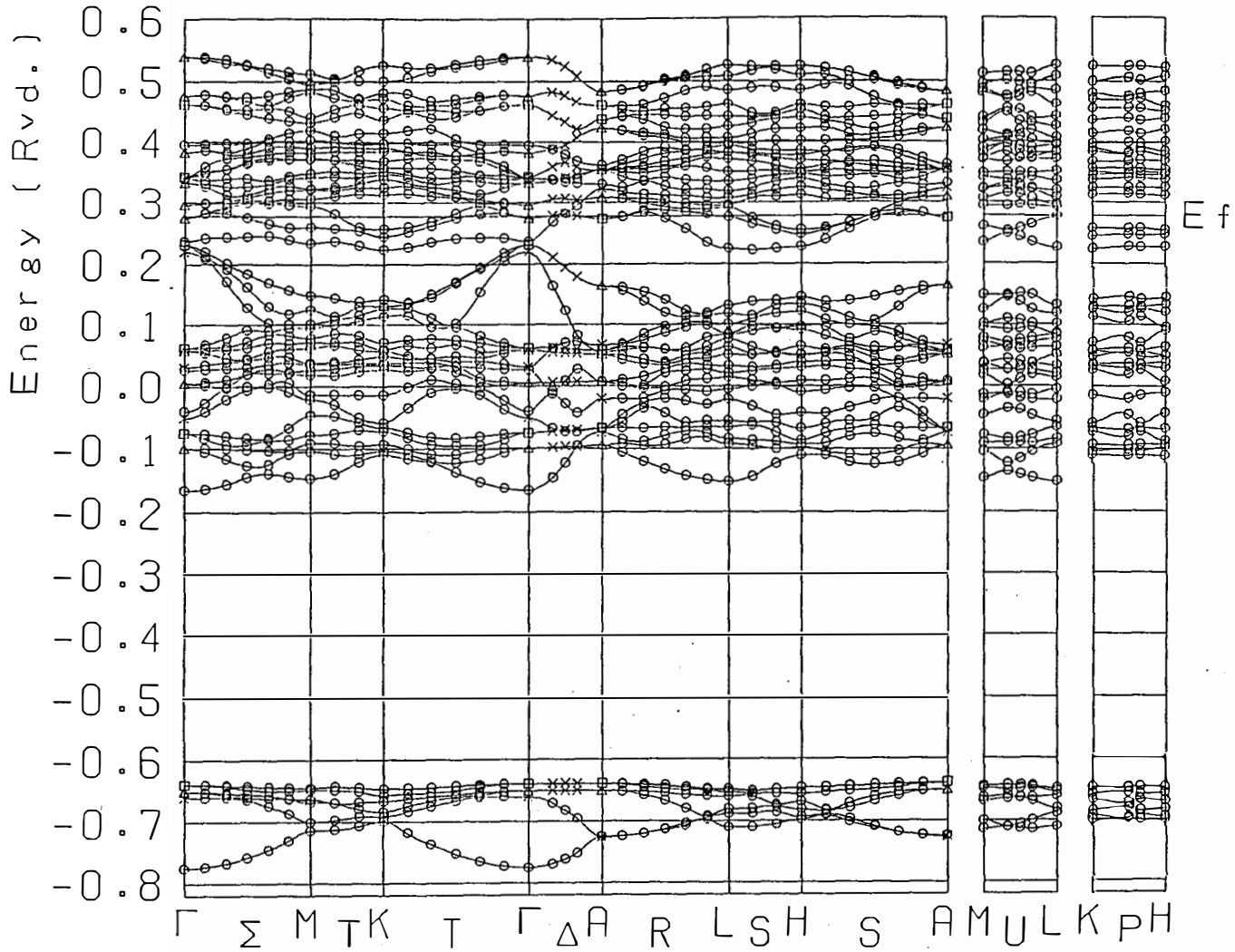

Fig. 3-3. The dispersion curves of $Ti_{1/3}TiS_2$.

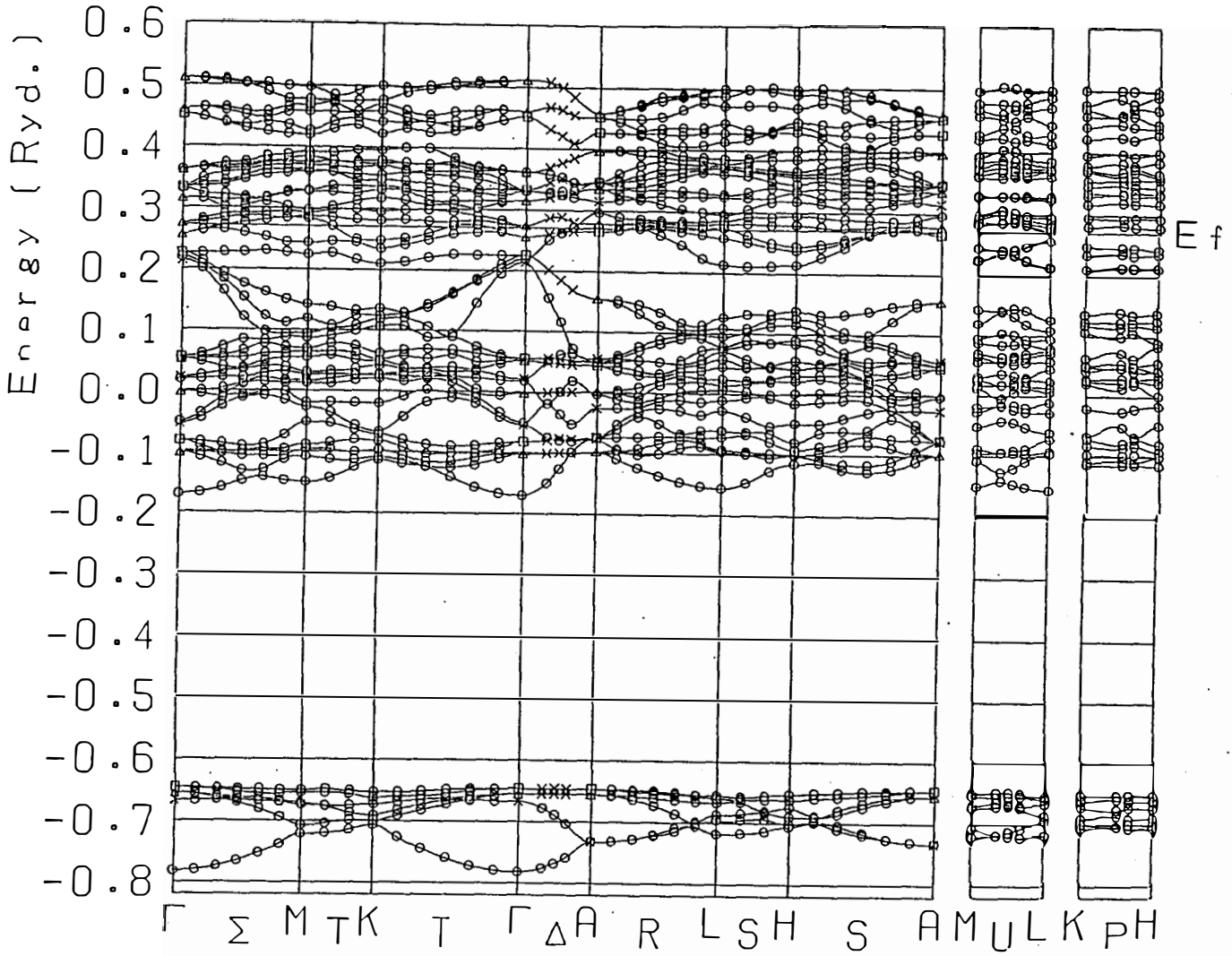

Fig. 3-4. The dispersion curves of $V_{1/3}TiS_2$.

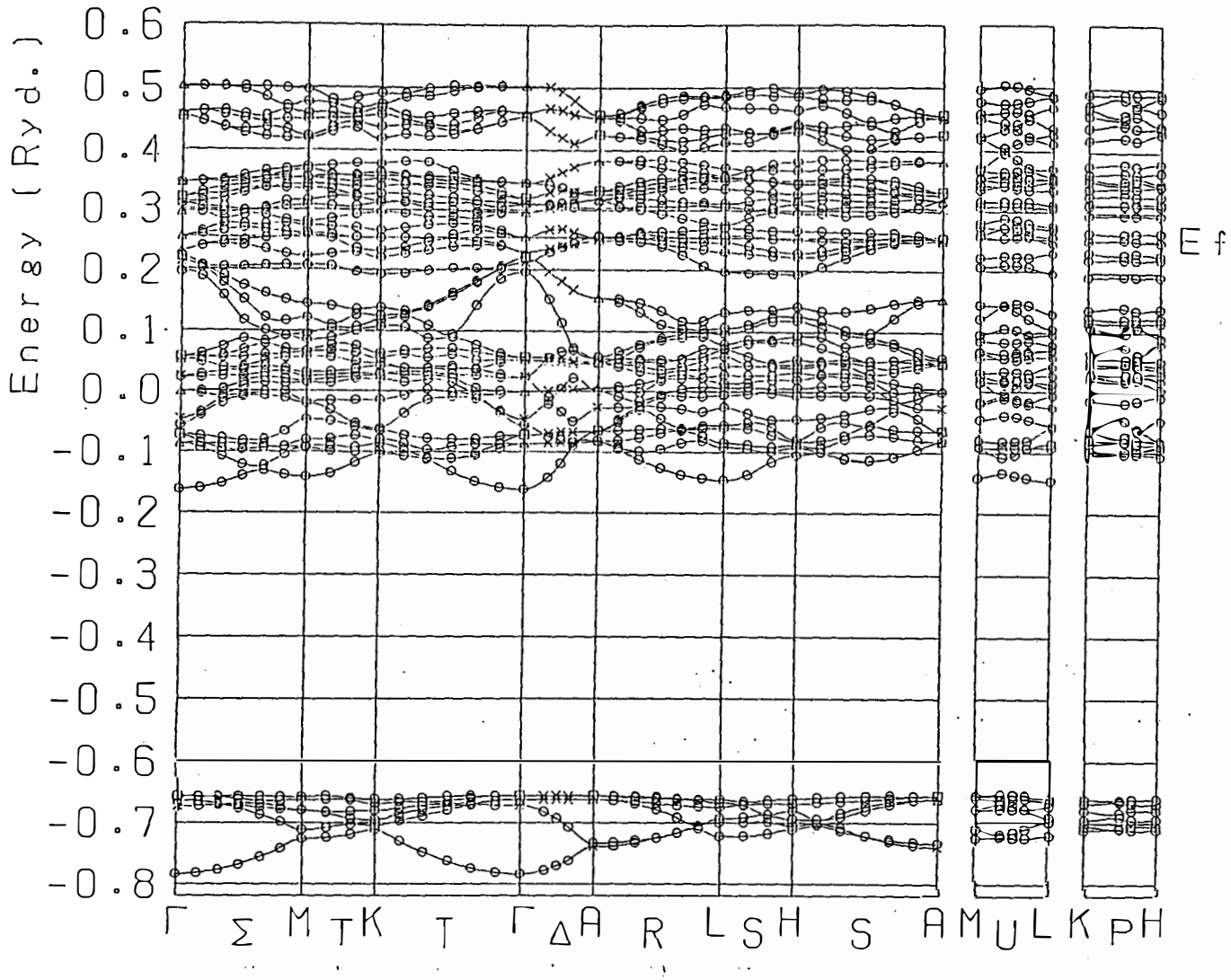

Fig. 3-5. The dispersion curves of $Cr_{1/3}TiS_2$.

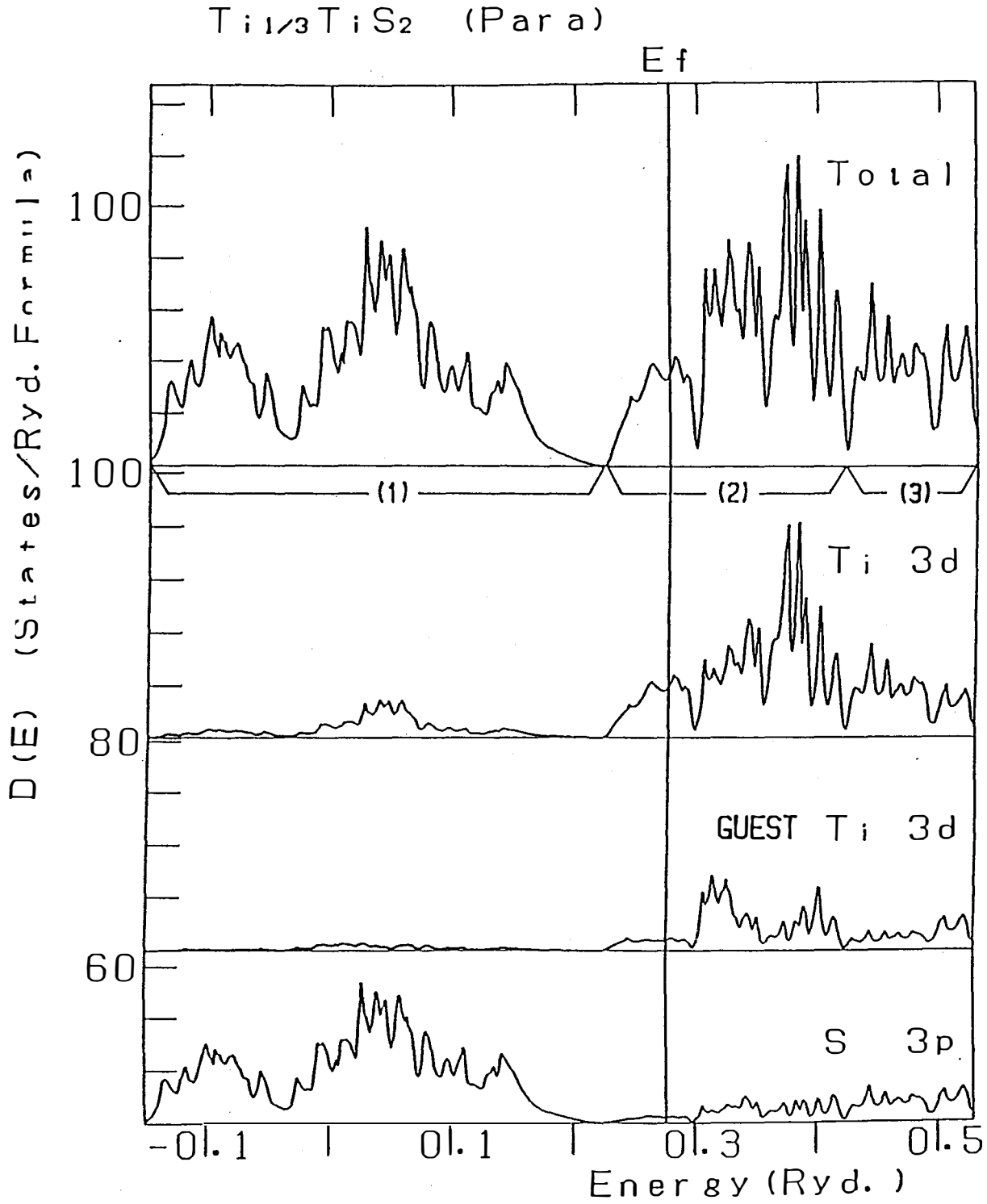

Fig. 3-6. The density of states of self-intercalation compound $Ti_{1/3}TiS_2$ (Ti_2S_3).

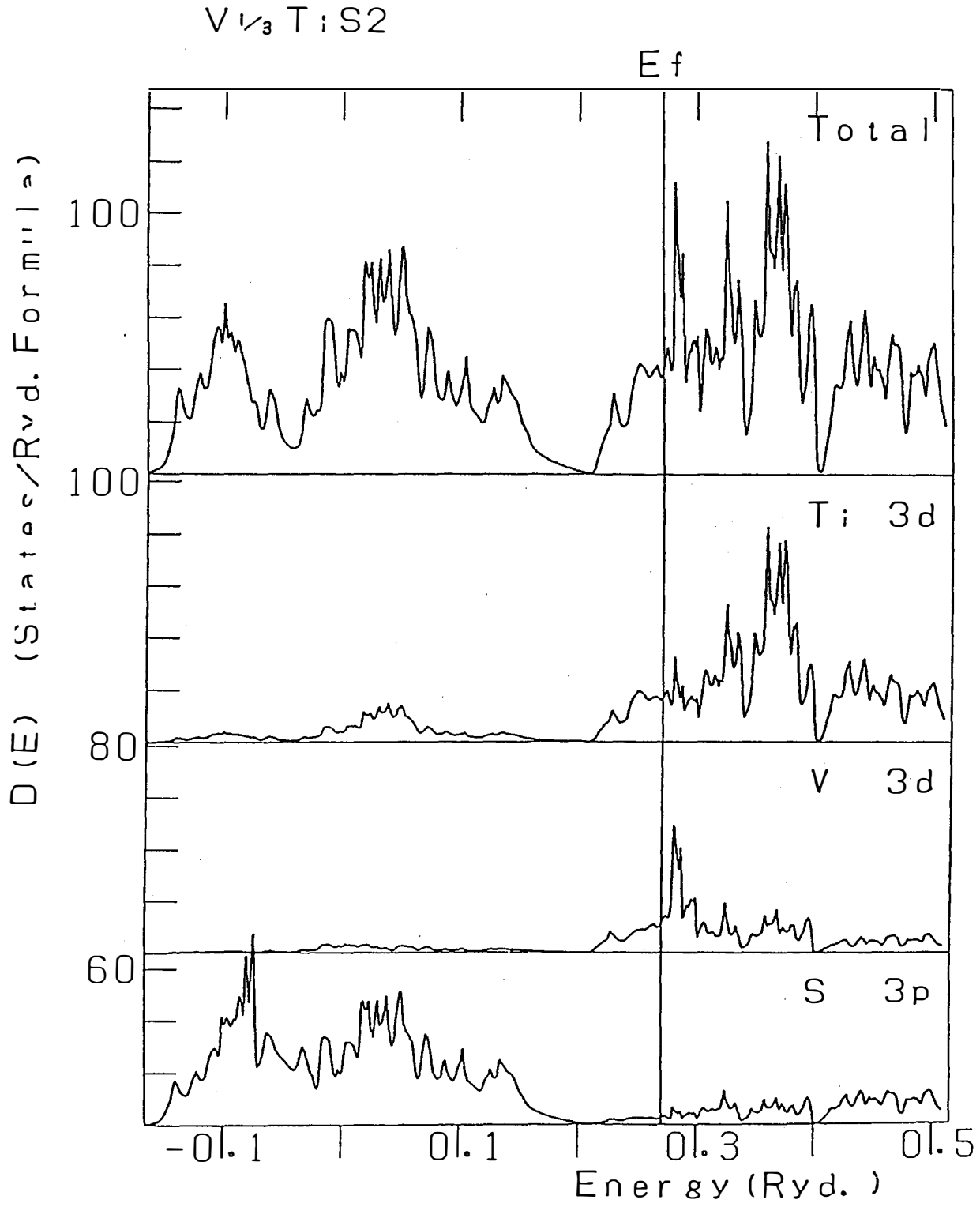

Fig. 3-7. The density of states of $V_{1/3}TiS_2$.

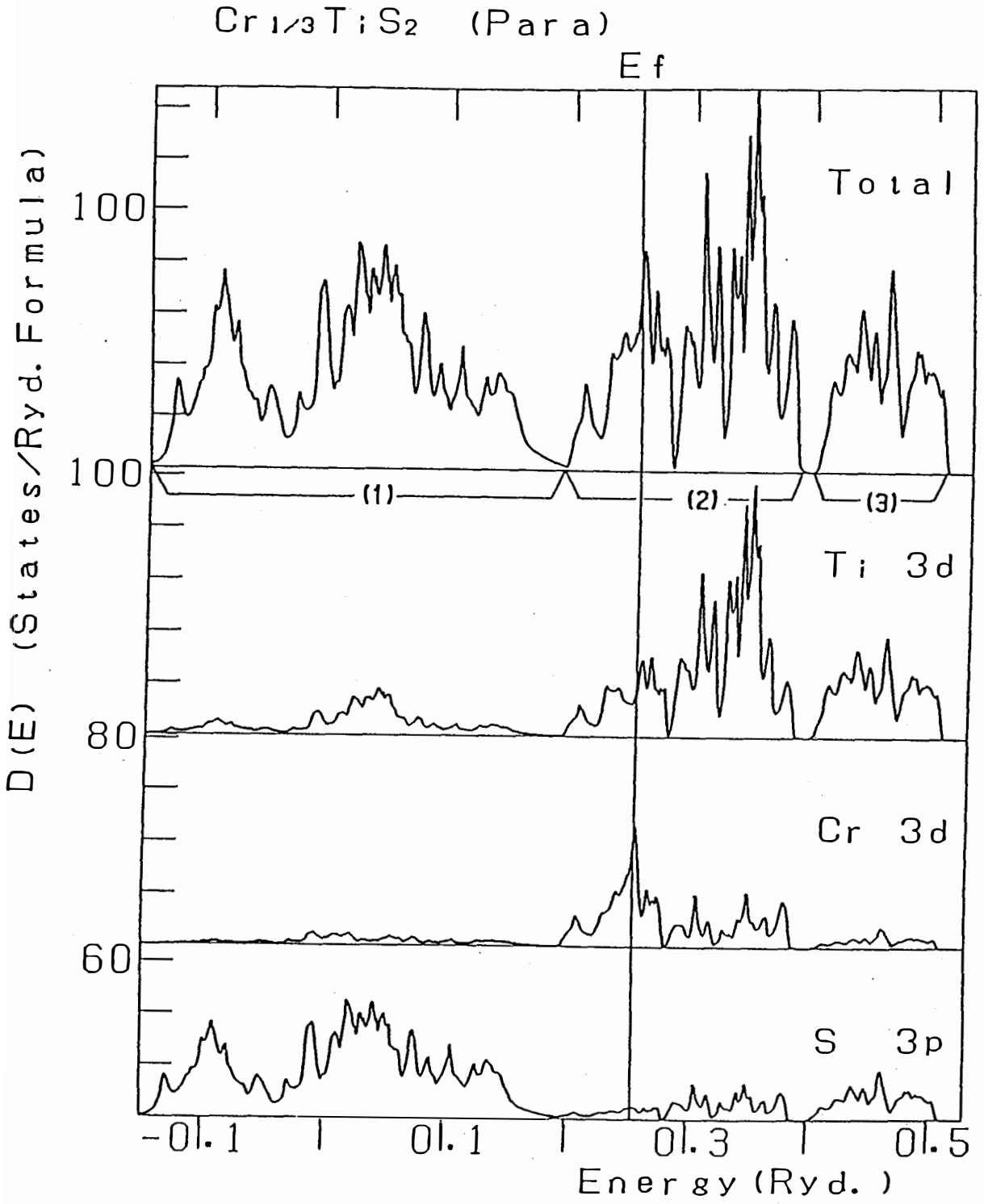

Fig. 3-8. The density of states of $Cr_{1/3}TiS_2$ in non-magnetic state.

3-2 Band Structures of Ferromagnetic $Cr_{1/3}TiS_2$ and $Co_{1/3}TiS_2$

In Sec. 3-1, it has been shown that the 3d states of the guest atoms are strongly hybridized to the electronic states of the host and form a band whose width is larger than 0.1 Ryd. Hence, to discuss the magnetism of $M_{1/3}TiS_2$, where M denotes transition elements, we must treat it on the basis of itinerant picture. In this section we calculate the electronic band structures of ferromagnetic $Cr_{1/3}TiS_2$ and $Co_{1/3}TiS_2$ by the self-consistent APW method.

We have used the same values for K_{max}, ℓ_{max} and MT radii as those used for the non-magnetic calculation. The initial spin polarization has been assumed only on the site of the guest 3d elements since the correlation effect on Ti and S sites is expected to be small. The electronic configuration for up- and down-spin states and MT radii are shown in Table.3-2.

We have evaluated the magnitude of the total magnetic moment by using the total DOS. The magnetic moment on each atom has also been obtained from the respective partial DOS, by calculating the difference in the number of electrons for up- and down spin-bands inside each MT sphere. In addition, for self-consistency in the magnetic state we have introduced the criterion that the magnetic moment at each MT are stationary.

3-2-1 $Cr_{1/3}TiS_2$

The DOS for up- and down-spin bands are shown in Fig. 3-9

together with the partial DOS. Splitting between up- and down-spin states occurs mainly in the Cr-3d bands. Due to the exchange splitting the DOS at the Fermi level, $\rho(E_F)$= 39.1 states/(Ryd·Formula), is significantly reduced compared with that of the non-magnetic state 70.9 states/(Ryd·Formula). Both the up- and down-spin states are well hybridized to the host. The down-spin band of Cr-3d has a larger width than that of the up-spin band, because exchange splitting raises the energy levels of the down spin states toward the enegy levels of the Ti-3d states and it brings about the large hybridization to the non-bonding and anti-bonding bands of the host. Thus the gap between the non-bonding and anti-bonding bands vanishes.

It should be mentioned that the hybridization nature of the Cr-3d states is different for up- and down-spin states. Since the shape of density of states is quite different for up- and down-spin bands, the exchange spin splitting is not described by a rigid splitting of the non-magnetic band.

The total magnetic moment per formula and partial magnetic moment within each MT sphere are summarized in Table 3-2. The magnetic moment at Cr site is 2.60μ_B, which is the largest value among the intercalation compounds of 3d-elements. As shown in Sec.3-1, the total DOS at the Fermi level of $Cr_{1/3}TiS_2$ in the non-magnetic band is large, and the peak of the partial DOS of Cr-3d states was located at the energy very close to E_F (see Fig.3-8). This significant contiribution of Cr-3d at E_F will cause the large magnetic moment. The magnitude of the total moment, 2.9

μ_B, is about four times larger than the experimental value 0.73 μ_B.[7)]

3-2-2 $Co_{1/3}TiS_2$

The calculated DOS is shown in Fig.3-10. The exchange splitting between the up- and down-spin bands is about 0.05 Ryd. For both spin states the electrons occupy the states below the energy level higher than that of the peak of the Co-3d partial DOS. The hybridization of the down-spin state of Co-3d with Ti-3d is larger than that of the up-spin state. This causes a difference in the number of up- and down-spin states below E_F. The obtained total magnetic moment per formula is 0.79 μ_B. This is comparable to the experimental value, 0.5 μ_B, determined by the measurement of high-field magnetizaion.[7)] Such a small magnetic moment cannot be explained in the localized picture. The magnetic moment of $Co_{1/3}TiS_2$ is much smaller compared with that of $Cr_{1/3}TiS_2$ or $Fe_{1/3}TiS_2$. The DOS at the Fermi level of $Co_{1/3}TiS_2$ in non-magnetic state ($\rho(E_F)$=48.8 states/(Ryd·Formula)) is comparable to that of $Fe_{1/3}TiS_2$ ($\rho(E_F)$=54.6 states/(Ryd·Formula)).[31)] However the partial DOS of Co-3d states near E_F is much smaller than that of the Fe-3d states. This small contribution of the Co-3d states near E_F may be a principal reason for giving rise to a small moment. In $Ni_{1/3}TiS_2$, the energy levels of the Ni-3d states are far from E_F compared with that in $Co_{1/3}TiS_2$. Thus the total $\rho(E_F)$ and the contribution of Ni-3d states to $\rho(E_F)$ are much smaller. Indeed,

$Ni_{1/3}TiS_2$ is non-magnetic. Such tendency is also found in $V_{1/3}TiS_2$ and $Ti_{1/3}TiS_2$, namely the energy levels of the 3d-states of V and Ti are much higher than E_F, thus $V_{1/3}TiS_2$ and $Ti_{1/3}TiS_2$ are non-magnetic.

Table.3-2. The electronic configuration for up and down spin states and MT radii for ferromagnetic $Co_{1/3}TiS_2$ and $Cr_{1/3}TiS_2$.

		up spin state		down spin state	
$Co_{1/3}TiS_2$	Co	$[Ar](3d)^5(4s)$	Co	$[Ar](3d)^2(4s)$	
	Ti	$[Ar](3d)(4s)$	Ti	$[Ar](3d)(4s)$	
	S	$[Ne](3s)(3p)^2$	S	$[Ne](3s)(3p)^2$	
			Co	Ti	S
		M.T. radii	0.1855	0.1850	0.2260
$Cr_{1/3}TiS_2$	Cr	$[Ar](3d)^{2.5}(4s)$	Cr	$[Ar](3d)^{1.5}(4s)$	
	Ti	$[Ar](3d)(4s)$	Ti	$[Ar](3d)(4s)$	
	S	$[Ne](3s)(3p)^2$	S	$[Ne](3s)(3p)^2$	
			Cr	Ti	S
		M.T. radii	0.1855	0.1850	0.2260

Table 3-3. The magnetic moment within each MT sphere and the total magnetic moment per formula of $M_{1/3}TiS_2$ (M=Cr, Co)in unit of μ_B.

	guest	Ti	S	total	exp.*
$Cr_{1/3}TiS_2$	2.60	0.21	-0.20	2.92	0.73
$Co_{1/3}TiS_2$	0.69	0.04	0.01	0.79	0.5

* Inoue et.al.[7)]
Negishi et.al.[6)]

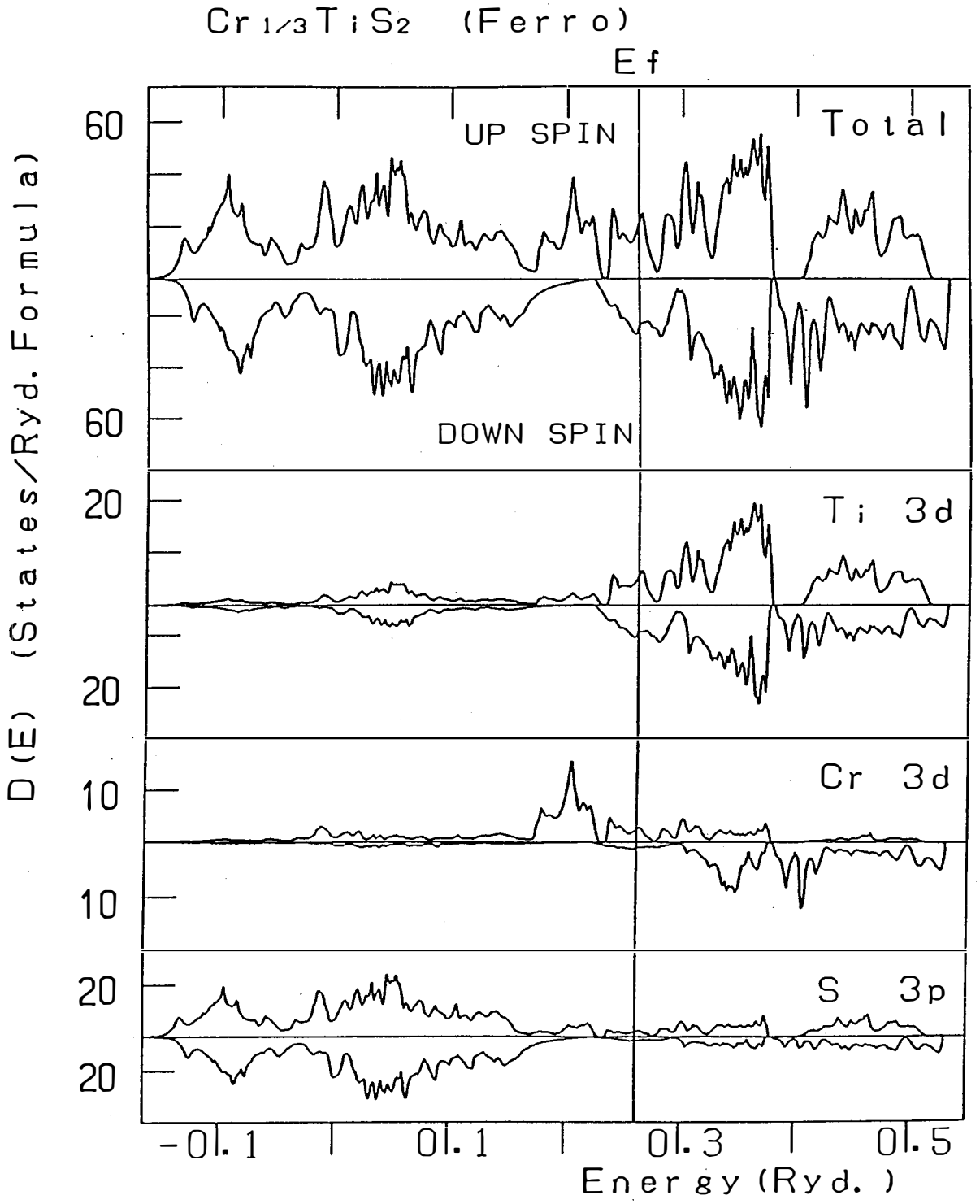

Fig. 3-9. The density of states of the ferromagentic bands of $Cr_{1/3}TiS_2$.

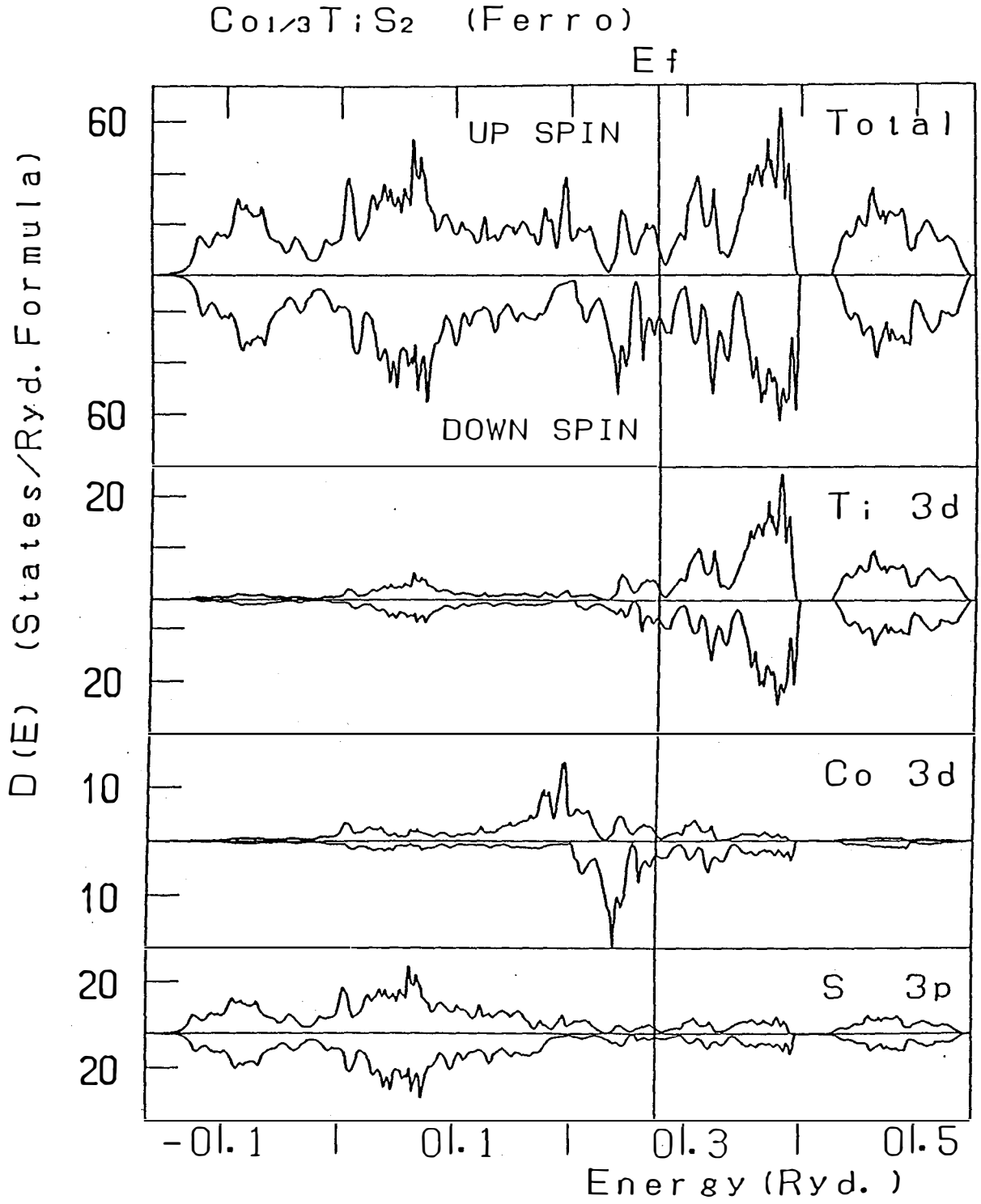

Fig. 3-10. The density of states of the ferromagnetic bands of $Co_{1/3}TiS_2$.

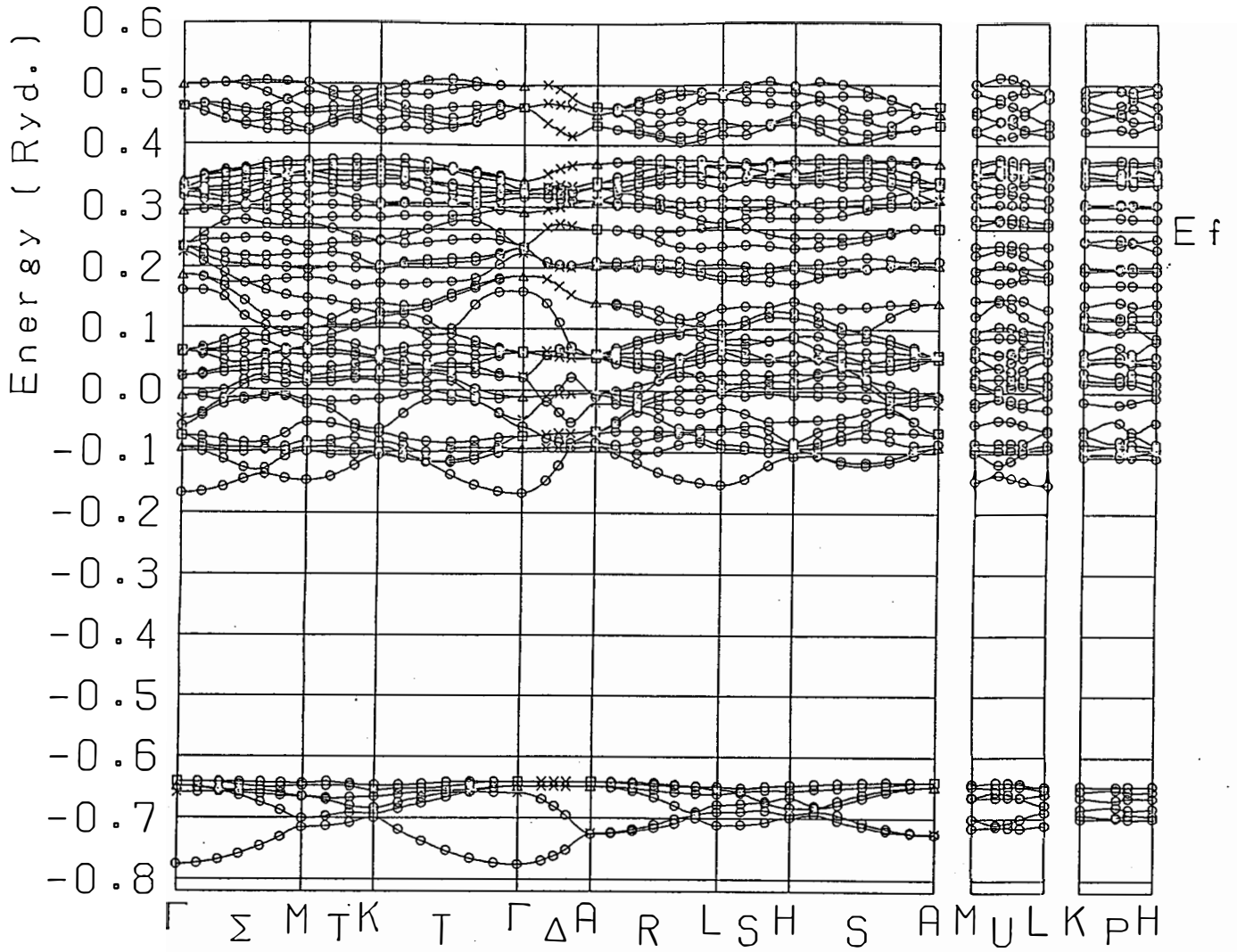

Fig. 3-11. The dispersion curves of the up-spin state of the ferromangentic $Cr_{1/3}TiS_2$

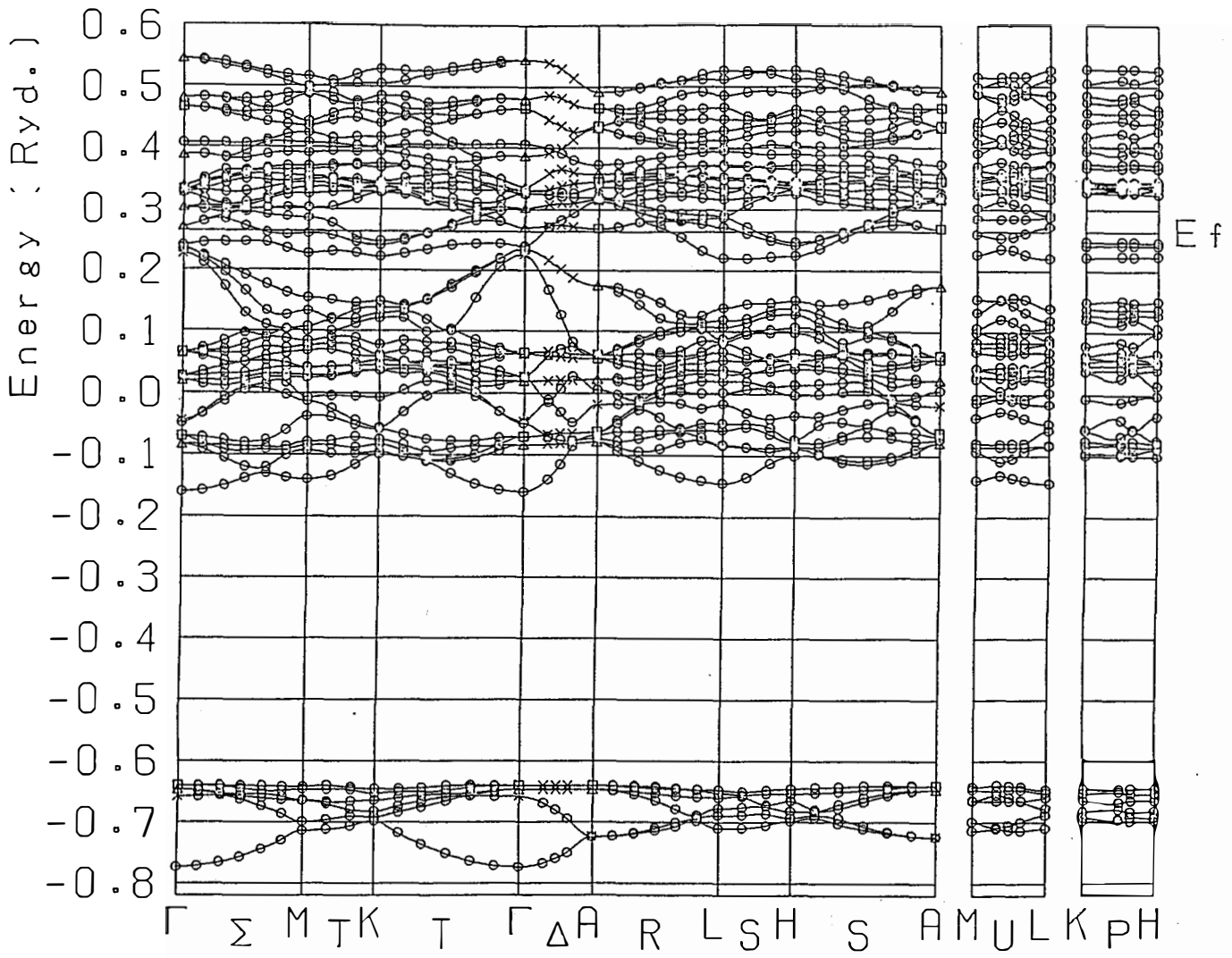

Fig. 3-12. The dispersion curves of the down-spin state of the ferromangentic $Cr_{1/3}TiS_2$

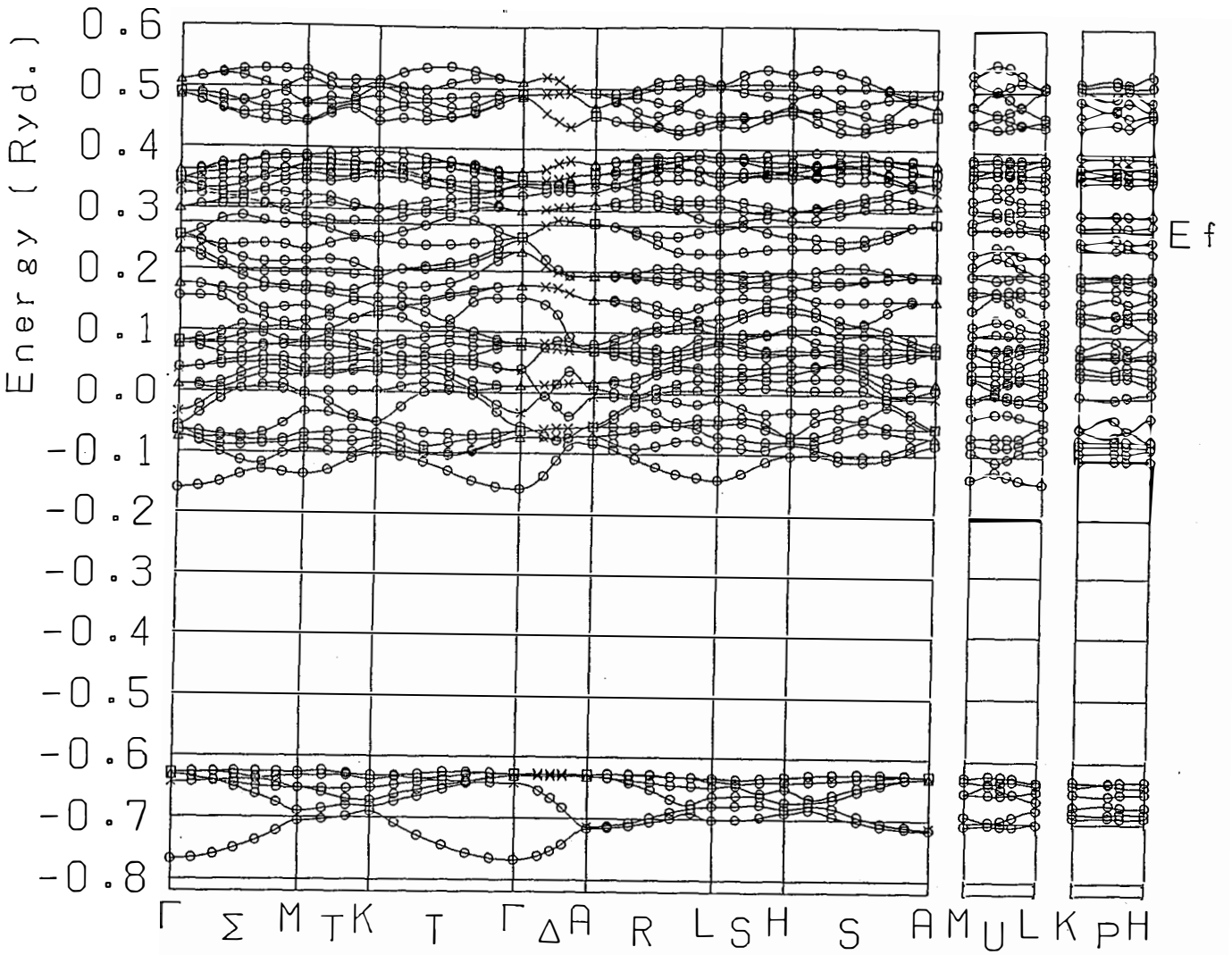

Fig. 3-13. The dispersion curves of the up-spin state of the ferromangentic $Co_{1/3}TiS_2$

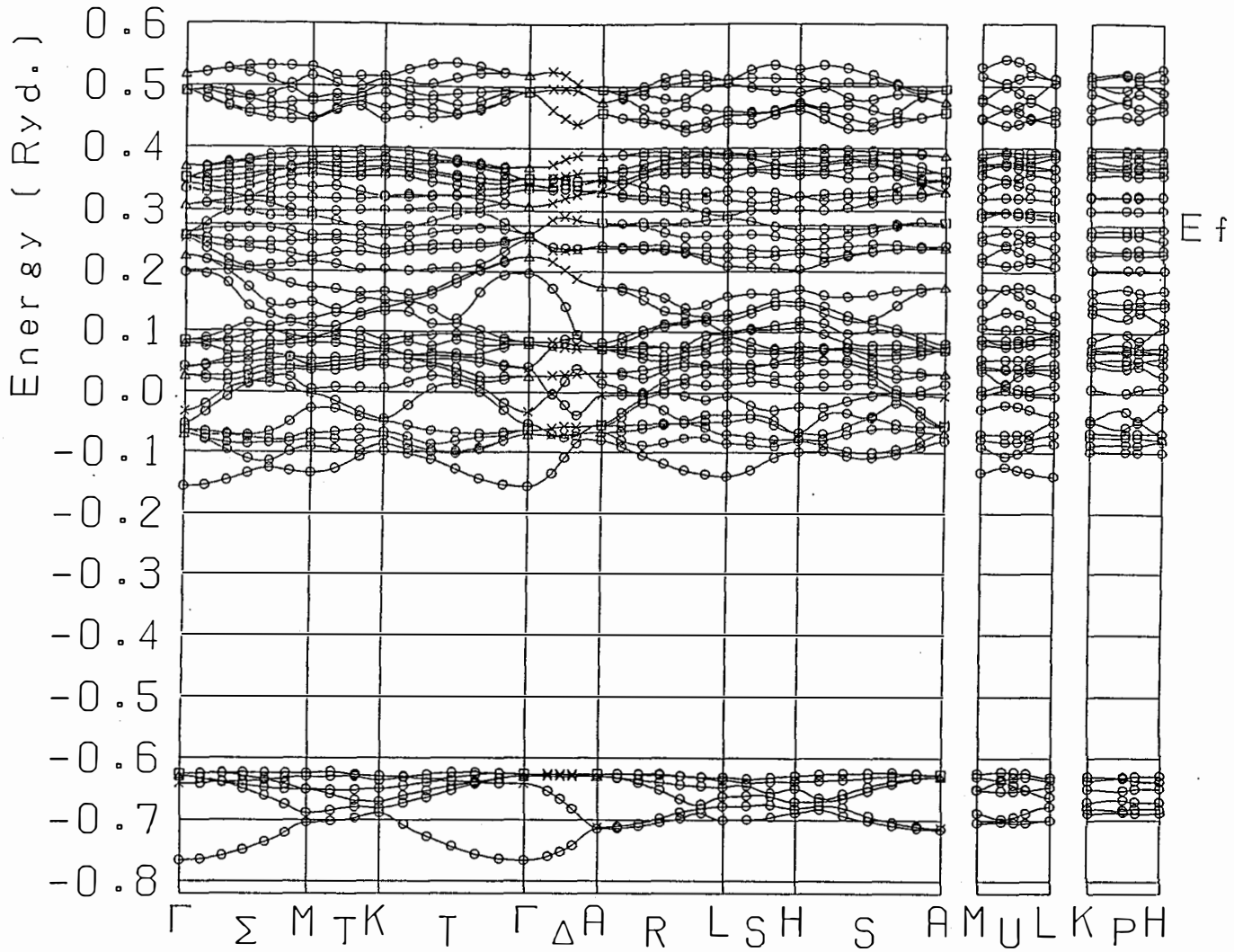

Fig. 3-14. The dispersion curves of the down-spin state of the ferromangentic $Co_{1/3}TiS_2$

3-3 Discussion

One of the physical quantities which are directly related to the DOS at the Fermi level is the electronic specific heat coefficient, γ, defined by

$$\gamma = \frac{1}{3}\pi^2 k_B^2 \rho(E_F) \qquad (3\text{-}1)$$

For the compounds of $Cr_{1/3}TiS_2$, $Fe_{1/3}TiS_2$, $Co_{1/3}TiS_2$ which become ferromagnet at low temperatures, we have evaluated the value of γ by using the value of $\rho_\uparrow(E_F)+\rho_\downarrow(E_F)$ for $\rho(E_F)$ in eq.(3-1). Inoue et.al.[8] have measured the specific heat C of the intercalation compounds having 3d transition elements as guest atoms. In their results, C/T is propotional to T^2 in high and medium temperature range, and to $-\ell nT$ in low temperature range below about 5K. Extrapolating the specific heat curve above 5K to 0K, they have evaluated the value of γ.

In Table 3-4 and Fig. 3-15, the theoretical values of γ are shown together with the experimental values. The partial DOS of guest 3d-states has a large contribution to the total DOS, then the relative position of E_F and the energy level of the guest 3d-states affects the value of γ. In $Ti_{1/3}TiS_2$ and $Ni_{1/3}TiS_2$ the value of γ is small because the levels of the guest 3d-states are much higher or lower than the Fermi level. The highest point of the γ curve shown in Fig. 3-15 is found for $Mn_{1/3}TiS_2$ which is a paramagnet. On the other hand, for the ferromagnetic Cr-, Fe-,

and Co-compounds the exchange splitting reduces the contributions of the guest 3d-states to $\rho(E_F)$, although the contributions are not small in the non-magnetic state, especially in Cr (see Fig.3-8) The absence of magnetism permits the large value of γ in $Mn_{1/3}TiS_2$.

The dependence of γ on the species of guest, i.e. the relative magnitude of γ among different $M_{1/3}TiS_2$ compounds is well explained by our band calculation, although the calculated values of γ are 5 or 8 times smaller than the experimental ones. This difference will be attributed to the effective mass enhancement indueced by the electron-electron correlation effect and/or the electron-phonon interaction. Here it should be noted that the value of γ obtained by the rigid band model is much smaller compared with that obtained by the present band calculation. Furthermore the dependence upon the sort of the guest atoms as mentioned above can not be reproduced by the rigid band model. Therefore we can say that the results of specific heat measurements indicate clearly the inapplicability of the rigid band model and suggest modification of the electronic band structure of the mother crystal due to the intercalation.

As mentioned in Sec.3-2. the band calculation for ferromagnetic $Cr_{1/3}TiS_2$ predicts a magnetic moment much larger than the experimental value. This fact may indicate that spin fluctuation effects are important even at T=0 K in $Cr_{1/3}TiS_2$. The zero-point spin fluctuation may play an important role also in $Mn_{1/3}TiS_2$ because this compound does not show any magnetic ordering in spite of its large value of $\rho(E_F)$.

Table 3-4. The density of states at the Fermi level, $\rho(E_F)$, and the electronic specific heat coefficient γ. For ferromagentic Cr-, Fe- and Co-compounds the value of $\rho(E_F)$ is taken as $\rho_{\uparrow}(E_F)+\rho_{\downarrow}(E_F)$.

guest	$\rho(E_F)$	γ [mJ/mol k^2]	γ (exp)*
Ti	35.9	6.2	--
V	41.1	7.1	50
Cr	39.1	6.8	70
Mn	63.8**	11	90
Fe	34.7**	6.0	30
Co	25.8	4.5	30
Ni	9.4**	1.6	10

* Inoue et.al.[8] (1986)
Negishi et.al.[6] (1987)
** Yamasaki et.al.[28)-31)] (1988)

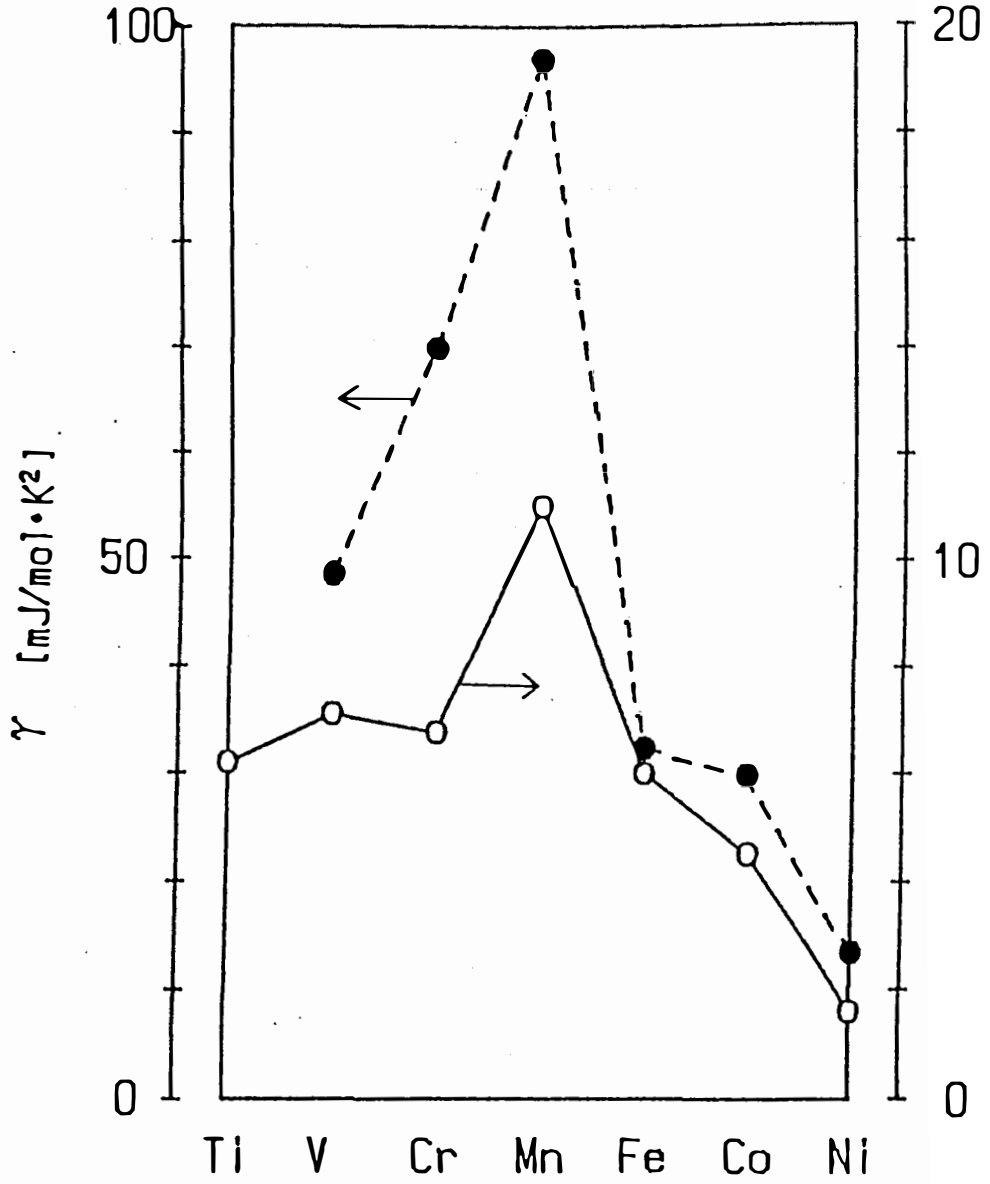

Fig. 3-15. The electronic specific heat coefficient γ of $M_{1/3}TiS_2$ (M=Ti, V, Cr, Mn, Fe, Co and Ni). The open circles denote the theoretical values evaluated from the band calculations and the closed circles the experimental values obtained by Inoue et al. The scale is different for the theoretical values (right) and for the experimental values (left).

§4. Electronic Structures of Noble-Metal and Alkali-Metal Intercalation Compounds

Electronic band structures of ordered silver intercalation compound, $Ag_{1/3}TiS_2$, and alkali-metal intercalation compounds, $K_{1/3}TiS_2$ and $Li_{1/3}TiS_2$, are calculated by using the self-consistent linearized APW (LAPW) method. The muffin-tin approximation and local density approximation by Gunnarsson and Lundqvist have been used. In order to compare the obtained results directly with the electronic structures of $M_{1/3}TiS_2$ (M=transition metal) in which M atom layers stack as ABCABC···, the band calculations have been carried out for the hypothetical ABC-stacking $Ag_{1/3}TiS_2$ as well as for the first-stage AB-stacking $Ag_{1/3}TiS_2$. The crystal structure of the AB-stacking is shown in Fig. 4-1. The space group of the first stage $Ag_{1/3}TiS_2$ is D_{3d} whose generators are I, $\{C_2^y|(0,0,1/2)\}$ and C_3, the unit call contains twenty atoms in total, i.e. two Ag, six Ti and twelve S atoms while the space group of ABC-stacking $Ag_{1/3}TiS_2$ is C_{3i} and the primitive unit cell contains one Ag, three Ti and six S atoms. In the band calculations of $Li_{1/3}TiS_2$ and $K_{1/3}TiS_2$, the crystal structure of the ABC-stacking is assumed.

Table.4-1. The lattice constats, MT radii and electronic configurations for $Ag_{1/3}TiS_2$, $Li_{1/3}TiS_2$ and $K_{1/3}TiS_2$.

lattice constant [19,24-26]		a	c
$Ag_{1/3}TiS_2$	(AB)	5.917	12.572
$Ag_{1/3}TiS_2$	(ABC)	5.917	18.858
$Li_{1/3}TiS_2$		5.934	17.584
$K_{1/3}TiS_2$		6.036	17.952

(unit in Å)

M.T. radii		Ag	Ti	S
$Ag_{1/3}TiS_2$	(AB)	0.2208	0.1904	0.2210
$Ag_{1/3}TiS_2$	(ABC)	0.2100	0.1800	0.2300
$Li_{1/3}TiS_2$		0.2220	0.2220	0.1900
$K_{1/3}TiS_2$		0.2300	0.1730	0.2300

(unit in a)

electronic configuration

$Ag_{1/3}TiS_2$	Ag	$[Kr](4d)^{10}(5s)$
$Li_{1/3}TiS_2$	Li	[He](2s)
$K_{1/3}TiS_2$	K	$[Ne(3s)^2](3p)^6(3d)^0(4s)$

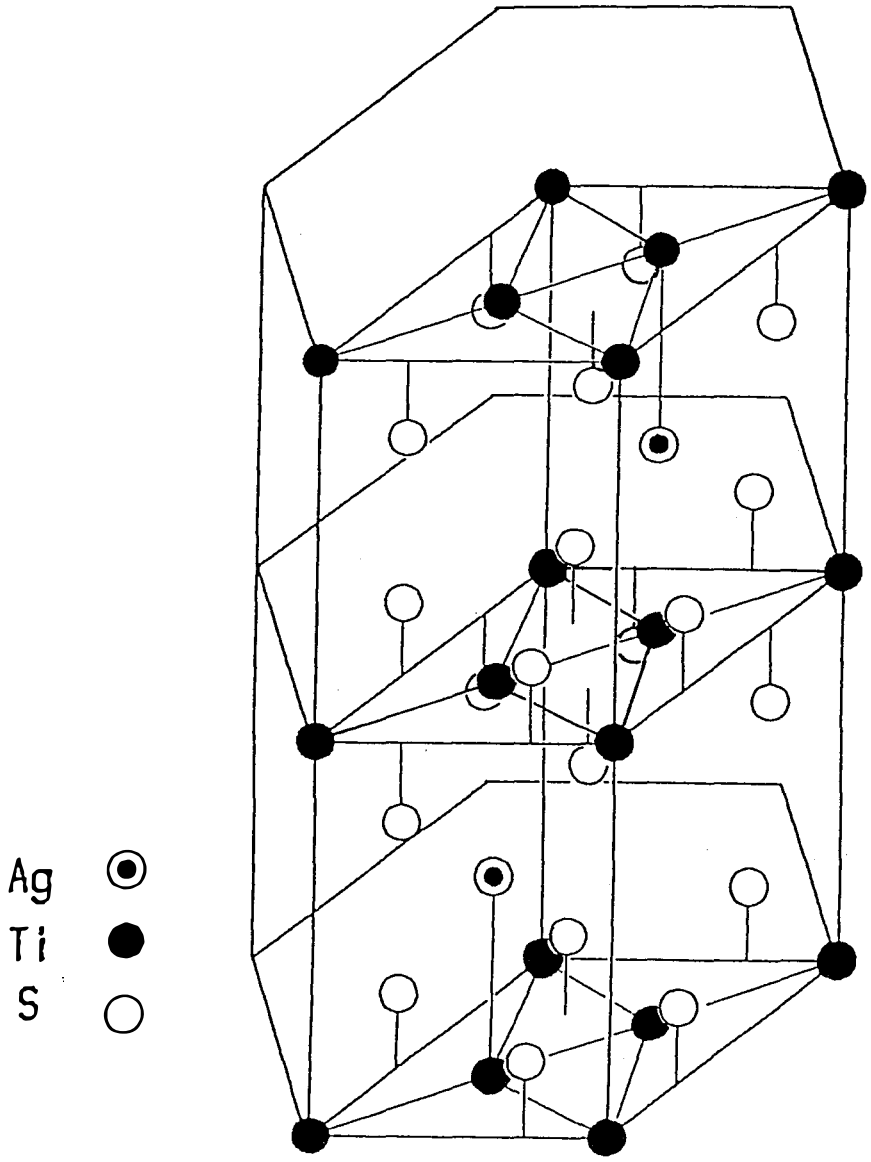

Fig. 4-1. The crystal structure of $Ag_{1/3}TiS_2$ with AB-stacking.

4-1 Noble-Metal Intercalation Compound $Ag_{1/3}TiS_2$

For AB- and ABC-stacking, the electronic configuration ,the lattice constants and MT radii are summarized in Table.4-1. The value of K_{max} is $4.5\times(2\pi/a)$ for AB-stacking and $4.1\times(2\pi/a)$ for ABC-stacking. The value of $\ell_{max}=7$ has been used for both kinds of stacking.

The dispersion curves along the symmetry lines are shown in Fig. 4-2 and Fig. 4-3 for AB- and ABC-stacking, respectively. The lower 12 (AB-stacking) and 6 (ABC-stacking) bands consist mainly of 3p states of sulfur. Above the energy gap, the mixing bands among Ag-4d, Ti-3d and S-3p have a width of about 0.6 Ryd for both AB- and ABC-stacking.

The densities of states of the mixing bands obtained for AB- and ABC-stacking are shown in Fig. 4-4 and Fig. 4-5, respectively. Overall feature of the DOS resembles each other. Since the number of bands in AB-stacking is two times larger than that in ABC-stacking, the peak of the non-bonding bands are shrunk in the case of AB-stacking and the DOS curve is more spiny. Comparing the DOS of the compounds of Ag with that of 3d-elements the most striking aspect is the Ag-4d band, i.e. it hybridizes strongly and overlaps energetically with S-3p bands. The width of the guest-4d band of the intercalation compound of Ag is larger than those of all $M_{1/3}TiS_2$ (M = 3d transition elements). This feature is consistent with the tendency that the guest-d states are hybridized with S-3p rather than Ti-3d when the guest belongs to the transition metal group of right hand

side in the periodic table, for example in the compound of $Ni_{1/3}TiS_2$. Now it should be noted that in the Ag intercalation compound the hybridization between the guest-4d and Ti-3d is remarkably small in contrast with the transition-metal intercalation compounds in which the guest-3d states hybridize fairly well with the Ti-3d states. In addition the mixing between Ti-3d and S-3p is reduced because of the large hybridization between Ag-4d and S-3p. As the result the bonding between Ti and S of the host is weakened by intercalation of Ag. Note that the large hybridizaion between Ag and S is not favorable for energy gain because almost all the mixing states are occupied. On the other hand the mixing bands which consist of guest-3d, Ti-3d and S-3p are occupied partially for the compounds of 3d-elements; for example $Cr_{1/3}TiS_2$(Fig.3-8). The energy gain is, therefore, large in the case of intercalation of 3d-elements. These features of the electronic structure seem to be related to the experimental results that the Ag atoms can not be intercalated more than $x=0.42$ [17] and also that the Ag atoms show the order-disorder transition in the interstitial layer at finite temperature.

Next, we have calculated the total enegy both for AB- and ABC-stacking to discuss which stacking is more favorable. The obtained result will be presented in §5. Furthermore the comparison of the total energies of the intercalation compounds of 3d-elements, alkali-metal and Ag will be made also in §5.

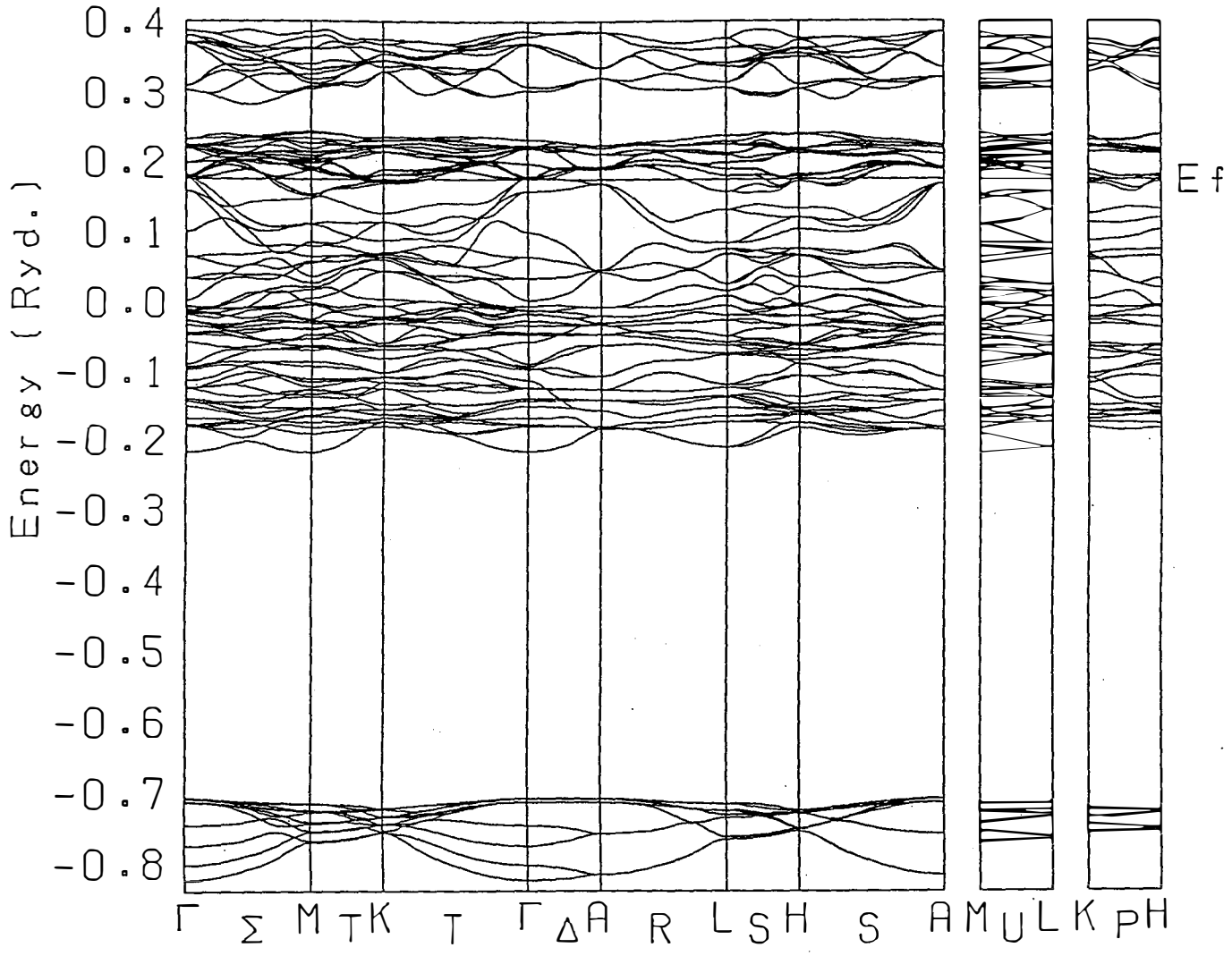

Fig. 4-2. The dispersion curves of $Ag_{1/3}TiS_2$ (AB-stacking).

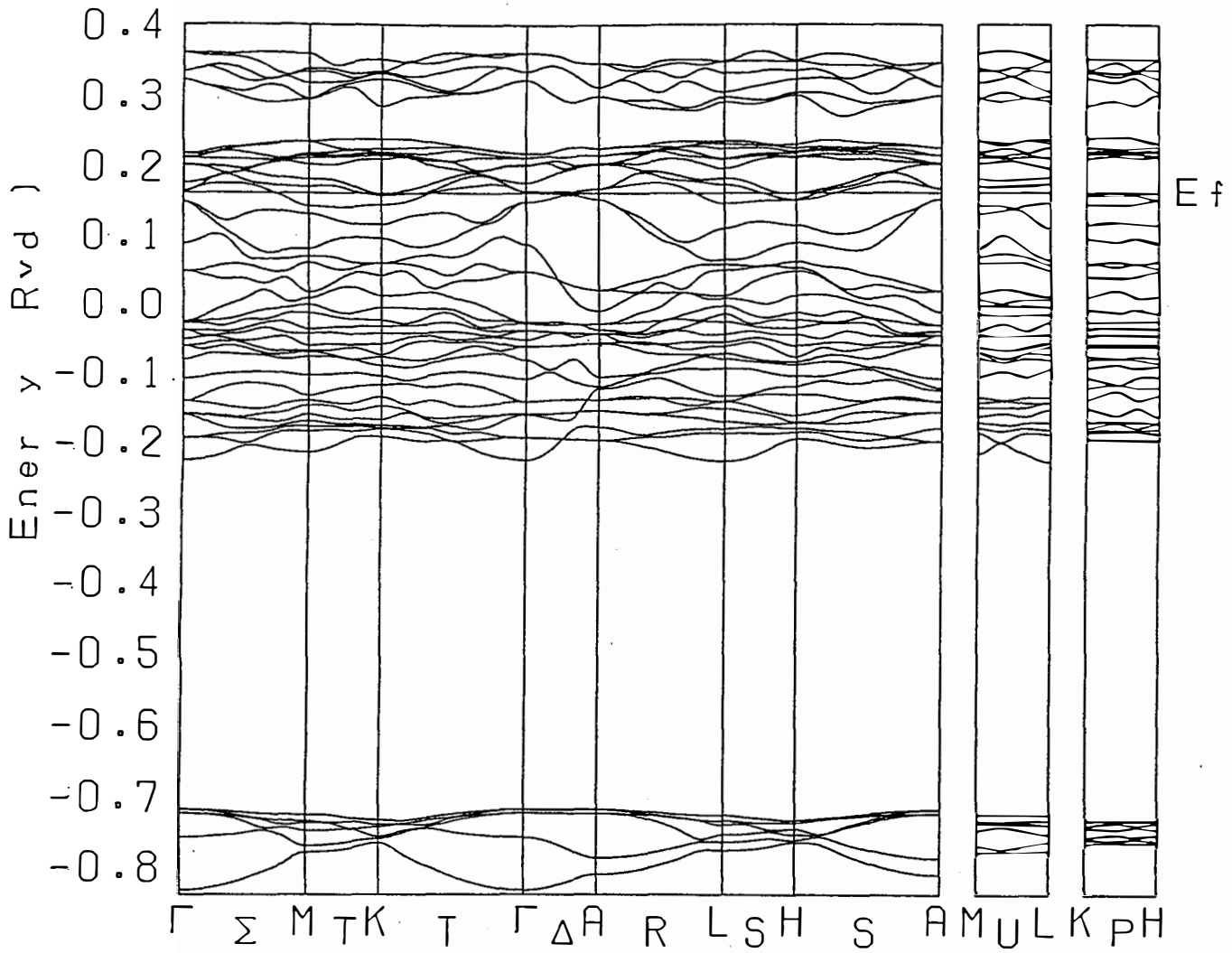

Fig. 4-3. The dispersion curves of $Ag_{1/3}TiS_2$ (ABC-stacking).

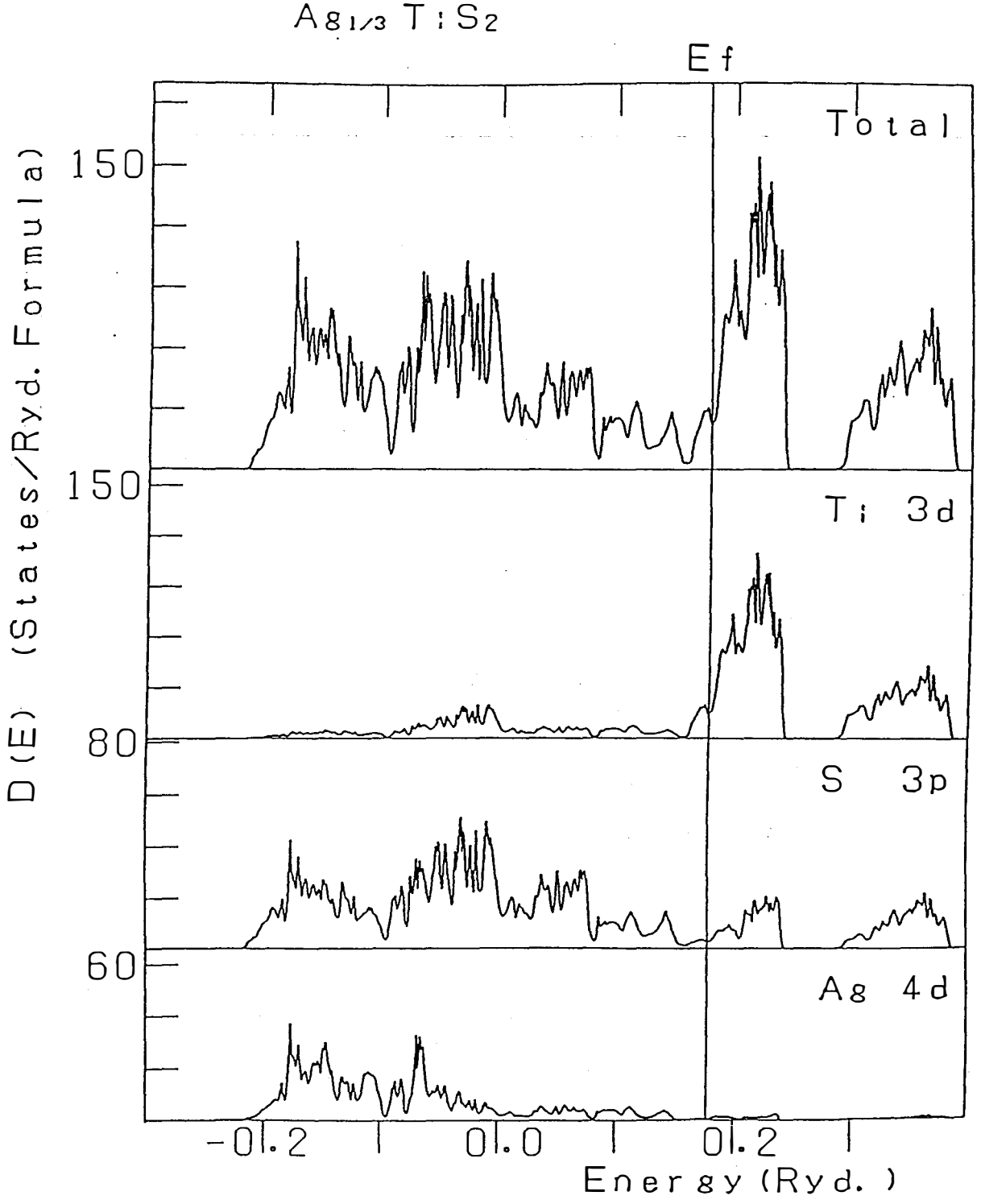

Fig. 4-4. The density of states of $Ag_{1/3}TiS_2$ (AB-stacking).

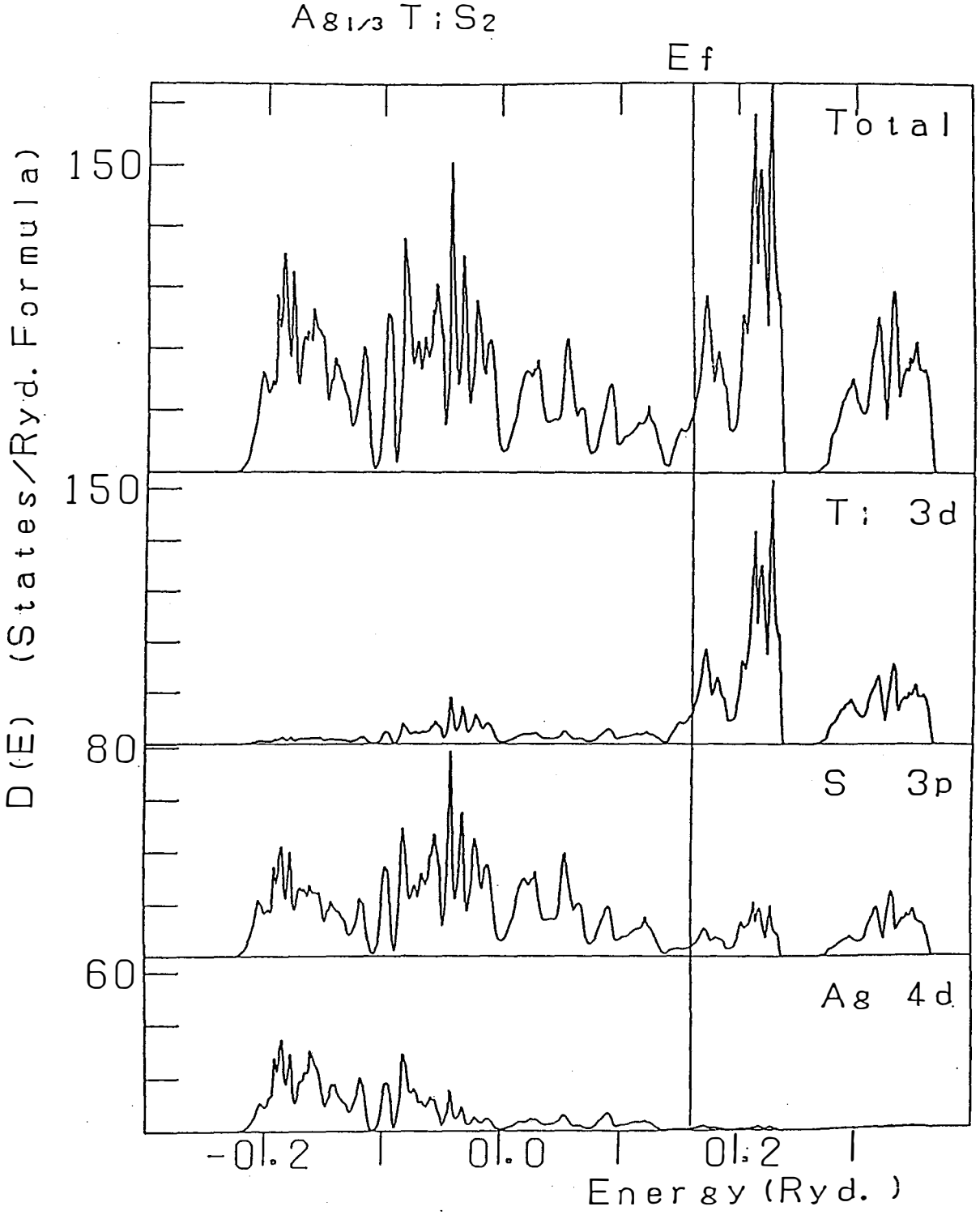

Fig. 4-5. The density of states of $Ag_{1/3}TiS_2$ (ABC-stacking).

4-2 Alkali Metal Intercalation Compounds, $Li_{1/3}TiS_2$ and $K_{1/3}TiS_2$

In our calculation for $Li_{1/3}TiS_2$ and $K_{1/3}TiS_2$, it has been assumed that the stacking along the c-axis is ABC. The space group for these compounds is C_{3i}. The K_{max} is taken to be $4.4\times(2\pi/a)$, and thus the number of basis function is about 470 for both $Li_{1/3}TiS_2$ and $K_{1/3}TiS_2$. The electronic configurations, the lattice constans and MT radii are summarized in Table.4-1.

4-2-1 $Li_{1/3}TiS_2$

The dispersion curves along the symmetry lines are shown in Fig.4-6. The lowest 6 bands consist mainly of S-3s states. The higher energy 38 bands are mixing bands which consist mainly of Ti-3d, S-3p states. The overall feature of the dispersion curves resembles to those of $M_{1/3}TiS_2$ (M = 3d transition element).

The density of states for the mixing bands are shown in Fig.4-7 together with the partial DOS. As seen in the figure, it is clear that the small hybridization of the guest with the host distinguishes $Li_{1/3}TiS_2$ from $M_{1/3}TiS_2$ (M = 3d transition elements) or $Ag_{1/3}TiS_2$, although the dispersion curves of $Li_{1/3}TiS_2$ are similar to both systems. Thus the bonding of Li atoms with the host is weak, and it may correspond to the experimental result that the Li atoms can move in interstitial layers. The shape of DOS of $Li_{1/3}TiS_2$ is similar to that of the host-TiS_2. Small difference between $Li_{1/3}TiS_2$ and TiS_2 should be derived mainly from the effect of folding due to intercalation. As the

unit cell is enlarged 3 times of original volume because of intercalation, the curve of DOS of $Li_{1/3}TiS_2$ is more spiny compared with that of the host and the peaks of DOS are somewhat broadened in $Li_{1/3}TiS_2$. The Fermi level is shifted toward higher energy side compared with TiS_2. For the electronic structure of $Li_{1/3}TiS_2$, therefore, we can say that the rigid band model is applicable; the guest atoms provide the electrons to the host without modifications of varying the electonic structure of the host. For $LiTiS_2$, the ASW (Augumented Spherical Wave) band calculation has been done by Dijkstra et.al.[23] The obtained results are similar to our results.

4-2-2 $K_{1/3}TiS_2$

The dispersion curves are shown in Fig. 4-8. The lowest 6 bands consist mainly of S-3s states and the others are the mixing bands of Ti-3d, S-3p and K-3p states. The gross features of the dispersion curves of $K_{1/3}TiS_2$ resemble those of $Li_{1/3}TiS_2$, except the 3 bands lying around -0.15 Ryd with small dispersion (about 0.05 Ryd.)

The density of states of the mixing bands are given in Fig. 4-9. As seen in the figures the lowest 3 bands among the mixing bands consist mainly of K-3p states and there are certain admixture of S-3p states. The bands which consist of inner p-states of the guest is not found in the mixing bands of $Li_{1/3}TiS_2$ or $NaTiS_2$ (Dijkstra et.al.). For Li, obviously, there is no p-symmetric orbits of the guests. As for $NaTiS_2$, an

absence of p-states in the mixing bands may be attributed to the deep energy levels of Na-2p orbits compared to K-3p orbits: the energy difference between Na-3s and Na-2p orbits is 2.26 Ryd for free atomic sodium, while the energy difference between K-4s and K-3p orbits is 1.43 Ryd. The above discussion may also be applicable for $Na_{1/3}TiS_2$. Thus the shallow p-states of $K_{1/3}TiS_2$ are distinctive character for the intercalation compounds of alkali metal. The 3p-bands of sodium raise the energies of the bonding- and non-bonding bands of the host toward higher energy side, then the gap between non-banding and anti-bonding bands is reduced. The density of states at E_F increases because bonding- and anti-bonding bands are approached each other.

gap between Ti-3dε and Ti-3dγ (Ryd.)

TiS_2	0.09
$Li_{1/3}TiS_2$	0.08
$LiTiS_2$	0.02 [23]
$NaTiS_2$	0.02 [23]
$K_{1/3}TiS_2$	0.06

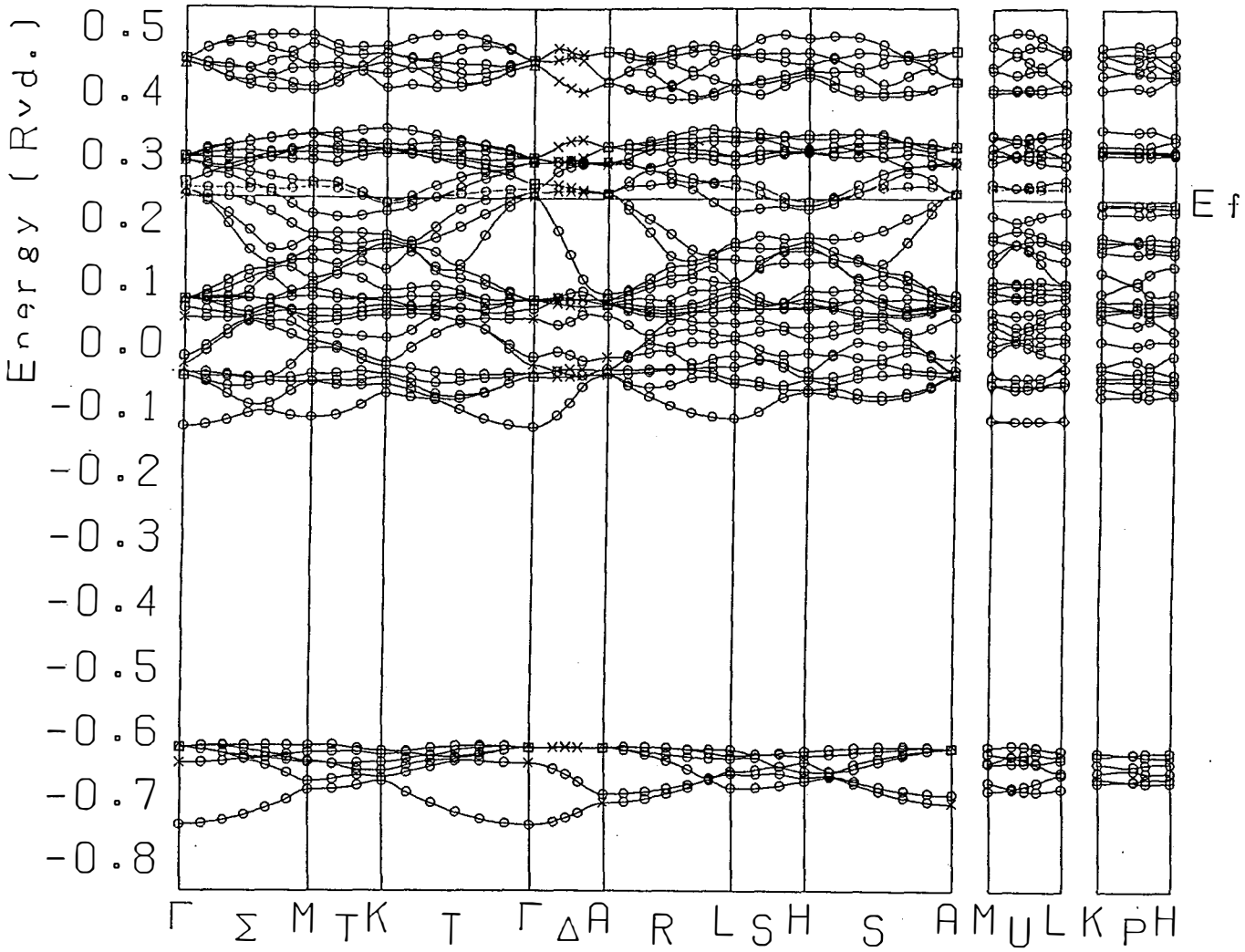

Fig. 4-6. The dispersion curves of $Li_{1/3}TiS_2$.

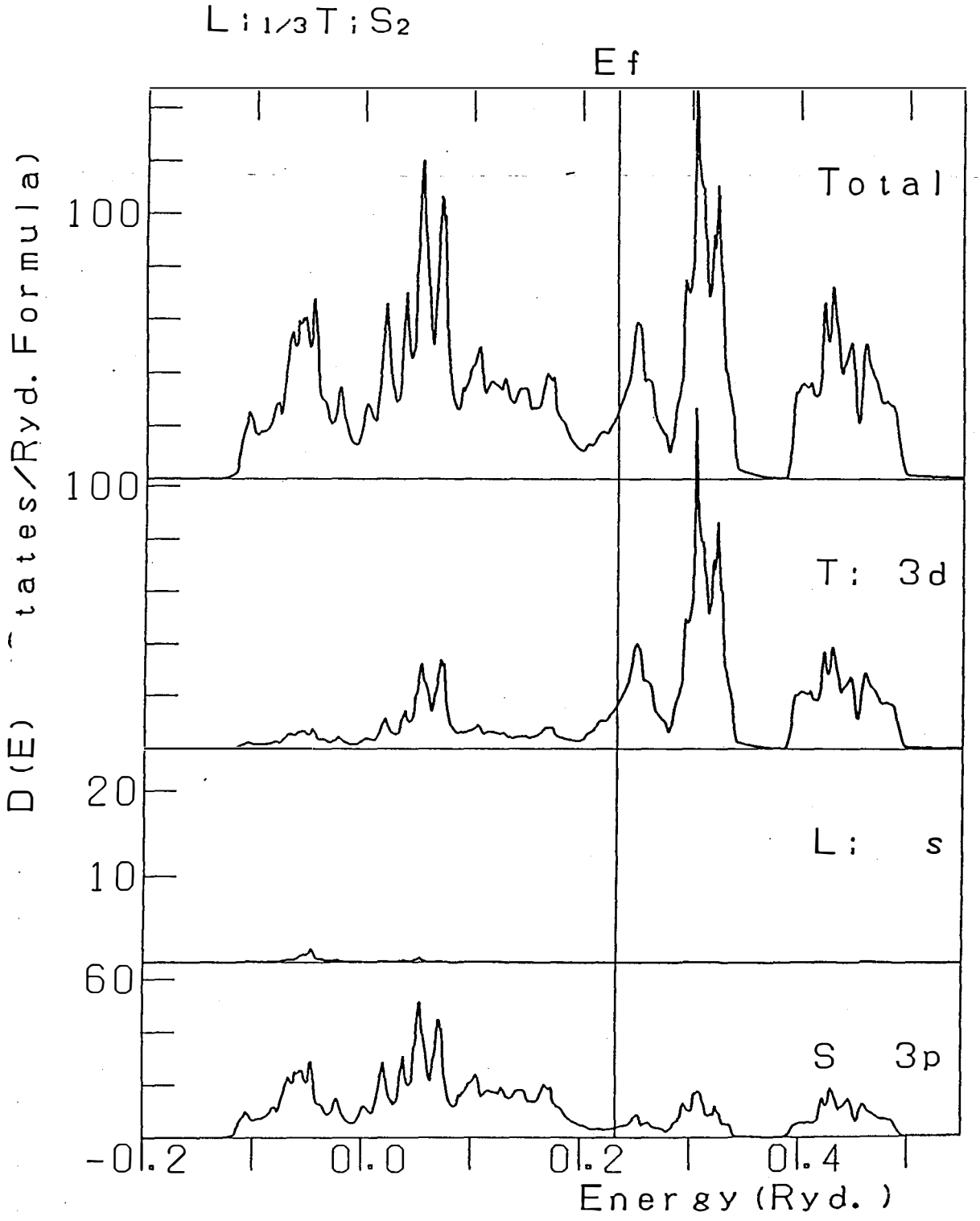

Fig. 4-7. The density of states of $Li_{1/3}TiS_2$.

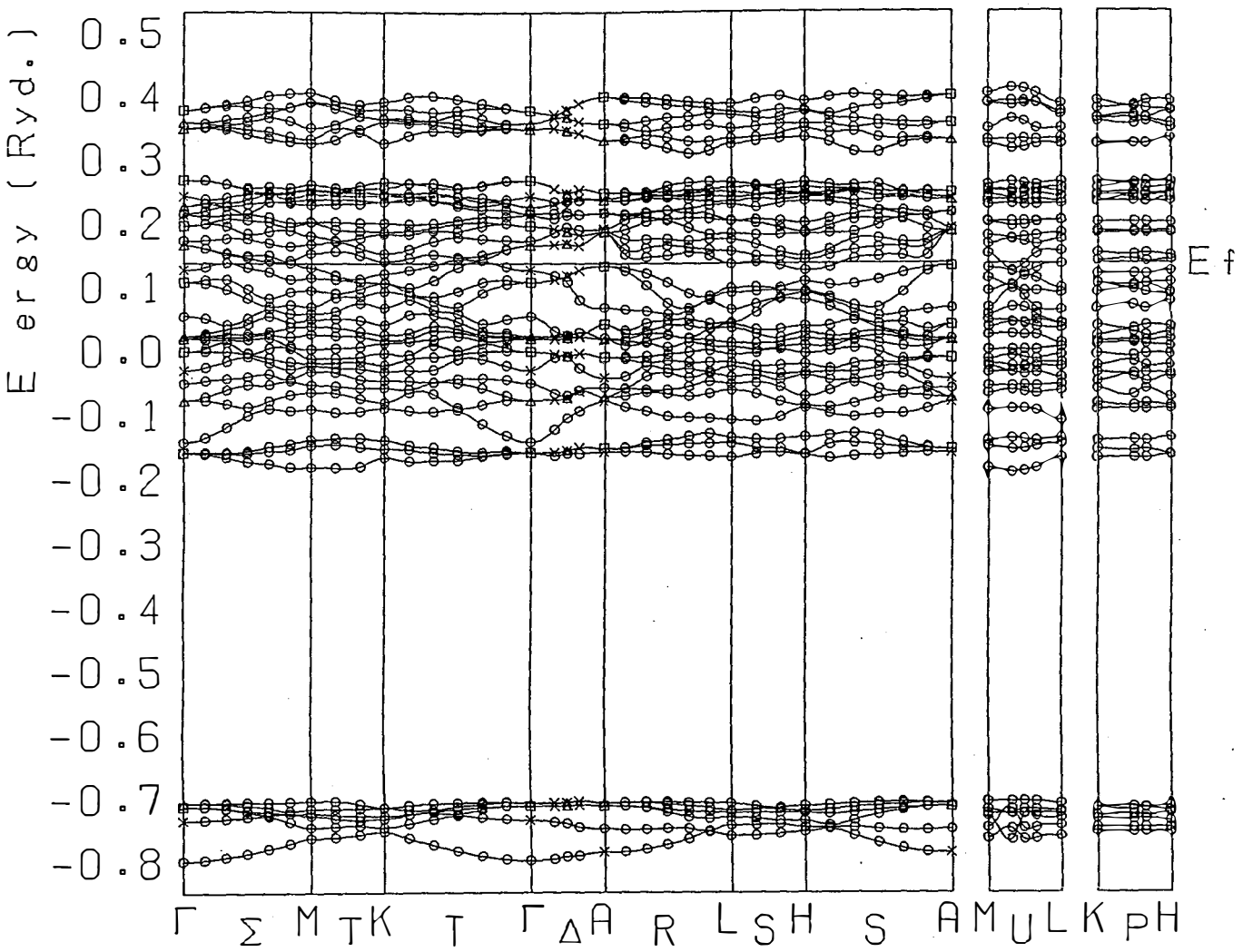

Fig. 4-8. The dispersion curves of $K_{1/3}TiS_2$.

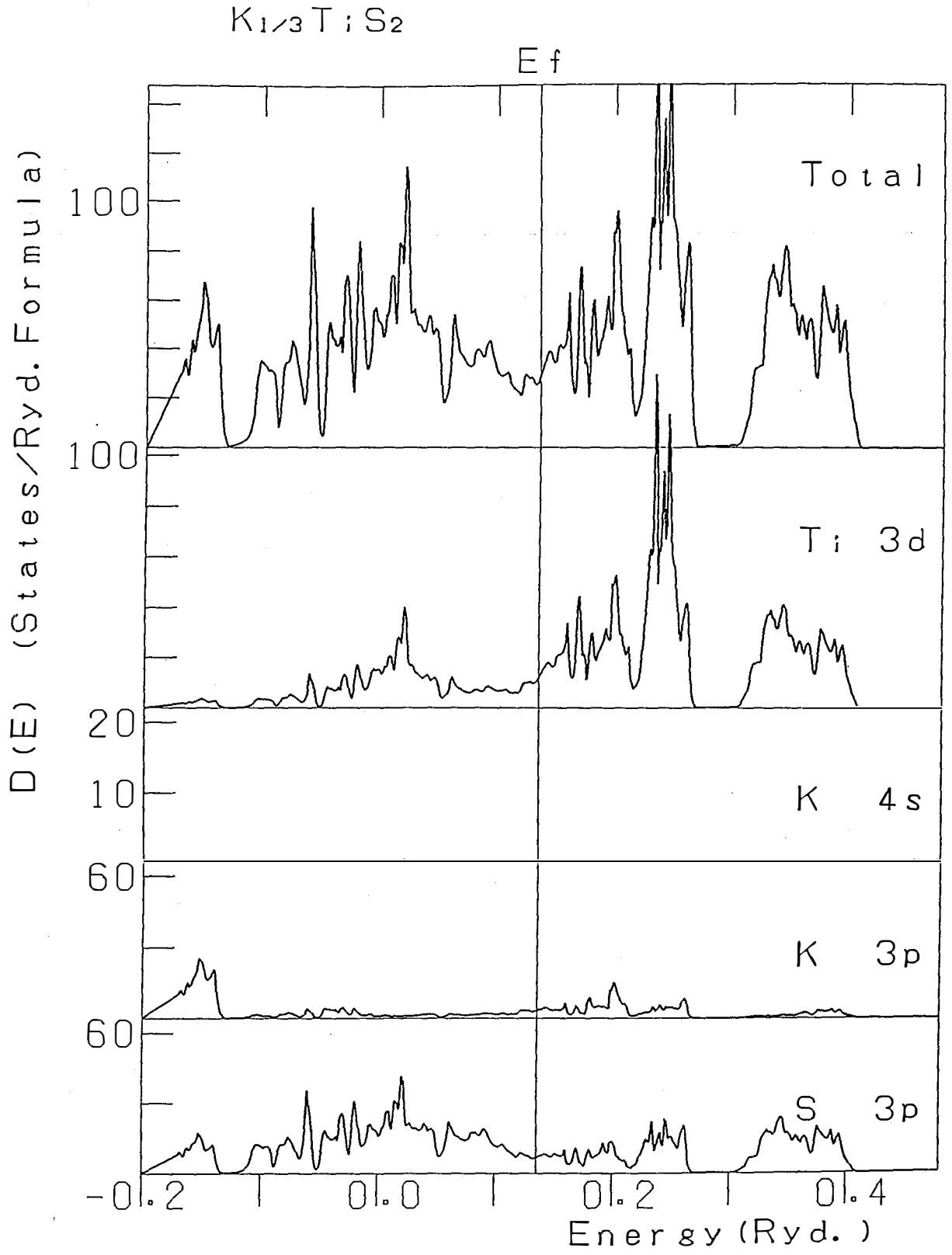

Fig. 4-9. The density of states of $K_{1/3}TiS_2$.

§5. Total Energy

In the preceding sections we have shown the obtained band strutures and discussed the differences between intercalation compounds of 3d transition metal intercalates, Ag intercalates and alkali-metal intercalates. For the strength of bonding between the host and the guest, only the qualitative discussion has been given. In this section we will show the results of total energy calculation in order to give the quantitative discussion for different bonding natures among the three kinds of intercalates.

5-1 Practical aspect for calculation

We have assumed that the sandwiches are rigid, in other words the intercalation causes only the displacement of the inter-sandwich distance without changing the atomic structure within a sandwich. We set the lattice parameters to the experimental values. Although the optimization of total energy as regard to the position of the host-Ti and -S has not been done, it should be noted that the energy variation in the optimization for the local displacement of the lattice is often in the order of several mRyd for a few percent of the displacement. In our calculations we have used the MT approximation for the crystal potential. In bcc or fcc iron, the difference between the total energy obtained by MT approximation and that obtained by

including warping correction is usually the order of 10 mRyd. (Terakura). If we use full potential instead of MT potential, the extra correction for the total energy is the order of one mRyd in metallic iron. Hence the approximation that we have used will not change principal result, since we will discuss the energy difference of the order of 0.1 Ryd.

For total energy calculation we have employed the criterion of 0.001 Ryd for self-consistency. We have taken much more number of plane waves for calculating total energy than that for evaluating only DOS or dispersion relation: for $Ag_{1/3}TiS_2$ with AB-stacking about 2100 APW's have been taken, and for other compounds about 500-600 APW's. The number of k-points, which have been used in calculating the charge density in each iteration step of the self-consistent calculation, is 4 for $Ag_{1/3}TiS_2$ and 6 for other compounds. The obtained total energies are shown in Table 5-1.

We have evaluated also the cohesive energy E_{coh} which is defined as

$$E_{coh} = E_{tot}(atom) - E_{tot}(bulk) \qquad (5\text{-}1)$$

where $E_{tot}(bulk)$ denotes the total energy for the bulk of the object and $E_{tot}(atom)$ means the sum of the total energies of all atoms which construct the bulk. By calculating E_{coh} we can discuss formation property for different crystals: the large E_{coh} leads to more stability.

5-2 Result

The evaluated cohesive energies are summarized in Table 5-1 and Fig.5-1. Their magnitude is about 1 to 2 Ryd., which is reasonable order of magnitude. Since the values in Table 5-2 are those for the total energy per unit cell which contains 10 atoms, the values per atom are the order of 0.1 Ryd. Note that cohesive energy for an ionic crystal is more than 0.5 Ryd., about 0.1 to 0.4 for a covalency crystal and about 0.1 to 0.5 for a simple metal.

As clearly seen from Fig.5-2 and Table 5-1, the $Ag_{1/3}TiS_2$ with AB-stacking is more stable energetically than that with ABC-stacking. This result is consistent with the experimental result because the observed stacking of Ag atom layers along the c-direction is ABAB$\cdots$.[18] The energy difference between AB-stacking and ABC-stacking is 0.153 Ryd/[$AgTi_3S_6$].

As for the alkali-metal intercalation compounds, the cohesive energies of $Li_{1/3}TiS_2$ and $K_{1/3}TiS_2$ are comparable to each other. They are also comparable to that of $Ag_{1/3}TiS_2$ with AB-stacking. Furthermore they are considerably small compared to that of the intercalation compound of transition metal, $Fe_{1/3}TiS_2$. This result indicates that the strengh of the bonding between the guest and the host is weak for both Ag and alkali metal intercalates. Here, it should be noted that the Ag atoms have large hybridization to the host (sometimes it is larger than that of 3d- transition element) while the alkali metals have weak hybridization as shown in the preceeding section, although their

cohesive energies are comparable. This result may be explained as follows. It is obvious for intercalation compound of alkali metal that the small hybridization leads to the small energy gain. For $Ag_{1/3}TiS_2$, the hybridization between Ti and S is lessened compared with that for the host-TiS_2. This reduction is caused by the large hybridization of Ag-4d with S-3p and it brings the loss of bonding energy of the host. This energy loss cannot be compensated by the energy gain arising from the hybridization between the Ag and S atoms, since the mixing bands of Ag-4d and S- 3p are almost occupied (see Sec.3-3). Thus the small cohesive energy in $Ag_{1/3}TiS_2$ will be ascribed to the reduction of the bonding between Ti-3d and S-3p of the host due to the intercalation of Ag.

For $Fe_{1/3}TiS_2$, the cohesive energy is markedly large compared with that of intercalation compound of alkali metal or Ag. The 3d-states of the guest atom are hybridized not only to S-3p states but also to Ti-3d states. Furthermore the mixing bands of three kinds of atoms, Ti, S, and transition-metal, are occupied partially. Therefore the energy gain due to intercalation will be large and the bondings among Ti, S and the guest atoms are expected to be large. This will lead to good stability of the 3d transition-metal intercalates compared with alkali metal or Ag intercalates.

We have also presented the sequence of magnitude of cohesive energy among $Li_{1/3}TiS_2$, $Ag_{1/3}TiS_2$(AB) and $K_{1/3}TiS_2$. However the difference in cohesive energy among them are about 0.02

Ryd/unitcell. We may only conclude that they have almost same stability. To discuss the correct sequence of the magnitude of the cohesive energy of them, it will be necessary to take farther correction for potential (full potential) and to make optimization of the total energy with respect to the atomic structure within a sandwich. But it beyonds the scope of this paper.

Table.5-1. The total energies and the cohesive energies for $M_{1/3}TiS_2$ (M= Fe,Ag,Li,K) with ABC-stacking and $M_{1/3}TiS_2$ (M = Fe,Ag) with AB-stacking. The E_{tot} denote total energy per MTi_3S_6, it corresponds to unit cell for ABC-stacking and a half of unit cell for AB-stacking: the value in () denotes the total energy per unit cell. The E_{coh} is defined by eq.5-1. The ΔE_{coh} is a difference from the E_{coh} of $Ag_{1/3}TiS_2$ (ABC).

(ABC)	E_{tot}(bulk)	E_{coh}	ΔE_{coh}	[Ryd/MTi_3S_6]
$Fe_{1/3}TiS_2$	12425.9439	1.756	0.744	
$Ag_{1/3}TiS_2$	20504.8070	1.012	0.000	
$Li_{1/3}TiS_2$	9899.9981	1.165	0.153	
$K_{1/3}TiS_2$	11086.1724	1.116	0.104	
(AB)				
$Fe_{1/3}TiS_2$	12425.8412	1.653	0.641	
	(25851.6824)	(3.306)		
$Ag_{1/3}TiS_2$	20504,9390	1.144	0.132	
	(41009.8780)	(2.288)		

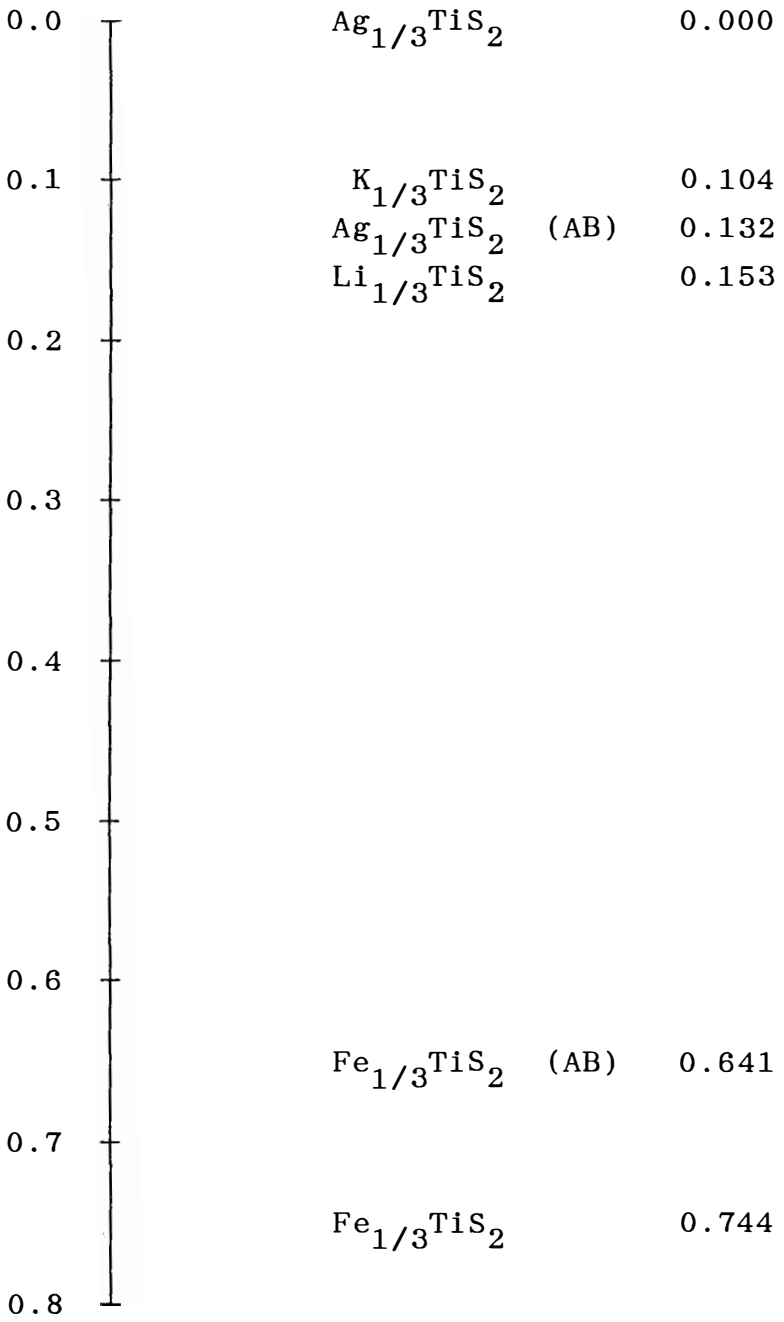

Fig. 5-1. The relative cohesive energy ΔE_{coh} [Ryd/MTi_3S_6] for the intercalation compounds. The ΔE_{coh} denotes the difference of the E_{tot} from that of $Ag_{1/3}TiS_2$ (ABC). The lower position denotes the more stability.

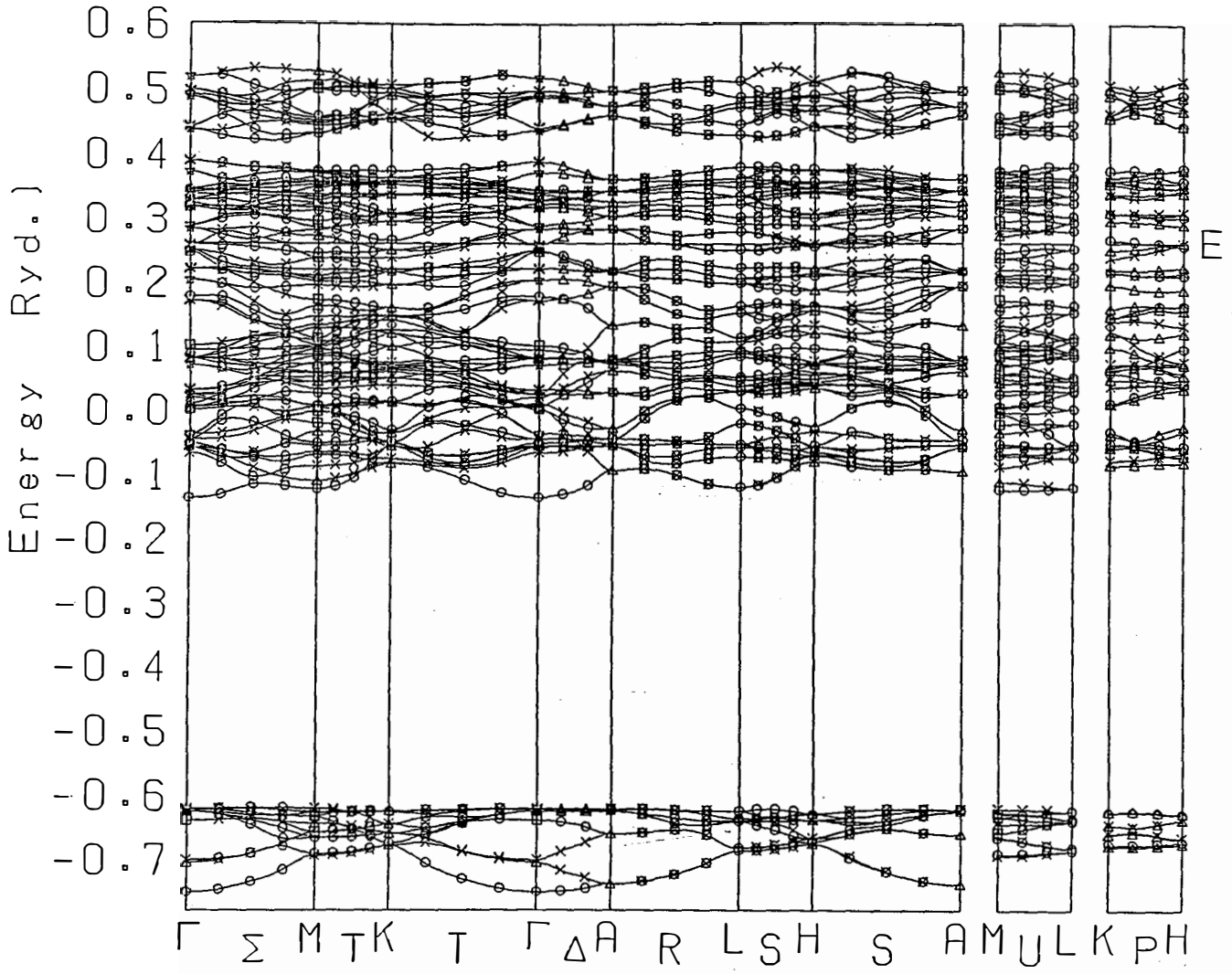

Fig. 5-2. The dispersion curves of $Fe_{1/3}TiS_2$ (AB-stacking).

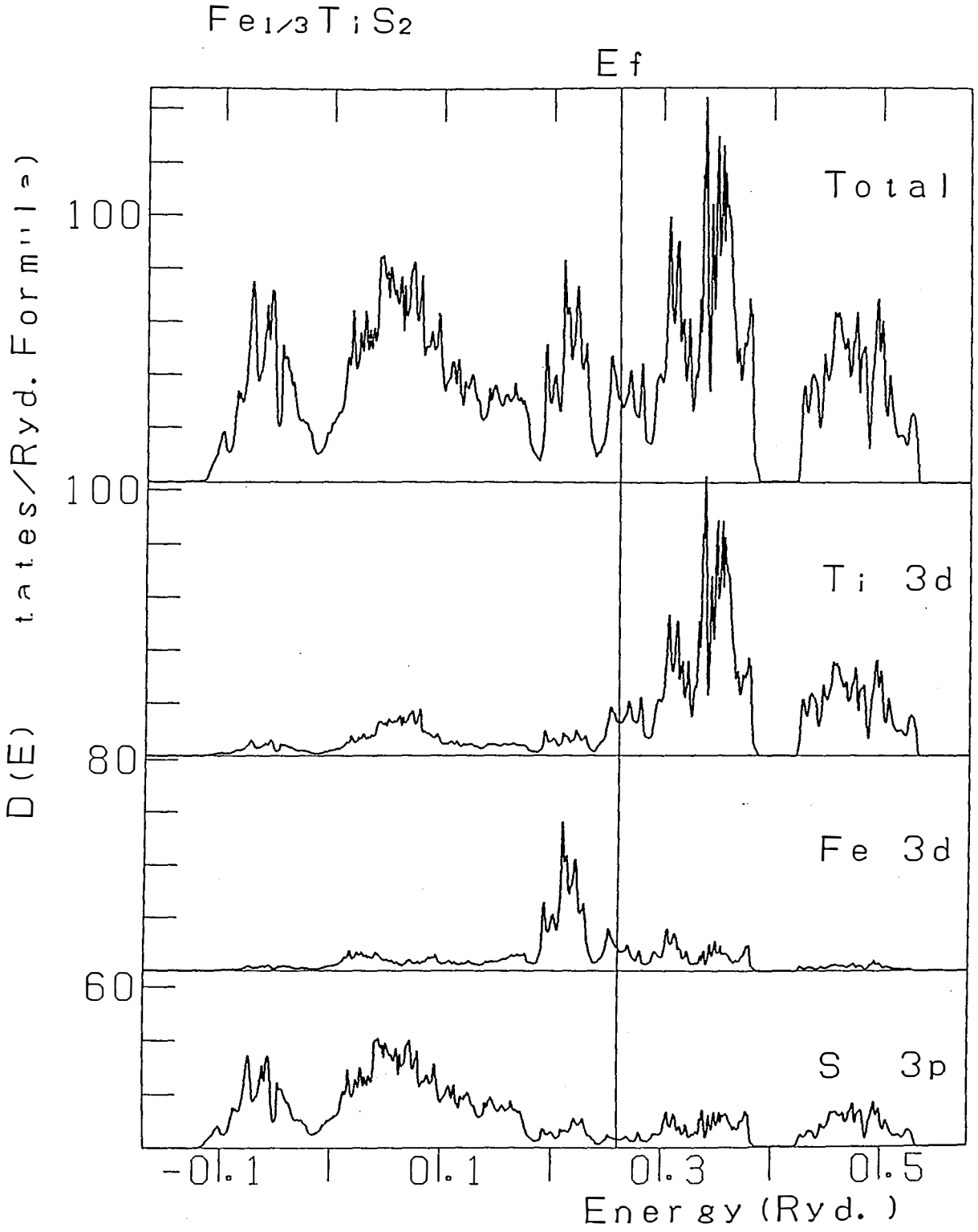

Fig. 5-3. The density of states of $Fe_{1/3}TiS_2$ (AB-stacking).

§6. RKKY Interaction in M_xTiS_2

As mentioned in section 1, intercalation compounds M_xTiS_2 (M = Cr, Fe, Co) show various magetism which depends on the sort of M and the concentration x. In section 3-2 we have calculated the band structures of the ferromagnetic state of $Cr_{1/3}TiS_2$ and $Co_{1/3}TiS_2$ since the guest M-3d states are well hybridized to the host electronic states and have itinerant character as shown in section 3-1.

When the concentration x is small ($x \approx 0$), modification of the band structures of the host TiS_2 may be small and the distance between the guest M atoms is large. Then it is expected that the M-3d electrons are localized to form localized spin moments at the M sites. In that case dominant magnetic interaction between two localized spin moments will be an indirect exchange interaction via spin polarization of conduction electrons due to the s-d exchange interaction between the conduction electron spins and the localized spins. The exchange interaction between the localized spins derived from the second order perturbation with respect to the s-d exchange interaction has been known as Ruderman-Kittel-Kasuya-Yosida (RKKY) interaction.[43-46]

When the guest atoms are rare earth elements, the guest-4f states will be well localized to form well defined localized magnetic moment and the rigid band model can be applicable. Thus we may expect that the magnetism in M_xTiS_2 (M = rare earth element) is explained by using the RKKY interaction even in case of rela-

tively high concentration (x=1/4 or 1/3).

We have calculated for the first time RKKY coupling between two spin moments in M_xTiS_2 by using the realistic band structures of the host to provide the starting point for understanding the magnetism of the low-concentration intercalates of the 3d transition element and the intercalation compound of the rare earth element.

6-1 Method for Calculation

6-1-1 Expression for RKKY Interaction

We assume the guest atoms provide their electrons to the host TiS_2 without modifying the band structure of TiS_2 (rigid band model). We also assume the s-d exchange interaction H_{s-d} can be expressed by using a δ-function as

$$H_{s-d}(\mathbf{r},\mathbf{R}) = j\,\delta(\mathbf{r}-\mathbf{R})\,\mathbf{s}(\mathbf{r})\cdot\mathbf{S}(\mathbf{R}) \qquad (6\text{-}1)$$

where $\mathbf{s}(\mathbf{r})$ denotes a conduction electron spin at $\mathbf{r}$ and $\mathbf{S}(\mathbf{R})$ is a localized spin at the guest site $\mathbf{R}$. This assumption is reasonable approximation when the valence orbital of the guest atoms (3d or 4f) does not spread compared with the wave length of conduction electrons.

As the result of the second order perturbation the RKKY interaction between two localized spins, $\mathbf{S}_1$ at $\mathbf{R}_1$ and $\mathbf{S}_2$ at $\mathbf{R}_2$,

is obtained in the following form:

$$J(\mathbf{R}_1-\mathbf{R}_2 \quad \$_1\cdot\mathbf{S}_2 \tag{6-2}$$

where the exchange coupling $J(\mathbf{R}_1-\mathbf{R}_2)$ is expressed as

$$J(\mathbf{R}_1-\mathbf{R}_2\ ) = \frac{1}{2}\sum_{n\mathbf{k}}\sum_{n'\mathbf{k}'}\frac{f(E_{n\mathbf{k}})-f(E_{n'\mathbf{k}'})}{E_{n\mathbf{k}}-E_{n'\mathbf{k}'}}\times \tag{6-3}$$

$$\{M_{n\mathbf{k},n'\mathbf{k}'}(\mathbf{R}_2)\,M_{n'\mathbf{k}',n\mathbf{k}}(\mathbf{R}_1)+\text{h.c.}\}$$

Here n is the band index, $\mathbf{k}$ denotes the wave number in the B.Z., f(E r)epresents Fermi distribution function, and $M_{n'\mathbf{k}',n\mathbf{k}}$ is a matrix element of the s-d exchange interaction defined by

$$\begin{aligned} M_{n'\mathbf{k}',n\mathbf{k}}(\mathbf{R}_1) &\equiv \int \psi^*_{n'\mathbf{k}'}(\mathbf{r})\,J\,\delta(\mathbf{r}\ \mathbf{R}-_1)\psi_{n\mathbf{k}}(\mathbf{r}\ d\mathbf{r}) \\ &= j\quad \psi^*_{n'\mathbf{k}'}(\mathbf{R}_1)\ \psi_{n\mathbf{k}}(\mathbf{R}_1) \end{aligned} \tag{6-4}$$

Here $\psi_{n\mathbf{k}}(\mathbf{r}$ d)enotes the Bloch eigenfunction of the host specified by n and $\mathbf{k}$. It has been assumed that the guest atoms occupy the octahedral site in the van der Waals gap layers. Then we can use the Bloch theorem

$$\psi_{n\mathbf{k}}(\mathbf{R}_2) = e^{i\mathbf{k}(\mathbf{R}_2-\mathbf{R}_1\ )}\ \psi_{n\mathbf{k}}(\mathbf{R}_1) \tag{6-5}$$

because $\mathbf{R}_2-\mathbf{R}_1$ must be a lattice vector. We write $\mathbf{R}_1-\mathbf{R}_2$ as $\mathbf{R}$ and consider the case of T=0. Then eq.(6-3) becomes

$$J(\mathbf{R}) = \frac{j^2}{2} \sum_{n\mathbf{k}}^{occ} \sum_{n'\mathbf{k}'}^{unocc} \frac{|\psi_{n'\mathbf{k}'}|^2 |\psi_{n\mathbf{k}}|^2}{\varepsilon_{n\mathbf{k}} - \varepsilon_{n'\mathbf{k}'}} \cos(\mathbf{k}-\mathbf{k}')\cdot\mathbf{R}. \qquad (6\text{-}6)$$

If we neglect the $\mathbf{k}$-dependence of the s-d exchange matrix elements $M_{n'\mathbf{k}',n\mathbf{k}}$ and assume the electronic structure is an electron gas-like, $J(\mathbf{R})$ is expressed as follows:

$$J(|\mathbf{R}|) = \frac{j^2 m k_F}{(2\pi)^3 h^2} \left(\frac{\cos 2k_F R}{R^3} - \frac{\sin 2k_F R}{2k_F R^4} \right) \qquad (6\text{-}7)$$

where m is an effective electron mass and k_F is the Fermi wave number. This expression is known as Ruderman-Kittel type interaction.[40)]

In the present calculation we have used the band structure of the host-TiS2 calculated by the APW method and we have also evaluated the matrix elements of the s-d exchange interaction by using the eigenfunctions obtained by the APW calculation. Then RKKY interaction is written as

$$J(\mathbf{R}) = \frac{j^2}{2} \sum_{n\mathbf{k}}^{occ} \sum_{n'\mathbf{k}'}^{unocc} \frac{\left| \sum_{\xi} C_{\xi}^{(n'\mathbf{k}')} \right|^2 \left| \sum_{\mu} C_{\mu}^{(n\mathbf{k})} \right|^2}{E_{n\mathbf{k}} \quad E_{n'\mathbf{k}'}} \cos(\mathbf{k}-\mathbf{k}')\cdot\mathbf{R} \qquad (6\text{-}8)$$

where $C_{\mu}^{(n\,\mathbf{k})}$ is the μ component of the eigenvector for $E_{n\,\mathbf{k}}$ in eq.(2-2), and μ and ξ denote the reciprocal lattice.

6-1-2 Practical Aspect in Calculation

In actual calculation we cannot perform exactly the summation over n and **k** in eq.(6-8). We have taken account of two valence bands and three conduction bands near the Fermi level E_F (see Fig.6-1) since a large contribution comes from energy bands near E_F because of the energy denominator in eq.(6-8). We have confirmed that taking the other bands into calculation changes the calculated value of J(**R**) only within 0.1 percent.

Accuracy of the calculated value of J(**R**) depends on the number of sampling **k**-points more sensitively rather than the number of bands. In order to estimate the influence of the number of **k**-points upon the accuracy of J(**R**) we have calculated J(**R**) with varying the number of **k**-points from 4000 to 15000. According to the results the values of J(**R**=6**a**) calculated with use of 12000 **k**-points and of 15000 **k**-points differ by one percent. Thus, in the following section we have calculated J(**R**) for $|\mathbf{R}| \leqq 6a$ by using 15000 **k**-points. It is noted here that if we want to calculate J(**R**) for $|\mathbf{R}| > 6a$ in the same accuracy as for $|\mathbf{R}| \leqq 6a$ we have to use sampling **k**-points more than 15000.

As noted in ref.28) our APW band calculation for the host TiS_2 gives a semimetallic band structure with a negative gap of -0.2 eV. Experimentally, on the other hand, stoichiometric TiS_2

is a semiconductor with a gap of 0.2 eV. Therefore, in actual calculation of J(**R**) we have raised by 0.4 eV all the conduction bands obtained by our APW band calculation in order that we achieve the realistic electronic band structure of TiS_2.

6-2 Result

On the basis of eq.(6-8) we have calculated the RKKY coupling J(**R**) in M_xTiS_2 at T=0K. Actual calculations have been performed for the following cases:

(1) x=0
(2) x=1/4, M^{2+}
(3) x=1/3, M^{2+}
(4) x=1/4, M^{3+}

The case (1) corresponds to an ideal situation when only two spin moments are put into the host TiS_2 and hence the semiconducting band structure of the host TiS_2 is used for calculating J(**R**). However, the results of calculation for this case will be applicable also to a case of finite but low concentration. In the case of (2)∿(4) the conduction band is partly filled and Fermi surfaces are formed because electrons are donated from the intercalant to the host. The Fermi level for each case is indicated in Fig.6-1.

The RKKY coupling have been calculated for each direction defined by Fig.6-2. Fig.6-3 shows coupling constants $J(\mathbf{R})$ calculated as a function of $\mathbf{R}$ for the case (1). Both values of $J(\mathbf{R})$ evaluated with and without $\mathbf{k}$-dependence of the s-d matrix elements $M_{n'\mathbf{k}',n\mathbf{k}}$ are shown together. As seen in the figure the value of $J(\mathbf{R})$ oscillates and decays as a function of distance R.

Reflecting the semiconducting band structure the value of $J(\mathbf{R})$ decays faster than that of Ruderman-Kittel expression, eq.(6-7). In fact it can be shown that $J(\mathbf{R})$ is proportional to $\exp(-\sqrt{\Delta}\,R)/R^3$ for large R, where Δ denotes the energy gap. Although the amplitude of $J(\mathbf{R})$ along the c-direction is comparable with that of the a- or x-direction, it should be noted that it is small at octahedral site itself ($\mathbf{R}= N\mathbf{c}$, N:integer). Thus the interaction between adjacent layers will be small compared with the intra-layer interaction.

As seen in Fig.6-3 the RKKY coupling for the nearest-neighbor site (position at 1a along the a-direction) and for the next nearest-neighbor site (position at $\sqrt{3}$a along x-direction) is antiferromagnetic while for the third neighbor site (position at 2a along the a-direction) it is ferromagnetic. This behavior of the RKKY interaction may play an important role in spin glass phase transitions observed at small concentration in Fe_xTiS_2 ($x<0.05$).[6,11,12]

In Fig.6-4 the RKKY coupling is shown for the case (2) (M^{2+} and $x=1/4$). The magnitude of $J(\mathbf{R})$ is order of 10^{-5} around $R \approx 1a$ while it becomes less than 10^{-6} for $|\mathbf{R}| > 4a$ in the a-direction

and for $|\mathbf{R}| > 5a$ in the x-direction. The value of $J(\mathbf{R})$ in this case decays gradually compared with that of the case (1). The coupling in the c-direction is small on the guest sites, and this situation is the same as in the case (1). These features of $J(\mathbf{R})$ for the case (2) are also seen for the cases of (3) and (4) as shown in Figs.6-5 and 6-6, respectively

In order to get an insight into the spin structure in the interstitial layer we have calculated $J(\mathbf{q})$, which is the Fourier transform of $J(\mathbf{R})$ for a superlattice of the guest M atoms. We have considered that the M atoms form a $2a \times 2a$ superlattice in the interstitial layer when x=1/4, and a $\sqrt{3}a \times \sqrt{3}a$ superlattice are formed when x=1/3.[3-5] The result is shown in Fig.6-7. As seen in the figure the maximum of $J(\mathbf{q})$ is located at the K point $(\pi/3,\pi/3)$ in the case (2), and the stable spin structure is a triangular arrangement. When we ignore the $\mathbf{k}$-dependence of the s-d matrix elements, $J(\mathbf{q})$ takes the maximum value at the M point $(\pi/2,0)$. This indicates that the consideration of the $\mathbf{k}$-dependence of the s-d matrix elements is important. In the case (3) (M^{2+}, x=1/3) $J(\mathbf{q})$ has the maximum value at the M point as seen in Fig.6-7, and the stable spin arrangement is an antiferromagnetic structure corresponding to the M point. The maximum of $J(\mathbf{q})$ for the case (4) (M^{3+}, x=1/4) is located at the Γ point (0,0).

It has been reported that the ferromagetic behavior is observed for $Co_{1/3}TiS_2$ and $Fe_{1/3}TiS_2$,[6,7] while our obtained results predict antiferromagnetic or triangular spin arrangement. This disagreement is considered to indicate also inapplicability

of the rigid band model to the intercalation compounds of 3d transition elements with high-concentration. As noted previously the results obtained for the cases (2)~(4) can be applicable well to intercalation compounds of rare earth elements. Unfortunately, however, magnetic measurements for Eu_xTiS_2 and Yb_xTiS_2 have been done only for $x < 0.10$.[47,48] The measurement for higher concentration intercalates of rare earth elements is desired.

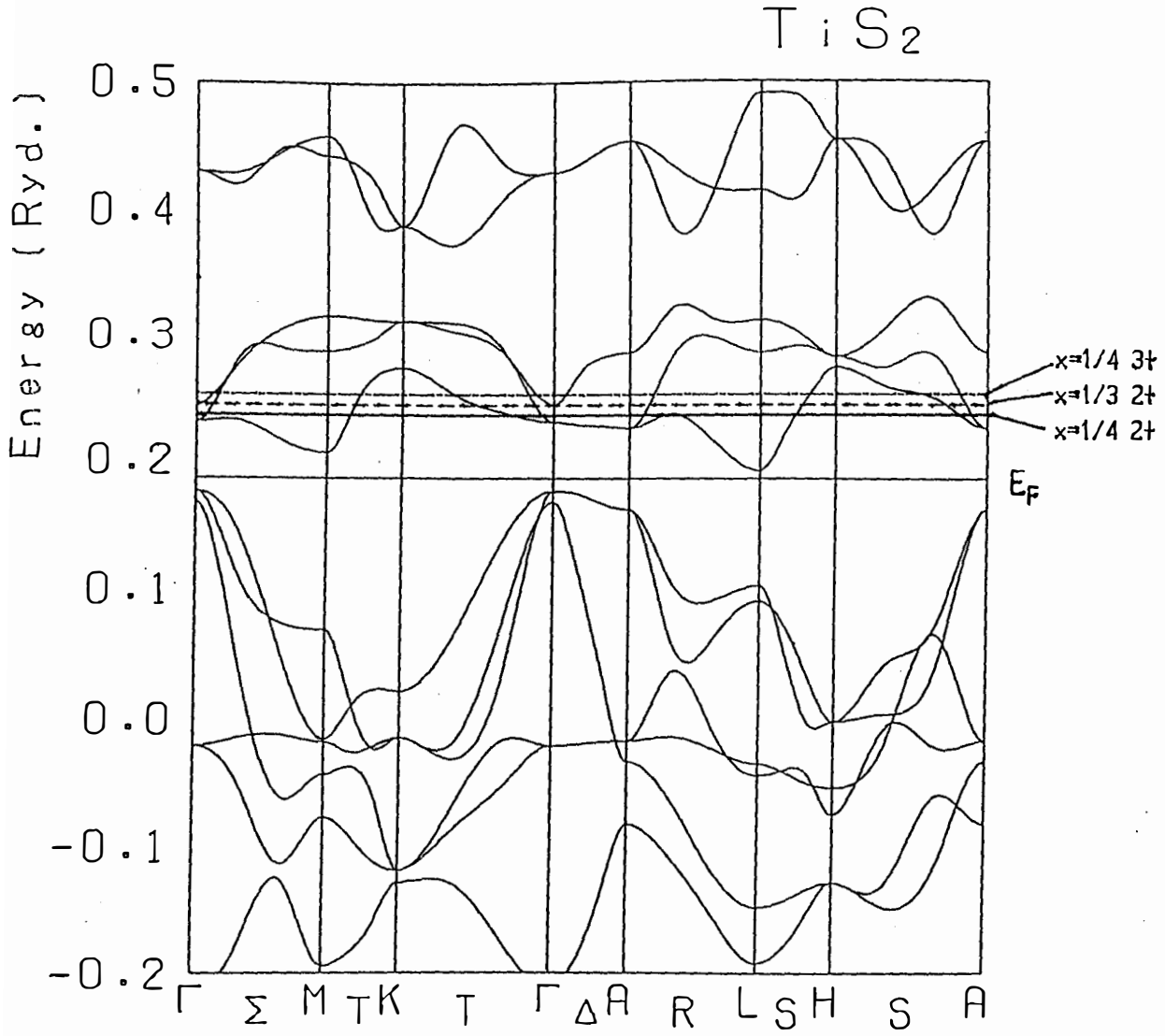

Fig. 6-1. The dispersion curves of TiS_2 for mixing bands consist of Ti-3d and S-3p. The Fermi level in the case of x=1/4 M^{2+}, x=1/3 M^{3+} and x=1/4 M^{2+} are shown by the solid line, broken line and chain line, respectively.

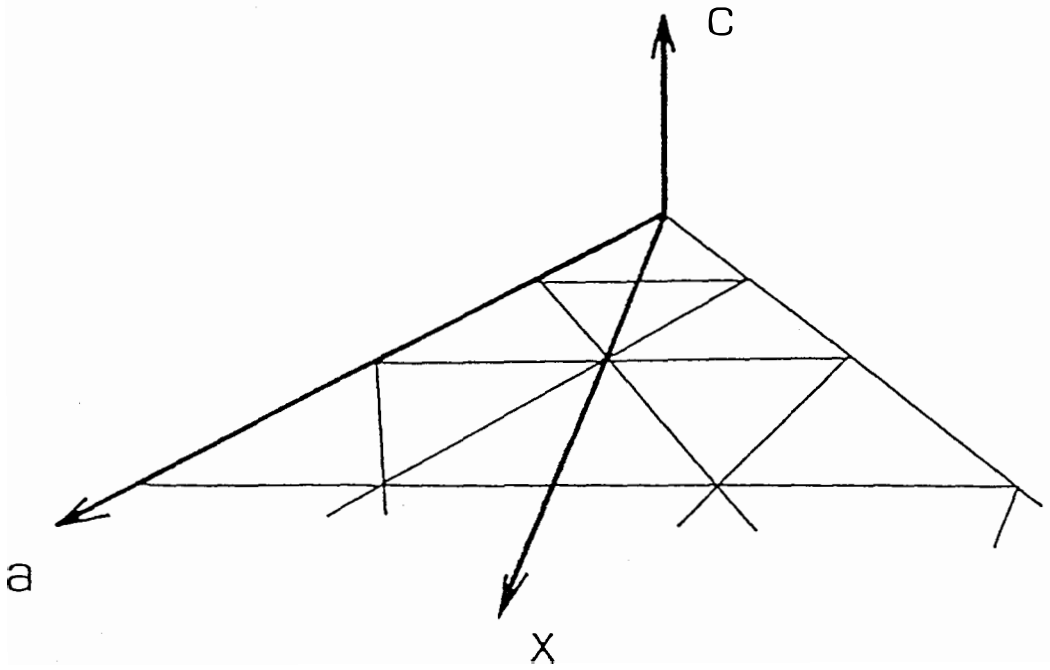

Fig. 6-2. The directions for which the RKKY coupling J(**R**) are calculated are defined as above. The triangular lattice site in the figure corresponds to the octahedral site in interstitial layer.

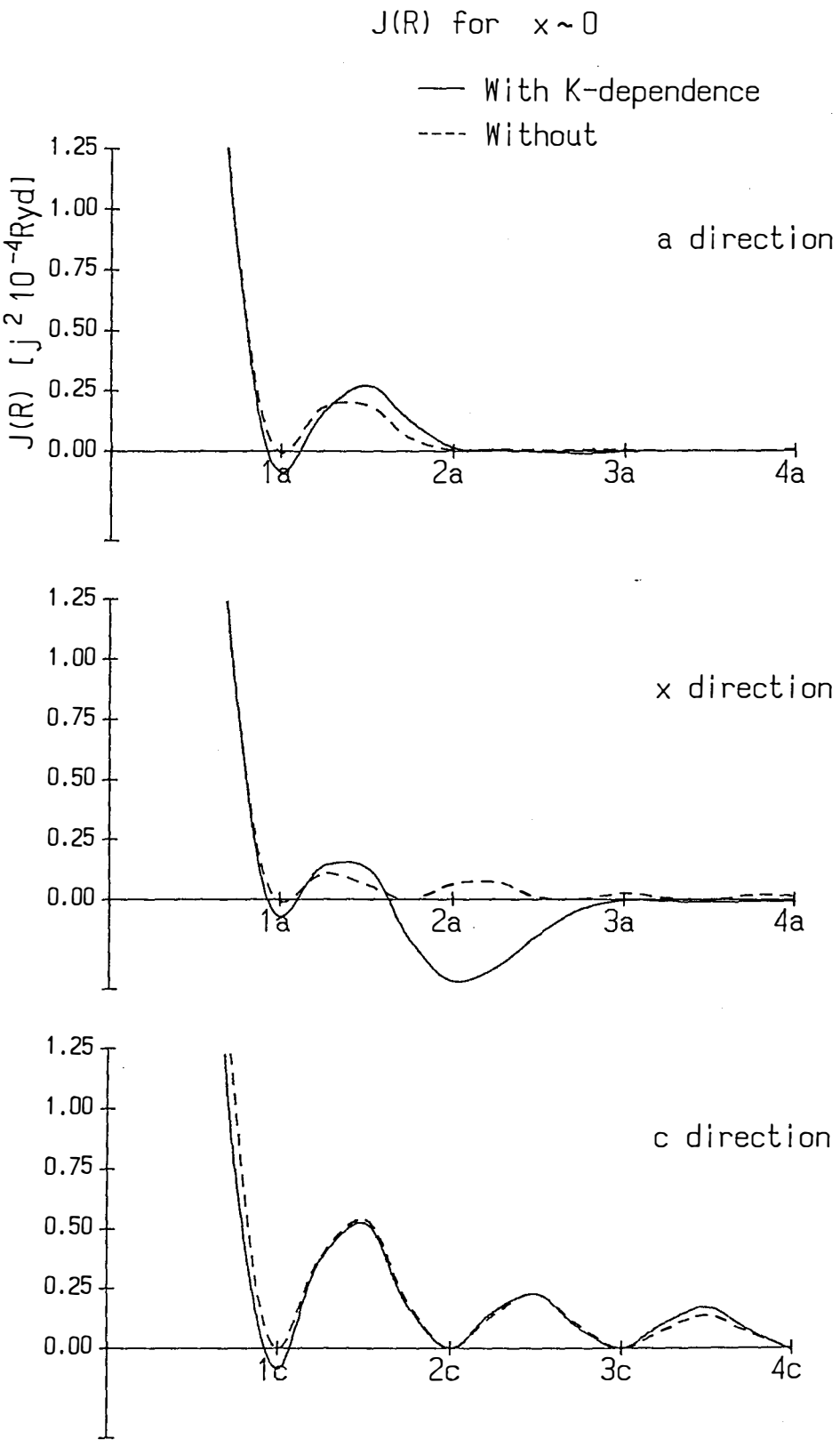

Fig. 6-3. The RKKY coupling in real space J(R) along each direction for $x \approx 0$.

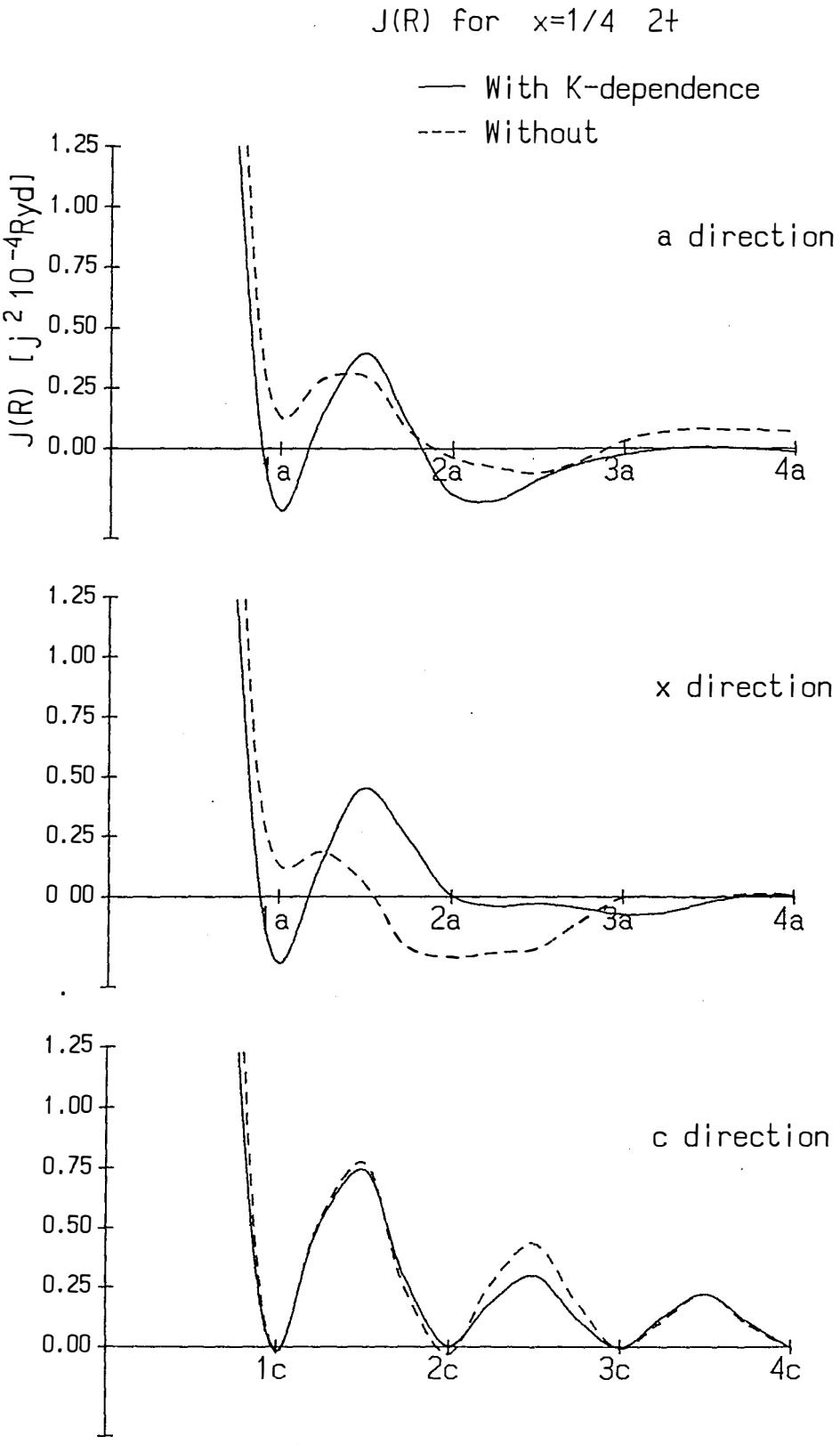

Fig. 6-4. The J(R) for x=1/4 M^{2+}

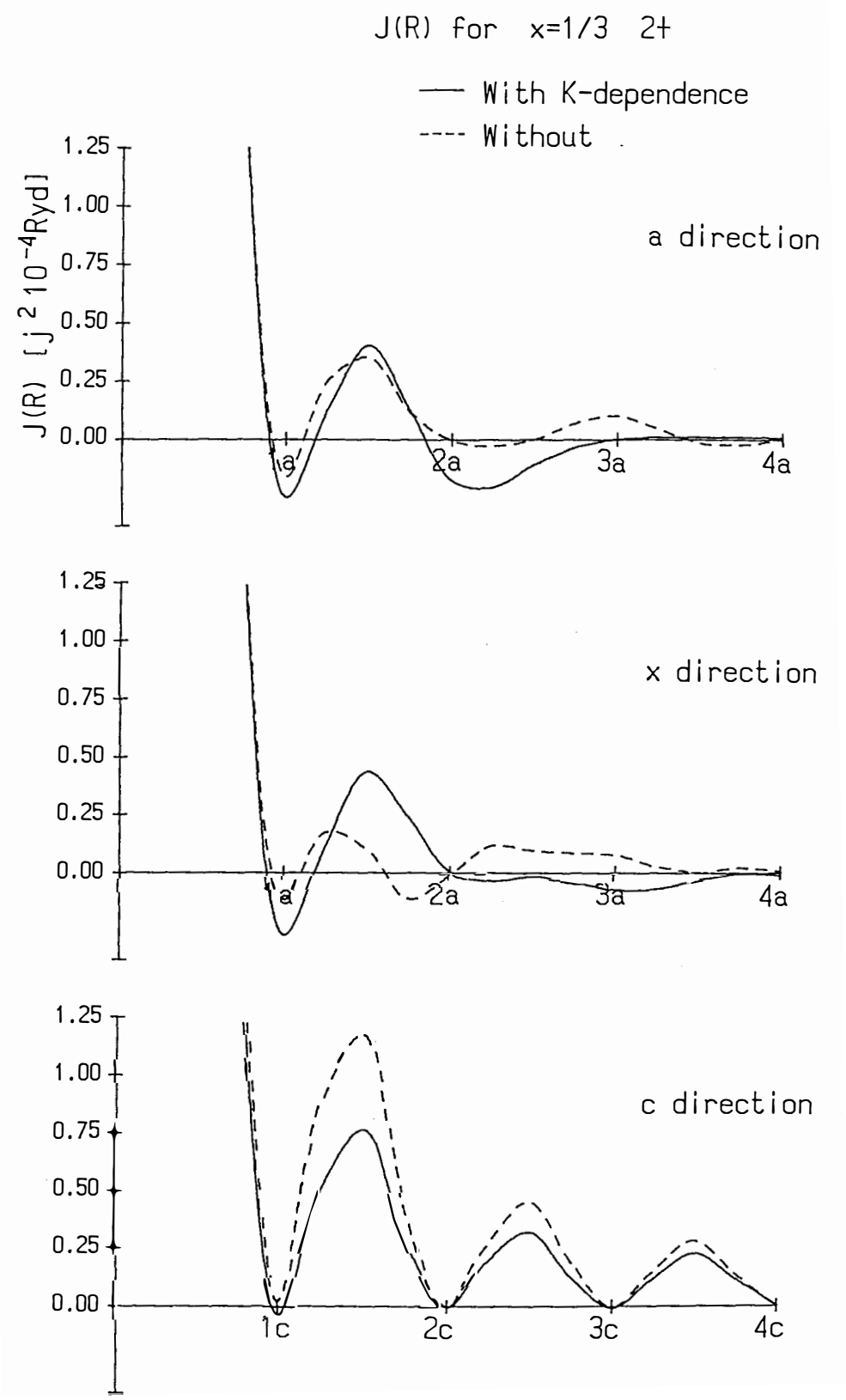

Fig. 6-5. The J(R) for x=1/3 M^{2+}

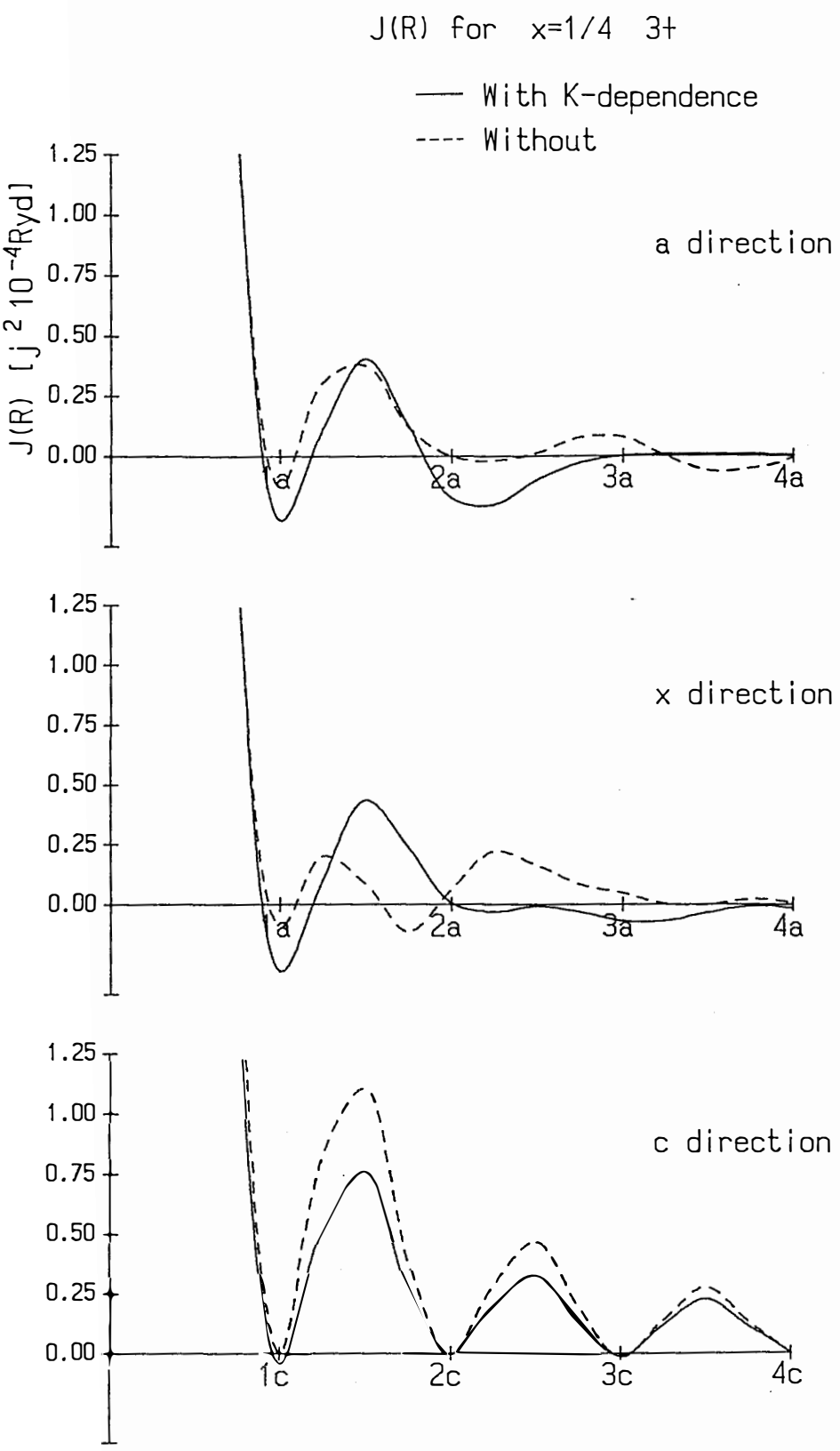

Fig. 6-6. The J(R) for x=1/4 M^{3+}

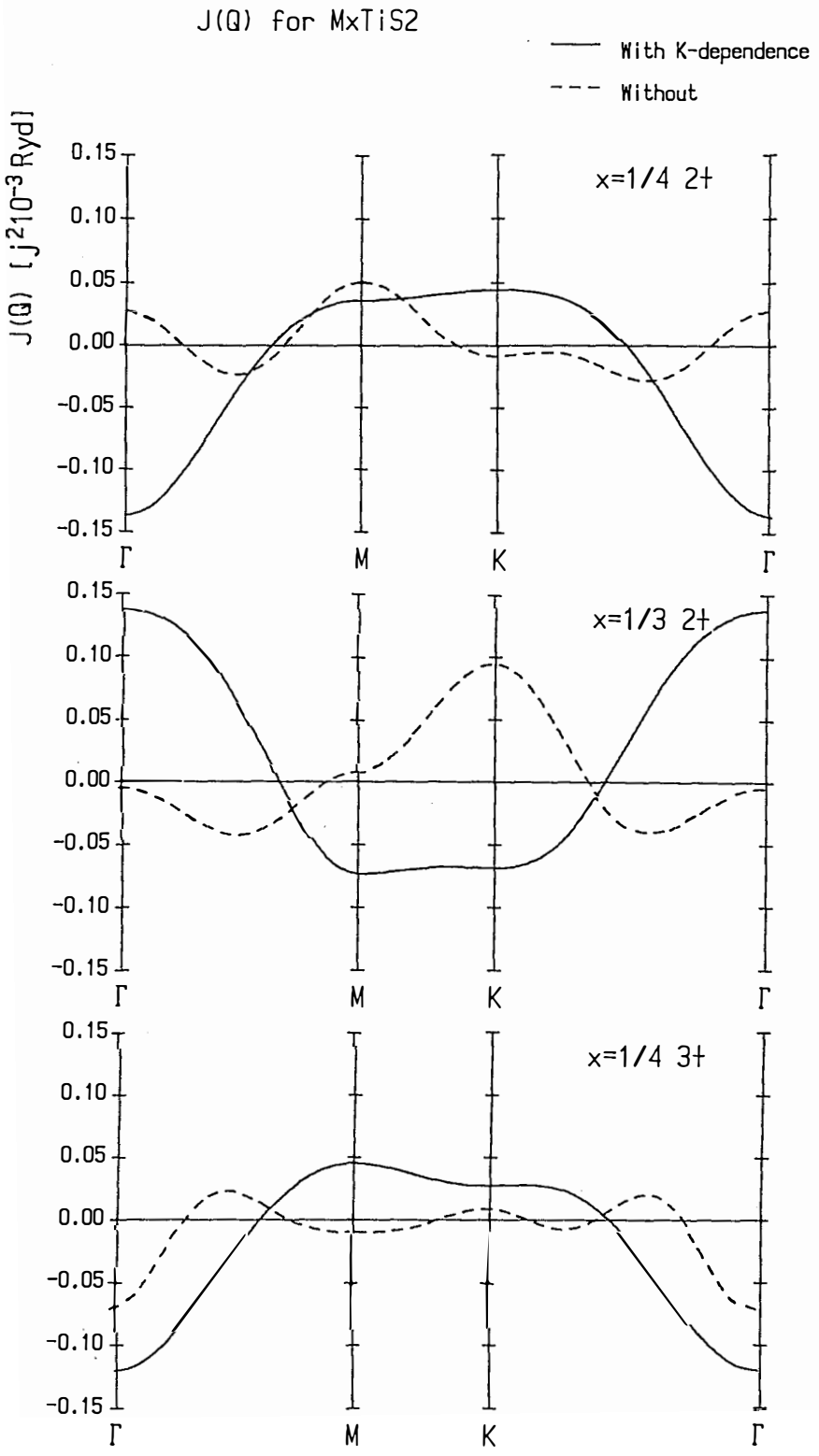

Fig. 6-7. The Fourier transform, J(**q**), of the RKKY coupling J(**R**) for corresponding superlattice; 2×2 for x=1/4, $\sqrt{3}\times\sqrt{3}$ for x=1/3.

§7. Summary

In this thesis we have performed systematic calculation of the electronic band structures and of the total energies for intercalation compounds of 3d-transition metal, Noble metal and Alkali metal as follows:

Band structure

3d-transition metal intercalation	$Ti_{1/3}TiS_2$
	$V_{1/3}TiS_2$
	$Cr_{1/3}TiS_2$
	$Cr_{1/3}TiS_2$ (ferromagnetic)
	$Co_{1/3}TiS_2$ (ferromagnetic)
Noble metal intercalation	$Ag_{1/3}TiS_2$
	$Ag_{1/3}TiS_2$ (AB-stacking)
Alkali metal intercalation	$Li_{1/3}TiS_2$
	$K_{1/3}TiS_2$

Total energy

3d-transition metal intercalation	$Fe_{1/3}TiS_2$
	$Fe_{1/3}TiS_2$ (AB-stacking)
Noble metal intercalation	$Ag_{1/3}TiS_2$
	$Ag_{1/3}TiS_2$ (AB-stacking)
Alkali metal intercalation	$Li_{1/3}TiS_2$
	$K_{1/3}TiS_2$.

Based on the band structures and the total energies, we have made clear the characteristic features of the three kinds of

compounds and have explained the difference among above mentioned compounds.

The principle results are summarized as follows:

3d-transition metal intercalation

(1) The guest-3d states are substantialy hybridized with Ti-3d and S-3p of the host and form bands with certain band width (more than 0.1 Ryd.). Then the guest-3d states have an itinerant character rather than localized one.

(2) The mixing bands of Ti-3d, S-3p and guest-3d are occupied partially by electrons, thus the energy gain due intercalation will be large.

(3) The magnetic moment in $Co_{1/3}TiS_2$ is 0.79 μ_B per unit cell and is comparable to the experimental value 0.5 μ_B. The magnetic moment of $Cr_{1/3}TiS_2$ is 2.92 μ_B and is four times larger than the experimental value.

(4) The calculated densitied of states at the Fermi level explain well the dependence of the specific heat coefficient γ on the sort of guest atoms, although the absolute magnitude of the observed γ is larger than the calculated one.

(5) The total energy calculation in $Fe_{1/3}TiS_2$ indicates that the intercalation compound of 3d element is stable enegetically and the ABC-stacking is favorable than the AB-stacking.

Noble metal intercalation

(6) The 4d states of guest are strongly hybridized with S-3p

states of the host, whereas that with Ti-3d is small. The hybridization of the guest 4d with S-3p is rather large in $Ag_{1/3}TiS_2$ compared with that in $M_{1/3}TiS_2$ (M=transition element). The strong hybridization between Ag-4d and S-3p destroy the covalent-like bond between Ti-3d and S-3p of the host, but does not yield an energy gain because almost all states of the hybridization bands of Ag-4d and S-3p are occupied by electrons. This feature seems to be related to the fact that Ag atoms cannot be intercalated more than x=0.42 and the Ag atoms show a temperature-induced order-disorder transition.

(7) The total energy calculation in $Ag_{1/3}TiS_2$ indicates that the ABC-stacking is more stable than the AB-stacking. The cohesive energy of $Ag_{1/3}TiS_2$ (AB) is comparable to that of the intercalation compound of alkali metals.

Alkali metal intercalation

(8) In the intercalation compound of Li or K the hybridization of Li-2s or K-4s with the host is weak, and the modification of the electronic structure of the host due to intercalation is small compared with that in the compounds of Ag or 3d-transition elements. Thus a rigid band model is applicable for the alkali metal intercalation compounds, especially for $Li_{1/3}TiS_2$. Since the Li atoms can be intercalated without breaking the intra-sandwich bond (Ti-S), the guest atoms can be intercalated to x=1 in contrast to Ag_xTiS_2 (6).

(9) In $K_{1/3}TiS_2$, narrow bands which consist of inner p states

(K-3p) are situated between S-3s bands and S-3p bands. It is distinguishable feature of $K_{1/3}TiS_2$ from other alkali-metal intercalation compounds.

(10) The guest atoms will be ionized nearly monovalency in both $Li_{1/3}TiS_2$ and $K_{1/3}TiS_2$, since the occupied states contain few s-symmetric valence states of the guest. It corresponds to experimental results of ionicity.[26)]

In the intercalation compounds of 3d transition-metal atoms inapplicability of the rigid band model and strong hybridization of guest-3d states with the host have been verified by experimental mesurements of specific heat, electronic properties and photoemission specta. The observed magnetic moments in $Cr_{1/3}TiS_2$, $Co_{1/3}TiS_2$ and $Fe_{1/3}TiS_2$ are much smaller than those expected from a free ionic state of the guest atom. Therefore the physical properties of the intercalation compounds of 3d transition element can be understood on the basis of the electronic band structures obtained by the APW band calculations. Now we should notice that the observed result specific heat coefficient and the photoemission spectra analysed by using cluster model (Fujimori and Suga[14)]) indicate a importance of the electron correlation effect. Investigations on the electron correlation effects in $M_{1/3}TiS_2$ (M = transition-metal) are left in future.

In the intercalation compounds of alkali metal and Ag, the weakness of bond between the guest and the host has been verified

by experiments: a diffusive motion of Li^+ was observed in Li_{TiS_2} ,[27] the order-disorder transition at finite temperature and the presence of gas phase were observed in Ag_xTiS_2.[21] Structural ordering of the guest and modification of the host layer in the intercalation compounds of Ag and alkali metal with large ionic radius such as K, Na have been also attracted much interest. The total energy calculation for the various arrangement of the guest and for the inner structure will reveal the structural features of the intercalation compounds of alkali metal. These calculations have to be performed with structural optimization and by the use of full potential, since the discussion of structural variation demands an accuracy of 10 mRyd.

We have also calculated RKKY interaction between localized spins on the guest atoms by using the realistic band structure of the host-TiS_2. The ground state spin arrangement evaluated by using RKKY coupling does not explain well the magnetic order observed in $Co_{1/3}TiS_2$ or $Fe_{1/3}TiS_2$. This indicates that the rigid band model is not adequate for these compounds. However we emphasize that the calculated result of the RKKY coupling should be applied to intercalation compounds with the low concentration guest atoms such as Fe_xTiS_2 with $x < 0.05$, and also applied to the intercalation compounds of rare-earth metal atoms, where the guest atoms are expected to have localized spin. Experimental study of magnetism in $R_{1/3}TiS_2$ (R = Eu,Yb) is desired.

Appendix.1. Construction of electronic charge density

The MT potential $V(\mathbf{r})$ consists of contributions from the interaction between an electron and nuclear charges and the electron-electron interaction. In the local spin density approximation (LSDA) the latter is expressed in terms of the electron charge density which should be determined self-consistently. Thus the construction of the electron charge density is an important task in the self-consistent band calculations.

In general the charge density of valence electrons, $\rho(\mathbf{r})$, is calculated from

$$\rho(\mathbf{r}) = \sum_{n\mathbf{k}}^{occup} |\Psi_{n\mathbf{k}}(\mathbf{r})|^2 \qquad \text{(A1-1)}$$

where $\Psi_{n\mathbf{k}}(\mathbf{r})$ represents the eigenfunction obtained for valence electrons with n being the band index, and the summation is taken over the occupied states. The spherically symmetric charge density in the νth MT sphere, $\rho_\nu(\mathbf{r}_\nu)$ is defined by

$$\rho_\nu(r_\nu) = \int \rho(\mathbf{r}_\nu) d\hat{r}_\nu \ .$$

In the LAPW method the eigenfunctions $\Psi_{n\mathbf{k}}(\mathbf{r})$ are not used directly in constructing the charge density. Instead the charge

density is obtained by making use of the partial density of state (DOS) as follows:

$$\rho_{\nu}(\mathbf{r}_{\nu}) = \rho_{\nu,\mathrm{core}}(\mathbf{r}) + \sum_{\ell} \int^{E_F} d\varepsilon\, \rho_{\ell\nu}(\varepsilon) |R_{\ell}(\mathbf{r}_{\nu};\varepsilon)|^2 \qquad \text{(A1-2)}$$

where $\rho_{\ell\nu}(\varepsilon)$ denotes partial DOS in MT sphere respect to ℓ which is angular momentum quantum number. It is reliabele to construct charge density in LAPW from partial DOS, because $E_{\mathbf{k}}$ s are determined variationally though basis functions are not good in comparison with APW. This notation (eq.A1-2) is exactly when one chose APWs as the basis functions. If radial wave function $R_{\ell}(\mathbf{r}_{\nu};\varepsilon)$ depends linearly on energy ε, the second term in eq.A1-2 can be represented only first three energy moments of the occupied partial DOS. When it has near limearly dependence, one can adoquatly express the charge density using few number of moments.

The charge density can be expressed as follows:

$$\rho_{\nu}(\mathbf{r}_{\nu}) = \rho_{\nu,\mathrm{core}}(\mathbf{r}_{\nu}) + \sum_{\alpha=1}^{N} \sum_{\ell} Q_{\ell\alpha\nu} |R_{\ell}(\mathbf{r}_{\nu};E_{\ell\alpha})|^2 \qquad \text{(A1-3)}$$

where the N is a integer, and the weight factor $Q_{\ell\alpha\nu}$ and the sampling energy $E_{\ell\alpha}$ are determined by following relation:

$$\sum_{\alpha=1}^{N} Q_{\ell\alpha\nu} E_{\alpha}^{\beta} = M_{\ell\beta\nu} \qquad (\beta = 0,1,\ldots 2N-1) \tag{A1-4}$$

The $M_{\ell\beta\nu}$ denotes the moment of order β

$$M_{\ell\beta\nu} \equiv \int^{E_F} \rho_{\ell\nu}(\varepsilon)\varepsilon^{\beta} d\beta \tag{A1-5}$$

In this paper the first four moments are taken (or let N = 2), then we can represent $\rho_{\nu}(\mathbf{r}_{\nu})$ exactly until the term propotion to ε^3 in $|R_{\ell}(\mathbf{r}_{\nu};\varepsilon)|^2$. The weight factor $Q_{\ell\alpha\nu}$,$E_{\ell\alpha}$ are used to make $\rho(\mathbf{r}_{\nu})$, $E_{\ell\alpha}$ are also used as $E_{\ell 1}$, $E_{\ell 2}$ which are parameter determines the form of basis functions.

Appendix.2. Exchange and Correlation in Electron Gas System

The exchange energy density in eq.2-36 for electron gas is

$$\varepsilon^{X}[\rho(\cdot)] = -\frac{3}{2\pi}(3\pi^2\rho)^{1/3} \quad , \tag{A2-1}$$

and the exchange potential energy density is defined by

$$v^{X}[\rho(\cdot)] \equiv \frac{d}{d\rho}(\rho\,\varepsilon^{X}[\rho(\cdot)]) \quad . \tag{A2-2}$$

Now we define density parameter r_s by

$$\frac{4}{3}\pi r_s^3 = \frac{1}{\rho} \quad . \tag{A2-3}$$

Then eq.A2-1 become

$$\varepsilon^{X} = -\frac{3}{2\pi\alpha r_s} \tag{A2-4}$$

and the potential energy density is give by using r_s

$$v^{X} = (1 - \frac{r_s}{3}\frac{d}{dr_s})\,\varepsilon^{X} \tag{A2-5}$$

then

$$= -\frac{4}{3}\frac{3}{2\pi\alpha r_s} \quad . \tag{A2-6}$$

where the α is given as $\alpha=(4/9\pi)^{1/3}$.

The eq.A2-4 and eq.A2-6 for polarized state are given by following interpolation expression.[36)]

$$\varepsilon^{x}(\zeta) = \varepsilon^{x}\{1 + (2^{1/3} - 1)\, f(\zeta)\} \tag{A2-7}$$

$$v^{x}_{\sigma}(\zeta) = \frac{4}{3}\varepsilon^{x}(1 + \sigma\zeta)^{1/3} \qquad (\sigma = +1, -1) \tag{A2-8}$$

where the σ denotes the spin $\uparrow$ (+1) and $\downarrow$ (-1), $\zeta=(\rho\uparrow-\rho\downarrow)/\rho$ and

$$f(x) \equiv \frac{1}{2(2^{1/3}-1)}\{(1+x)^{4/3} + (1-x)^{4/3} - 2\} \quad . \tag{A2-9}$$

The correlation energy density are estimated by following interpolation expression respect to r_s[36)]

$$\varepsilon^{c}_{p} = -c_p\, g(\frac{r_s}{r_p}) \quad , \qquad \varepsilon^{c}_{f} = -c_f\, g(\frac{r_s}{r_f}) \tag{A2-10}$$

where the p and f means the case of $\zeta=0$ and $\zeta=1$ respectively and

$$g(x) \equiv (1+x^3)\,\mathrm{log}(1+\frac{1}{x}) - x^2 + \frac{1}{2}x - \frac{1}{3} \tag{A2-11}$$

The C_p, C_f, r_p and r_f are constant given in Table.A2. The correlation potential density is given as

$$v_p^c = -c_p \log\left(\frac{r_s}{r_p}\right) , \qquad v_f^c = -c_f \log\left(\frac{r_s}{r_f}\right) \tag{A2-12}$$

The interpolation for intermediate spin polarization state, $0 < \zeta < 1$, are done by using following expression.

$$\varepsilon^c(\zeta) = \varepsilon_p^c + (\varepsilon_f^c - \varepsilon_p^c) f(\zeta) \tag{A2-13}$$

$$v_\sigma^c(\zeta) = v_p^c + \{ v_f^c - v_p^c - \frac{4}{3} (\varepsilon_f^c - \varepsilon_p^c)\} f(\zeta) + \frac{4}{3} (\varepsilon_f^c - \varepsilon_p^c) f'(\sigma\zeta) \tag{A2-14}$$

where

$$f'(x) = \frac{1}{2^{1/3}-1} \{(1+x)^{1/3} - 1\} \quad .$$

In our band calculation, the exchange-correlation terms are estimated by using eq.A2-4, A2-6, A2-13 and A2-14, and three type of the expressions are available: the von Barth & Hedin, the Gunnarson & Lundqvist and the Hedin & Lundqvist type.

Table. A2. Constants for the interpolation experssion.

	C_p	C_f	r_p	r_f
vB-H*	0.0504	0.0254	30	75
G-L**	0.0504	0.0225	11.4	15.9
M-J-W***	0.0450	0.0225	21	52.9

The C_f and r_f are defined by $C_f=C_p/2$ and $r_f=2^{4/3}r_p$

* von Barth and Hedin[36)]

** Gunnarsson and Lundqvist[38)]

*** Morruzi, Janak and Williams[34)]

Appendix.3. Atomic positions in unit cell

	ABC-stacking	AB-stacking
	(0 , 0 , 1/6)	(0 , 0 , 0)
Ti	(0 , 0 , 1/2)	(0 , 0 , 1/2)
	(0 , 0 , 5/6)	(2/3, 1/3, 0)
		(1/3, 2/3, 0)
	(1/3, 0 , u)	(2/3, 1/3, 1/2)
	(0 , 1/3, u)	(1/3, 2/3, 1/3)
S	(2/3, 2/3, u)	
	(1/3, 1/3, v)	(2/3, 0 , t)
	(2/3, 0 , v)	(0 , 2/3, t)
	(0 , 2/3, v)	(1/3, 0 , u)
		(0 , 1/3, u)
M	(0 , 0 , 0)	(2/3, 0 , v)
S		(0 , 2/3, v)
		(1/3, 0 , w)
		(0 , 1/3, w)
		(1/3, 1/3, t)
		(1/3, 1/3, v)
		(2/3, 2/3, u)
		(2/3, 2/3, w)
M		(2/3, 1/3, 1/4)
		(1/3, 2/3, 3/4)

	u	v
Ti	0.4170	0.5830
V	0.4166	0.5834
Cr	0.4168	0.5832
Fe	0.4169	0.5831
Co	0.4156	0.5844
Li	0.4190	0.5810
K	0.4206	0.5794
Ag	0.4243	0.5756

	Fe	Ag
s	0.1247	0.1135
t	0.3753	0.3865
u	0.6247	0.6135
v	0.8753	0.8865

References

1. J. A. Wilson and A. D. Yoffe, Adv. Phys. **18** (1969) 193
2. J. J. Bary, H. P. Hughes, P. C. Klipstein and R. H. Friend, J. Phys. C:Solid State Physics **16** (1983) 393
3. M. Inoue and H. Negishi, J. Phys. Soc. Jpn. **53** (1984) 943
4. M. Inoue and H. Negishi, J. Phys. Soc. Jpn. **54** (1985) 380
5. M. Inoue and H. Negishi, J. Phys. Chem. **90** (1986) 235
6. N. Negishi, A. Shoube, H. Takahashi, Y. Ueda, M. Sasaki, M.Inoue, J. Magn. Magn. Matt. **67** (1987) 179
7. M. Inoue and H. Negishi, J. Magn. Magn. Matt. **70** (1987) 199
8. M. Inoue, Y. Muneta, H. Negishi and M. Sasaki, J. Low. Temp. Phys. **63** (1986) 235
9. Y. Tazuke and T. Endo, J. Magn. Magn. Matt. **31-34** (1983) 1175
10. Y. Tazuke, A. Nomura and T. Ebina, J. Phys. Soc. Jpn. **56** (1987) 1250
11. T. Satoh, Y. Tazuke and T. Miyadai and K. Hoshi, J. Phys. Soc. Jpn. **57** (1988) 1743
12. T. Satoh, Y. Tazuke and T. Miyadai, J. Magn. Mang. Matt. **64** (1987) 179
13. T. Tazuke, K. Kuwazawa, Y. Onishi and T. Hashimoto, J. Phys. Soc. Jpn. **60** (1991) 2534
14. A. Fujimori and S. Suga, Phys. Rev. **B38** (1988) 3676
15. Y. Ueda, K. Fukushima, H. Negishi, M. Inoue, M. Tanigushi and S. Suga, J. Phys. Soc. Jpn. **56** (1987) 2471

16. Y. Ueda, H. Negishi, M. Koyano, M. Inoue, K. Soda, H. Sakamoto and S. Suga, Solid. State. Commun. **57** (1986) 839
17. G. A. Scholz and R. F. Frindt, Mat. Res. Bull. **15** (1980) 1703
18. R. M. Suter, M. W. Shafer, P. M. Horn and P. Dimon, Phys. Rev. **B26** (1982) 1291
19. A. G. Gerards, H. Roede, R. J. Haange, B. A. Boukamp and G. A. Wiegers, Synth. Metal. **10** (1984/85) 51
20. K. Ohshima and S. C. Moss, Acta. Cryst. **A39** (1983) 298
21. Y. Kuroiwa, K. Ohshima and H. Maeta, J. Appl. Crystallogr. **23** (1990) 77
22. Y. Kuroiwa, K. Ohshima And Y. Watanabe, Phys. Rev. **B42** (1990)
23. H. Dijikstra, C. F. van Bruggen and C. Haas, J. Phys. C: Solid State Physics **16** (1983) 393
24. J. Rouxel, J. Sol. St. Chem. **17** (1976) 223
25. J. Rouxel, **Physics and Chemistry of Layered Materials, Vol.6: Intercalated Layered Matterials**, F. Levy, Ed., Reidel, Dordrecht (1979)
26. M. S. Whittingham and A. J. Jacobson, **Intercalation Chemistry** (1982) Academic Press, New York
27. C. Berthier, **Fast Ion Transport in Solid** (1979) Elservier, North Holland.
28. T. Yamasaki, N. Suzuki and K. Motizuki, J. Phys. C **20** (1987) 395
29. N. Suzuki, T. Yamasaki and K. Motizuki, J. Magn. Magn. Matt. **70** (1987) 64

30. N. Suzuki, T. Yamasaki and K. Motizuki, J. Phys. C **21** (1988) 6133
31. N. Suzuki, T. Yamasaki and K. Motizuki, J. Phys. Soc. Jpn. **58** (1989) 3250
32. J. C. Slater, Phys. Rev. **51** (1937) 864
33. T. L. Loucks, **Augumented Plane Wave Method**, W. A. Benjamin, Inc. New York (1967)
34. T. Takeda and J. Kubler, J. Phys. F:Metal Physics **9** (1979) 661
35. P. Hohenberg and W. Kohn, Phys. Rev. **136** (1964) B864
36. W. Kohn and L. J. Sham, Phys. Rev. **140** (1965) A1133
37. V. L. Moruzzi, J. F. Janak and A. R. Williams, Calculated Electronic Properties Of Metal, Pergamon, Inc. New York (1987)
38. R. M. Dreizler and E. K. U. Gross, Density Functional Theoty, Springer-Verlag. New York (1990)
39. U. Von Barth and L. Hedin, J. Phys. C. **5** (1972) 1629
40. L. Hedin and B. I. Lundqvist, Solid State Physics **23** (1969) 1
41. O. Gunnarson and B. I. Lundqvist, Phys. Rev. **B13** (1976) 4274
42. D. M. Ceperley and B. J. Alder, Phys. Rev. Lett. **45** (1980) 566
43. M. A. Ruderman and C. Kittel, Phys. Rev. **96** (1954) 99
44. T. Kasuya, Prog. Theor. Phys. **16** (1956) 45
45. K. Yosida, Phys. Rev. **106** (1959) 893
46. L. M. Roth, H. J. Zeiger and T. A. Kaplan, Phys. Rev. **149** (1966) 519

47. S. P. Hsu and W. G. Glaunsinger, Mat. Res. Bull. **21** (1986) 1063

48. S. P. Hsu and W. S. Glaunsinger, J. Solid State Chem. **67** (1987) 109

List of Publications

1. "RKKY Interaction in Intercalation Compounds of Transition-Metal Dichalcogenides"
   N. Suzuki, Y. Yamazaki, T. Teshima and K. Motizuki, Physica **B156&157** (1989) 286

2. "Electronic Band Structure of Intercalation Compounds"
   N. Suzuki, T. Teshima and K. Motizuki, **Proceedings of Fourth Asia Pacific Physics Conference** (1990) 448

3. "Electronic Band Structure of 1T-Type TiS_2 Intercalation with Light 3d Transition-Metals"
   T. Teshima, N. Suzuki and K. Motizuki, J. Phys. Soc. Jpn. **60** (1991) 1005